THESIS

Investigating Machine Learning Applications for Monitoring Electrical Resistivity and Predicting Physical Properties in Permafrost Regions

Author:

SIAVASH ABGHARI

Supervisors:

ALBERTO GODIO

FARBOD KHOSRO ANJOM

MOHAMMADKARIM KARIMPOUR

09 DECEMBER 2024

POLITECNICO DI TORINO
DIATI

Acknowledgment

I would like to express my deepest gratitude to everyone who has supported and guided me throughout this thesis journey. First and foremost, I extend my heartfelt thanks to my supervisors, Professor Alberto Godio, Dr. Farbod Khosro Anjom, and Dr. Mohammadkarim Karimpour, for their invaluable guidance, encouragement, and expertise. Their insights and support were instrumental in shaping the direction and quality of this research.

I am profoundly grateful to my beloved wife, Fatemeh, whose unwavering love, patience, and encouragement have been my greatest source of strength and motivation. Your belief in me made this accomplishment possible, and I am forever indebted to you for your sacrifices and support.

To my friends who shared this journey with me, thank you for your companionship, inspiration, and constant encouragement. Your presence made this challenging path more meaningful and enjoyable, and I will always cherish the moments we shared.

Finally, I offer my deepest gratitude to all who contributed, directly or indirectly, to the completion of this thesis. This work would not have been possible without your support, and I am sincerely thankful for the role each of you played in this achievement.

Abstract

Permafrost, a critical component of Earth's cryosphere, plays a significant role in global climate systems and geotechnical stability in cold regions. Understanding its dynamics is essential for environmental monitoring and infrastructure planning. This thesis explores the potential of machine learning (ML) and geophysical methods to predict the petrophysical properties of permafrost and improve resistivity inversion techniques, focusing on synthetic 2D resistivity models and Convolutional Neural Network (CNN)-based inversion.

A key part of this thesis involves development of synthetic models representing typical permafrost regions, incorporating layers such as the active layer, thaw layer, permafrost, and base layer. For this, several models were trained using experimental data from the literature, with a neural network achieving the highest accuracy—an R^2 score of 0.975—in predicting realistic resistivity values of frozen soil based on temperature, dry density, and water content as input.

The thesis also evaluates ML models for predicting temperature and water content in permafrost body based on predicted resistivity value of permafrost from apparent resistivity which got an R^2 score of 0.588. Moderate and poor predictive performance was observed for predicting temperature and water content, respectively, with limitations attributed to the dependency on previously predicted resistivity values.

To address limitations in conventional inversion techniques, a CNN model was developed to invert apparent resistivity data into true resistivity distributions. The CNN model outperformed traditional methods, effectively capturing complex discontinuities and providing high-resolution resistivity maps. However, signs of overfitting and dependency on fixed configurations highlighted the need for richer datasets and validation with real-world data.

This research demonstrates the potential of ML and CNN-based inversion for advancing permafrost studies. It underscores the importance of comprehensive datasets and methodological refinement to improve model generalization and applicability in real-world scenarios. The findings contribute to geotechnical and environmental monitoring, offering a foundation for future research on permafrost dynamics and climate change mitigation.

Table of Contents

List of figures

List of tables

Chapter 1: Introduction

Permafrost, defined as ground that remains at or below 0°C for at least two consecutive years (Washburn, 1973), serves as a critical component in cold-region ecosystems, influencing landscapes, carbon storage, and infrastructure stability (Jin et al., 2021). As climate change accelerates, permafrost regions are increasingly at risk of thawing and degradation. These processes have profound implications, including the release of greenhouse gases such as carbon dioxide and methane, which amplify global warming. Furthermore, the destabilization of structures built on permafrost—such as buildings, roads, and pipelines—poses significant challenges to infrastructure integrity in Arctic and sub-Arctic regions. Therefore, continuous monitoring and assessment of permafrost are crucial for understanding its dynamics, mitigating associated risks, and informing climate change adaptation strategies (Hjort et al., 2022). Permafrost refers to the thermal state of subsurface ground. Unlike sea ice, glaciers, and ice sheets, it cannot be directly observed through satellite remote sensing on local to global scales. Detecting changes in permafrost instead requires subsurface measurements and/or indirect assessments using remote sensing techniques. Consequently, our understanding of permafrost dynamics remains fragmented, even amidst record-setting warming observed within the permafrost borehole monitoring network (Schuur et al., 2022).

Electrical resistivity tomography (ERT) has been widely used to map the ice-containing permafrost by its resistivity contrast compared to the surrounding unfrozen medium (Buckel et al., 2023). These measurements could be effective in monitoring permafrost conditions by mapping subsurface resistivity, which varies with temperature, water content, and other properties (Oldenborger & LeBlanc, 2018). However, traditional resistivity inversion techniques often struggle to accurately image permafrost in regions with complex lateral variations, fractures, and voids, underscoring the need for innovative solutions (Liu et al., 2024). For instance, in laterally discontinuous permafrost, wider frozen bodies cause the boundary at the base of the frozen region to become less distinct. So, the boundaries between unfrozen and frozen regions in ERT images should be interpreted with caution, particularly in ice-rich, laterally continuous permafrost where sensitivity at depth is low (Herring & Lewkowicz, 2018).

This research aims to bridge this gap by introducing a Machine Learning (ML)-based approach that leverages synthetic data to enhance the prediction and understanding of permafrost properties. The primary objective of this thesis is to develop and evaluate a multi-step ML framework to predict and analyze permafrost resistivity, temperature, and water content, as well as to explore the potential of Convolutional Neural Network (CNN)-based inversion for anomaly detection in permafrost regions.

The research questions for this thesis are as follows:

1. How effectively can ML models predict permafrost resistivity from apparent resistivity data?
    - This question explores the capability of various ML algorithms to estimate resistivity values accurately based on input features derived from apparent resistivity data.
2. What are the most suitable ML algorithms for predicting temperature and water content in permafrost regions?
    - This question aims to identify the optimal ML models and preprocessing techniques for accurately predicting temperature and water content, crucial parameters for characterizing permafrost conditions.
3. How well can a CNN model capture discontinuities in permafrost regions?
    - This question evaluates the ability of a CNN-based inversion technique to detect and map discontinuities and anomalies in permafrost regions, providing insights into the advantages and limitations of this pioneering approach in contrast to traditional methods.

This study focuses on synthetic data generation, model training, and evaluation using ML techniques. The research does not involve field data collection but relies on experimental data from the literature (Shan et al., 2015) to simulate realistic scenarios. The thesis explores predictive models for frozen soil, incorporating synthetic pseudo-sections that represent permafrost, thaw, and active layers.

This research contributes to both academic knowledge and practical applications in environmental monitoring and geophysical analysis. By improving the predictive modeling of permafrost properties using ERT, this work supports better decision-making for climate change mitigation, risk management for infrastructure, and environmental planning in cold regions. The insights gained can also inform future research on the use of synthetic data and ML in geoscience.

This thesis follows a structured approach as outlined below:

1. Developing a Model to Predict the Resistivity of Frozen Soils: A neural network model was trained using experimental data from the literature to predict the resistivity of frozen soil. Key input features for this model included temperature, dry density, and water content extracted from experiments of Shan et al., (2015). The resulting model served as a foundation for creating synthetic datasets for further analysis.
2. Simulating Synthetic 2D Resistivity Data: Synthetic pseudo-sections were generated to simulate realistic permafrost regions, capturing features such as discontinuities, thaw layers, and active layers. This step utilized forward modeling through the ResiPy library and resistivity inversion to produce comprehensive synthetic data.
3. Evaluating ML Algorithms for Predicting Resistivity from Apparent Resistivity Data: Various ML models, including Gradient Boosting, Random Forest, Support Vector Regressor, and Neural Networks, were trained and tested to predict permafrost resistivity. These models utilized generated apparent resistivity data and electrode configurations as input features.
4. Predicting Temperature and Water Content: ML models were employed to predict critical permafrost parameters, including temperature and water content. Features such as predicted resistivity and dry density were used to train and evaluate these models.
5. Creating a CNN Model for Inversion: A CNN model was developed and tested for resistivity inversion, aiming to capture and highlight discontinuities and anomalies in permafrost regions. This pioneering technique complements the earlier stages, providing detailed resistivity mapping and advancing the understanding of permafrost characteristics.

The thesis is structured into five main chapters, along with annexes to provide supplementary information:

- Chapter 2: background studies on the Application of Electrical Resistivity and ML Models for Monitoring Permafrost: discusses the background studies on the application of Electrical Resistivity (ER) and ML models for monitoring permafrost. The objective is to review and synthesize existing research on the use of ER and ML techniques in assessing permafrost conditions. The chapter covers the fundamentals of permafrost monitoring and its significance, provides an overview of Electrical Resistivity methods and their applications and reviews ML models applied in geophysical ER studies.
- Chapter 3: Prediction of Petrophysical Properties of Permafrost Using Electrical Resistivity: This chapter discusses the methodology for predicting the petrophysical properties of permafrost using electrical resistivity. It begins by emphasizing the importance of petrophysical properties in understanding permafrost dynamics and highlights the challenge of limited field data. The study

proposes generating synthetic 2D models based on established petrophysical characteristics, enabling the development of ML models for estimating permafrost properties.

- Chapter 4: ERT and CNN Inversion: Chapter 4 explores the use of ERT and CNN for imaging and analyzing permafrost regions. It discusses the principles of ERT, its applications in mapping permafrost layers, and the limitations of conventional inversion techniques. The chapter introduces a CNN-based inversion model as a novel method to enhance the resolution and accuracy of resistivity mapping, particularly in identifying sharp resistivity contrasts and discontinuities within permafrost zones.
- Chapter 5: Discussion and conclusion: concludes the thesis with a summary of key findings and their implications, while outlining recommendations for future research. It recaps the objectives and research questions, summarizes results and key insights from Chapters 3 and 4, and discusses the implications for environmental monitoring and geotechnical applications. The chapter also highlights limitations of the study and provides recommendations for future research, including model improvements and field applications.
- Annex 1: provides detailed information on the experimental data used as the foundation for synthetic model generation, specifically referencing the work of Shan et al. (2015). It includes critical data points such as resistivity values, water content, and temperature, all gathered from the mentioned literature. The annex also features tables that summarize these key data points, providing a clear and concise overview of the experimental setup and findings that underpin the synthetic modeling process.
- Annex 2: describes the ML models, evaluation metrics, and data normalization techniques utilized in this thesis. It provides an overview of models, including Random Forest and CNN, along with a justification for their selection based on the research objectives and data characteristics. It details the evaluation metrics employed, such as R^2, Mean Squared Error (MSE), Root Mean Squared Error (RMSE), and Mean Absolute Error (MAE), explaining their relevance in assessing model performance. Additionally, it discusses the normalization techniques applied, such as StandardScaler and MinMaxScaler, and their rationale for ensuring consistent scaling of features to enhance model accuracy and training stability. Figures and tables showcasing model architectures, configurations, and performance metrics are included to provide a comprehensive reference for the methodologies and results discussed in the thesis.

Chapter 2: background studies on the Application of Electrical Resistivity and ML Models for Monitoring Permafrost

2.1 Permafrost Definition and Description

The first mention of permanently frozen ground comes from Russia–Siberia from the Medieval Period but the first written mention dates back to 1598 and refers to its occurrence on Nova Ziemlya (Dobinski, 2011). The term "permanent frost" was originally used to describe ground that remains frozen indefinitely. However, this term was deemed scientifically inadequate, as it failed to account for the precise temporal and environmental conditions of frozen ground. To address this limitation, it was replaced by the term "perennially frozen" or "permafrost," which better encapsulates the concept of ground remaining frozen continuously over long periods. This refinement highlights the scientific effort to adopt terminology that more accurately represents the dynamic and time-dependent nature of geological phenomena (Dobinski, 2011).

In the glossary officially approved by the International Permafrost Association (IPA), definition number 390 defines permafrost as: "Ground (soil or rock, including ice and organic material) that remains at or below 0°C for at least two consecutive years" (van Everdingen, 1998). Permafrost is now defined in physical terms based on a temperature criterion, as the thermal state of the lithosphere and its contents, characterized by remaining at or below 0°C for at least two consecutive years. This definition carries two critical implications for understanding the nature of permafrost (Dobinski, 2011):

- Water Content in Permafrost: Permafrost may, but does not necessarily, contain water. When water is absent, the ground is referred to as *dry permafrost* (van Everdingen, 1998). This term describes frozen solid material that contains no water. However, this definition can be misleading, as ice itself is technically "dry." The term "wet" specifically refers to liquid water.
- States of Water in Permafrost: Water within permafrost can exist in frozen, unfrozen, or partially frozen states. The permafrost concept relies on 0°C as the threshold temperature, but water does not necessarily freeze at this point.

Permafrost forms when the extent of ground freezing during winter exceeds the extent of its thawing during summer. Initially, a thin layer of frozen or cryotic ground develops due to climatic cooling and persists through subsequent winters. If cooling continues, this layer thickens annually. Seasonal changes cause alternating penetration of cold and heat into the ground, resulting in wave-like thermal dynamics (Dobinski, 2011).

- During winter, as temperatures drop significantly below 0°C, the frozen ground layer extends from the surface to the depth of maximum winter freezing. This depth is influenced by the duration and severity of winter; prolonged exposure to the lowest temperatures results in deeper freezing. The penetration of cold is affected by factors such as the thickness of snow cover, the type of ground cover, and the physical properties of the ground, including heat capacity, thermal conductivity, and geothermal gradient.
- In summer, much of the frozen ground near the surface thaws, with some thawing occurring at the base of the frozen layer. The surface layer that thaws and refreezes seasonally is known as the active layer. The depth of thawing varies depending on summer warmth, with warmer summers causing deeper thawing, while cooler summers result in a shallower active layer. This dynamic interaction between freezing and thawing underscores the sensitivity of permafrost to seasonal and climatic variations.

Figure 3.1 illustrates the thermal structure of permafrost, highlighting the interactions between seasonally active layers, perennially frozen ground, and the geothermal gradient. The diagram identifies key elements such as the active layer, which undergoes seasonal freezing and thawing, the permafrost table, representing the upper boundary of permafrost, and the permafrost base, denoting its lower boundary.

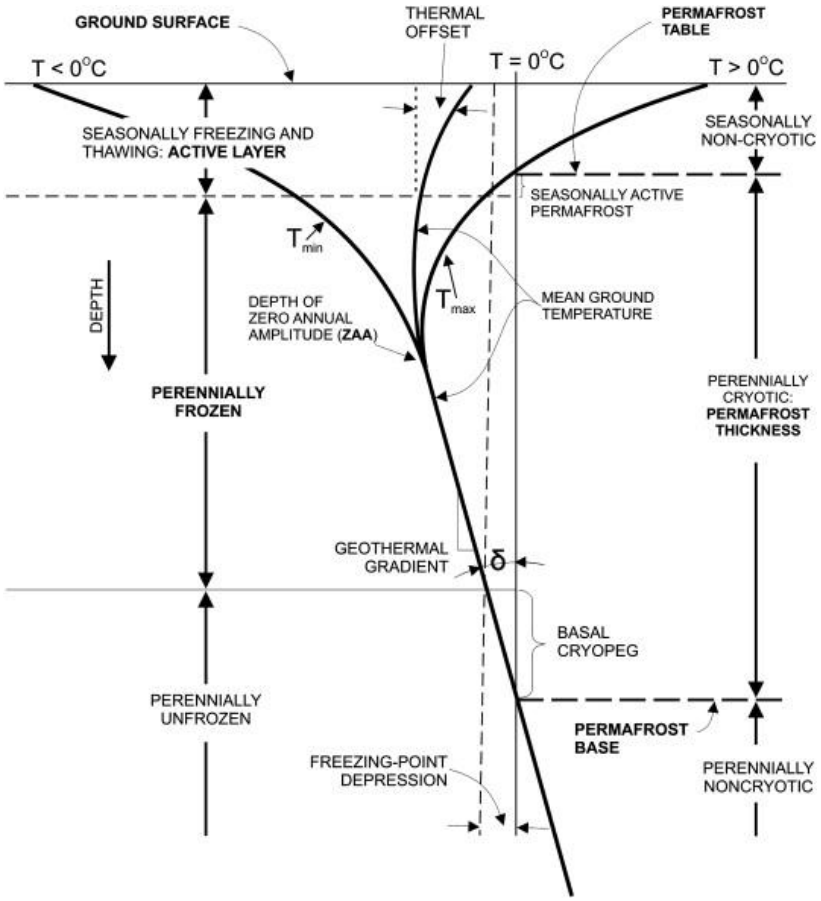

Figure 2.1 - Processes which may occur within permafrost body (shown as a process of degradation) (Dobinski, 2011).

2.1.1 Active Layer

An active layer is the ground or rock located above the permafrost table that undergoes seasonal freezing during the winter months. Although it is not part of the permafrost itself, the active layer plays a crucial role in the thermal dynamics of the permafrost system by transmitting heat (or cold) into the underlying lithosphere, thereby influencing the permafrost's stability and interaction with the atmosphere.

The thickness of the active layer is determined by several factors, with key influences being the temperature of the ground surface, the thermal properties of the soil and its cover, soil moisture levels, and the presence and thickness of snow cover (French, 2017). In mountainous environments, additional factors such as altitude, slope exposure, solar radiation, topographic conditions, and localized air circulation patterns also play a significant role in shaping permafrost occurrence and active layer dynamics. These factors can create microclimates that encourage the retention of cold in certain landforms (Delaloye and Lambiel, 2005).

2.1.2 Thawing

Thawing in permafrost occurs when the ground temperature rises above 0°C, leading to the phase change of ice into liquid water. This process has significant implications for both ecological and geotechnical systems. Thawing alters the physical and thermal properties of the soil, often resulting in subsidence and destabilization of infrastructure, particularly in areas where ice-rich permafrost dominates (Shur et al., 2005). Furthermore, thaw can lead to the release of previously trapped greenhouse gases, such as methane and carbon dioxide, from organic material stored in permafrost, contributing to global warming (Schuur et al., 2015).

The thawing process often begins in the active layer, which undergoes seasonal freezing and thawing. As warming intensifies, the thaw can extend deeper into the permafrost table, leading to the degradation of permafrost. This deepening of the thaw layer not only accelerates carbon release but also disrupts hydrological systems, affecting water flow and storage in cold-region ecosystems (Jorgenson et al., 2010).

The rate and extent of thawing depend on factors such as soil composition, ice content, vegetation cover, and climate conditions. Regions with higher organic content and ice-rich permafrost are particularly susceptible to rapid thawing, which exacerbates the impacts on both local and global scales (Romanovsky et al., 2010).

2.2 Overview of Permafrost Monitoring and Significance

Permafrost, an integral component of polar and subpolar regions, represents ground that remains frozen for at least two consecutive years. It plays a pivotal role in global ecological systems, influencing carbon cycling, hydrological processes, and ecosystem stability (Loranty et al., 2018). Permafrost regions act as vast carbon reservoirs, storing nearly twice as much carbon as the atmosphere, predominantly in the form of frozen organic matter (Schuur et al., 2015). As climate change accelerates, the thawing of permafrost poses significant risks, including the release of greenhouse gases such as carbon dioxide and methane, which further amplify global warming through positive feedback mechanisms (Biskaborn et al., 2019; Natali et al., 2021).

Monitoring permafrost is crucial for understanding these climate feedback processes and mitigating associated risks. Thawing permafrost can lead to widespread ground subsidence, known as thermokarst, which destabilizes natural landscapes and built infrastructure in cold regions. This has profound implications for communities and industries reliant on stable ground conditions, such as mining, oil extraction, and transportation (Shiklomanov et al., 2013; Romanovsky et al., 2010). Additionally, thawed permafrost alters local hydrology by changing soil water content, drainage patterns, and surface water availability, impacting ecosystems and water resources in these regions (Jorgenson et al., 2015; Walvoord & Kurylyk, 2016).

Effective monitoring of permafrost dynamics is challenging due to its subsurface nature. Unlike surface features such as glaciers, permafrost cannot be directly observed using traditional remote sensing techniques, making indirect methods like ERT and ground-penetrating radar (GPR) essential tools for its assessment (Kneisel et al., 2008). ERT, in particular, has proven effective for delineating permafrost boundaries and detecting thawing zones by mapping the electrical resistivity variations associated with changes in soil temperature and water content (Kneisel et al., 2014; Hilbich et al., 2008).

As climate-induced permafrost degradation progresses, the need for precise and efficient monitoring techniques has become increasingly evident. Advanced methods, such as combining geophysical techniques with ML models, offer the potential to enhance our understanding of permafrost stability and long-term dynamics. These approaches enable the analysis of large, complex datasets, improving

prediction accuracy and identifying critical changes in permafrost regions (Ran et al., 2022; McKenzie et al., 2021).

2.3 ERT for Permafrost Assessment and its limitations

ERT has become an important geophysical tool for subsurface exploration and environmental monitoring. Its non-invasive methodology and capability to delineate resistivity contrasts make it particularly effective for mapping permafrost, a key component of cold-region ecosystems. By measuring electrical resistivity, ERT provides detailed images of subsurface conditions, enabling researchers to identify permafrost boundaries, detect seasonal changes, and monitor degradation caused by climate warming (Herring et al., 2019; Kneisel et al., 2008).

ERT has been successfully utilized to track the distribution and seasonal dynamics of permafrost across diverse environments, from Arctic tundra to alpine permafrost regions. For instance, ERT has enabled the identification of thawing fronts in active layers and the vertical extent of frozen soils during warming events (Hilbich et al., 2008; Krautblatter et al., 2010). These studies underscore ERT's value in capturing the transition between frozen and thawed soil, providing critical insights into permafrost behavior under changing climatic conditions.

A significant advantage of ERT lies in its ability to highlight resistivity contrasts, which are closely associated with temperature, water content, and soil composition. Frozen soils exhibit high resistivity due to the presence of ice, while thawed soils show much lower resistivity, influenced by liquid water content and salinity (Kneisel et al., 2014). These properties make ERT particularly suited for monitoring permafrost in regions where ground conditions vary significantly over time.

However, ERT also faces limitations. Conventional inversion techniques often struggle with imaging in areas with significant lateral variations or complex subsurface structures. These challenges can result in smoothed resistivity maps that fail to capture sharp transitions or discontinuities, such as fractures, voids, or rapid changes in soil properties (Liu et al., 2024; Auken et al., 2015). Additionally, noise from environmental factors or instrumentation can further complicate data interpretation, reducing the accuracy of the inversion results (Schmidt et al., 2020).

To address these challenges, recent advancements in inversion algorithms and data processing techniques have been developed. Sophisticated approaches, such as regularized inversion, joint inversion with complementary datasets, and ML-based interpretation, have demonstrated the potential to enhance the resolution and reliability of ERT imaging (Zhong et al., 2020; Liu et al., 2020). These innovations improve the ability of ERT to resolve fine-scale features, such as discontinuities in lateral layers or localized anomaly zones, which are critical for understanding permafrost dynamics and their implications.

Moreover, integrating ERT with other geophysical methods, such as seismic refraction or ground-penetrating radar (GPR), has shown promise in overcoming some of these limitations. Multi-method approaches leverage the strengths of each technique, providing a more comprehensive understanding of subsurface conditions and reducing ambiguities in interpretation (Buckel et al., 2021; Hauck, 2013).

2.4 ML Applications in Permafrost Studies and ERT

The integration of ML techniques into permafrost research and ERT has significantly advanced the field by offering tools to analyze complex geophysical data and improve predictive accuracy (Liu et al., 2024). ML models such as neural networks, random forests, and support vector machines have been

instrumental in identifying and mapping permafrost regions, particularly in areas with heterogeneous subsurface structures where traditional methods face limitations (Baral & Haq, 2020).

ML algorithms have been employed to extract meaningful patterns from extensive datasets, enabling the prediction of permafrost extent and stability. For example, studies have demonstrated the ability of ensemble learning methods, such as random forests and gradient boosting, to enhance the interpretation of resistivity data by reducing noise and improving the detection of discontinuities in frozen ground layers (Baral & Haq, 2020). Neural networks, on the other hand, excel in capturing non-linear relationships between environmental variables, offering high-resolution mapping capabilities for permafrost regions (Liu et al., 2022).

ERT, a widely used geophysical method, benefits greatly from ML integration. ML models trained on ERT data can predict subsurface resistivity profiles more effectively than traditional inversion methods, especially in regions with significant lateral variations or complex geological structures (Zhuo et al., 2023). These models improve the resolution of resistivity maps, making them particularly valuable for studying seasonal freeze-thaw cycles and long-term permafrost degradation (Melo & Li, 2021; Xixi et al., 2023)

Despite its promise, the application of ML in permafrost studies has challenges, including the need for large, diverse datasets and the risk of model overfitting. Future research should focus on integrating multi-source datasets, optimizing model architectures, and exploring unsupervised learning techniques to further advance the field. Additionally, combining ML with improved ERT inversion techniques could provide a more comprehensive understanding of permafrost dynamics (Liu et al., 2024).

Chapter 3: Prediction of petrophysical properties of permafrost using electrical resistivity

Summary: Chapter 3 focuses on predicting the petrophysical properties of permafrost using electrical resistivity. It begins by highlighting the importance of these properties in understanding permafrost dynamics. Due to the scarcity of high-resolution field data, the study proposes generating synthetic 2D models based on established petrophysical characteristics. This approach enables the development of ML models to estimate properties of permafrost body. Figure 3.1 represents the overall flowchart of the methodology used in this chapter.

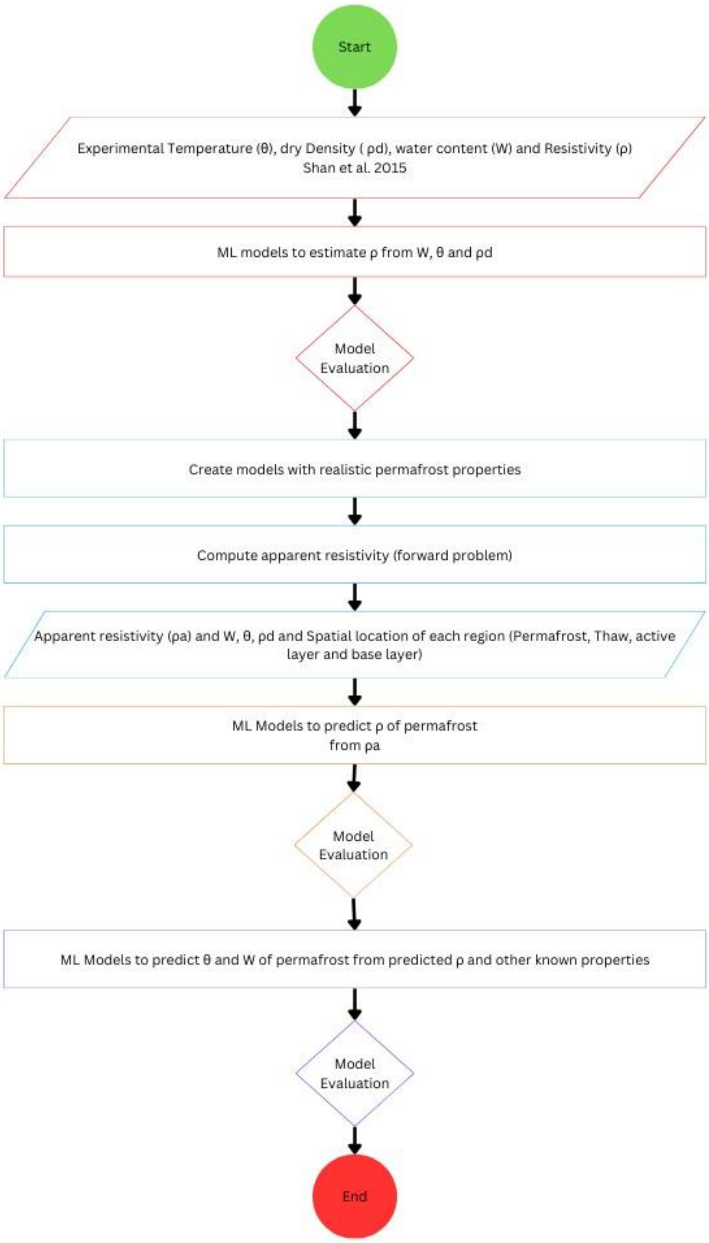

Figure 3.1 - The workflow of predicting petrophysical properties of permafrost body

3.1 Petrophysical Properties of Permafrost

Petrophysical properties encompass the physical and chemical characteristics of soil and rock that influence their interactions with thermal, hydraulic, and mechanical processes. In permafrost regions, these properties are essential for understanding subsurface dynamics, stability, and responses to environmental changes. Key properties include thermal conductivity, electrical resistivity, permeability, porosity, mineral composition, and temperature, all of which contribute to the behavior of frozen ground (Williams & Smith, 1989).

A major challenge in permafrost research is the lack of comprehensive and high-resolution field data on its petrophysical properties. Collecting such data across vast, remote, and climatically extreme regions is both logistically challenging and costly. Additionally, the significant spatial and temporal variability of permafrost makes it difficult to establish detailed subsurface profiles that account for local heterogeneities, such as fractures, voids, and mixed soil compositions.

This scarcity of reliable datasets limits the ability to develop predictive models for permafrost dynamics and hinders the effectiveness of geophysical monitoring techniques.

To address the data gap, this study emphasizes the generation of synthetic 2D models that represent various permafrost conditions. These models are designed based on established petrophysical characteristics for typical sedimented permafrost regions, allowing for the simulation of realistic subsurface scenarios.

3.2 Selecting Petrophysical Properties

A critical question in this study was determining how to model or develop an equation capable of predicting the resistivity of frozen soils based on their petrophysical properties. Shan et al. (2015) provided significant insights into this challenge through their seminal research on the electrical resistivity of frozen soils. The study emphasized the distinct differences in resistivity between frozen and unfrozen soils, primarily driven by phase changes in pore water during freezing.

Shan et al.'s model incorporates various soil properties, including unfrozen water content, temperature, initial water content, and dry density, to establish a comprehensive framework for resistivity prediction. This integrative approach builds upon earlier foundational studies, such as Archie (1942) and Waxman and Smits (1968), which introduced methodologies for understanding soil resistivity under diverse conditions. These models laid the groundwork for predicting electrical resistivity, providing a theoretical basis for understanding how soil properties interact in frozen environments.

The resistivity model proposed by Shan et al. (2015) is mathematically expressed as follows:

$$\rho = \left[A \times \frac{a\theta^{-b}}{W} + \rho_d \left(B \times \frac{a\theta^{-b}}{W} + C \right) + D \right]^{-1} \qquad \textit{(Equation 3.1)}$$

where A, B, C, and D are coefficients linked to the structural characteristics and electrical resistivity of the soil components; W is the water content; $a\theta^{-b}$ represents the unfrozen water content; θ is the absolute temperature; and ρ_d is the dry density of the soil.

They Performed Experiments on silty clay samples to measure electrical resistivity under different conditions of temperature, water content, and dry density. The experimental results supported the model's predictions, aligning with theoretical expectations.

Given the challenges and time-intensive process of determining the experimental coefficients in the model proposed by Shan et al. (2015), this study sought to develop predictive ML models to estimate the resistivity of frozen soil. Experimental data from Shan et al. were digitized from their published figures (figure 3.2) using the online tool Plot Digitizer. This method enabled the extraction of key data points, including resistivity, temperature, dry density, and water content, which were then utilized as input features for the ML models.

The resulting dataset, consisting of 156 data points, is detailed in Annex 1 and was employed as input features for training and testing the ML models. This approach provided a scalable and efficient alternative for resistivity prediction while validating the potential of ML in modeling complex soil behavior.

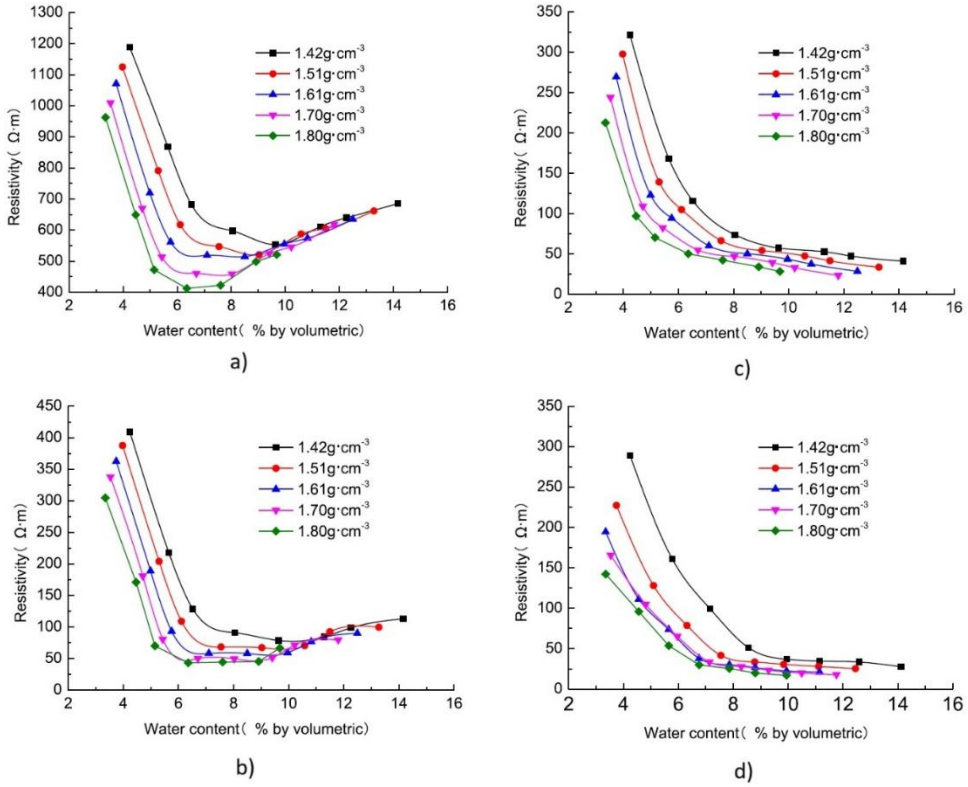

Figure 3.2 - Curves of the relationship between the electrical resistivity of the frozen soil and water content under different dry density conditions, a at t = -17°c, b at t = -3°c, c at t = 3°c and d at t = 17°c (reproduced from Shan et al. 2015)

3.3 Predicting Resistivity of frozen soil based on selected properties

The extracted dataset was utilized to train and test several ML models, including Neural Networks, Random Forest, Gradient Boosting, Support Vector Regressor, and k-Nearest Neighbors. The performance of these models was evaluated to determine how well their predictions aligned with the results of Shan et al. (2015). In Annex 2, a comprehensive overview of the ML algorithms utilized in this thesis is presented, offering a general description of each algorithm's functionality, strengths, and applicability.

Below, each model is described in detail.

- The Neural Network model was designed as a deep learning framework to capture complex, nonlinear relationships within the data. It was structured with four dense layers to progressively learn features from the input data. The network had 250 neurons in the first layer, 150 in the second, and 40 in the third, all employing the Rectified Linear Unit (ReLU) activation function to

introduce nonlinearity and enable the model to learn intricate patterns. The output layer consisted of a single neuron with a linear activation function, suitable for regression tasks, producing continuous resistivity predictions. To mitigate overfitting, dropout layers were added after each dense layer, randomly deactivating 20% of neurons during training. The network was optimized using the Adam optimizer, a popular choice for its adaptive learning rate capabilities, and trained to minimize the MSE loss function, ensuring that predictions closely matched actual resistivity values.

- The Random Forest algorithm, an ensemble method, was employed for its robustness and ability to handle nonlinear relationships. This model constructs multiple decision trees, each trained on different subsets of the data, and averages their outputs for final predictions. This ensemble approach reduces overfitting and enhances generalization. A grid search optimization identified the best parameters for the model, including an unlimited maximum depth for trees, a minimum sample split of 2, and 100 estimators. These parameters enabled the Random Forest model to balance predictive accuracy with computational efficiency.
- The Support Vector Regressor (SVR) was applied to fit a hyperplane that best represents the data while maintaining a specified margin of tolerance. SVR is particularly effective for datasets with fewer samples, as it minimizes overfitting by maximizing the margin between the hyperplane and the nearest data points. For this study, the optimal parameters were a regularization parameter (C) of 10, a linear kernel to simplify the relationship between inputs and outputs, and the 'scale' gamma setting to adapt to feature variability. These settings allowed the SVR to provide stable predictions while accommodating the complexities of the dataset.
- Gradient Boosting was used as a sequential ensemble method where trees are built iteratively. Each subsequent tree focuses on correcting the errors made by the previous ones. This iterative refinement minimizes a loss function, leading to progressively better predictions. The best parameters, identified through grid search, included a learning rate of 0.2 to balance convergence speed and precision, a maximum tree depth of 3 to prevent overfitting, and 200 estimators to ensure sufficient model complexity. Gradient Boosting is well-suited for this task due to its ability to model complex relationships with high accuracy.
- Finally, the k-Nearest Neighbors (k-NN) algorithm was employed as a non-parametric method. It predicts the output for a given data point by averaging the outputs of its nearest neighbors in the feature space. The proximity of neighbors is determined using a distance metric, ensuring that predictions reflect local data patterns. The best parameters included using 3 neighbors and assigning distance-based weights to prioritize closer neighbors in the predictions. This approach made k-NN particularly effective in capturing localized patterns in the resistivity data.

Together, these models provided a diverse set of approaches for predicting frozen soil resistivity, with each leveraging its unique strengths to address the challenges of the dataset.

3.3.1 Data Preprocessing

To ensure consistency and enhance the performance of ML models, a careful normalization strategy was implemented for the input data. Different normalization techniques were chosen based on the characteristics of each feature and their expected impact on model performance:

- Temperature and Density (MinMaxScaler): The MinMaxScaler was used for scaling temperature and dry density features, as these variables have a finite and well-defined range. MinMaxScaler normalizes data by rescaling each feature to lie within a specified range, typically [0, 1]. This method preserves the relationships among data points without distorting their distribution, which is crucial for features like temperature and density that directly influence the resistivity of permafrost.
- Water Content (StandardScaler): The StandardScaler was applied to water content because this feature has a more variable distribution and may include values that deviate significantly from the

mean. StandardScaler transforms data to have a mean of 0 and a standard deviation of 1, making it ideal for features that do not have strict bounds or follow a normal-like distribution.

3.3.2 Model Evaluation and Comparison

Summary of the results and comparison between different ML algorithms performances represented below:

Table 3.1 – results and comparison between models' performance for predicting resistivity (ρ) of frozen soil

Model	MSE	MAE	MAPE	R^2 score
Neural Network	1320.31	26.22	18.68	0.975
Random Forest	1435.29	27.15	17.65	0.973
Gradient Boosting	1719.55	27.15	18.26	0.967
Support Vector Regressor	21529.49	124.310	116.3	0.597
K-Nearest Neighbors	1729.68	30.49	23.32	0.967

All models, except the Support Vector Regressor, demonstrated strong performance. The neural network achieved the highest R^2 score (0.975) and the lowest MSE, MAE, and MAPE, indicating that it was the most accurate in predicting resistivity. The Random Forest model followed closely, with a comparable R^2 score of 0.973 and similar MAE.

The low MSE and high R^2 score indicate that the neural network captured 97.5% of the variance in the target variable, achieving high accuracy in resistivity predictions. Additionally, the low MAE and MAPE values confirm that the neural network model's predictions closely approximate actual resistivity values, demonstrating minimal average error.

In contrast, the SVR exhibited significantly higher error rates and a much lower R^2 score of 0.597, indicating a poor fit with the data. This lower performance suggests that SVR is less suitable for resistivity prediction in this context compared to the neural network and other tree-based models.

3.3.3 fit the proposed model prediction on experimental data

This section evaluates the proposed Neural Network (NN) model by comparing its predictions with experimental data from Shan et al. (2015). Shan et al.'s model, grounded in theoretical principles, incorporates key soil properties such as unfrozen water content, temperature, initial water content, and dry density to estimate resistivity. While their model (Equation 3.1) is highly accurate in describing frozen soil resistivity, it requires the determination of experimental coefficients, which is labour-intensive and time-consuming.

In contrast, the model presented in this study offers a streamlined approach to resistivity prediction, bypassing the need for coefficient calibration. Figures 3.3 to 3.6 illustrate this comparison for temperatures of -17°C, -3°C, 3°C, and 17°C, respectively. Each figure includes plots for varying dry densities (ρ = 1.8, 1.7, 1.61, 1.51, and 1.42 g/cm^3), labeled as a to e, and highlights the relationship between resistivity and water content.

Key Observations:

- Actual Resistivity (Blue Line): The experimental data from Shan et al. (2015) show that resistivity generally decreases with increasing water content up to a threshold, beyond which it stabilizes or slightly increases. This reflects the intricate interplay between water content and resistivity in frozen soils.
- Predicted Resistivity (Red Dashed Line): The NN model effectively captures the main resistivity trends observed in the experimental data. Although minor deviations exist, particularly at lower water content levels, the predicted values align closely with the experimental results.

The figures underscore the ML model's ability to replicate resistivity patterns across different soil conditions and temperatures, particularly under sub-zero conditions. This suggests that the ML approach is a viable and efficient alternative to traditional models, offering comparable accuracy without the need for exhaustive parameter calibration.

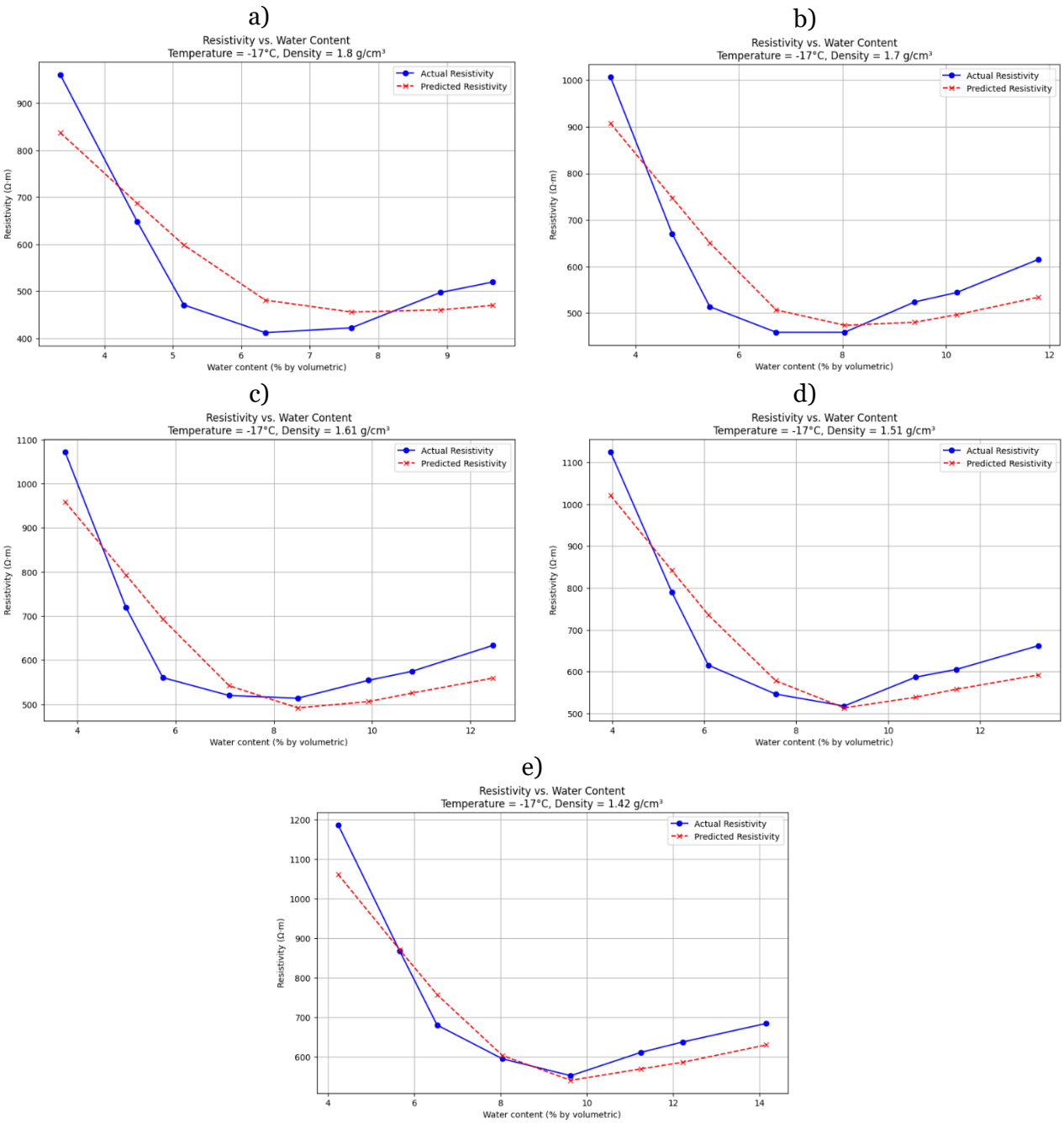

Figure 3.3 - Comparison between experimental data and the proposed model for different dry densities at a constant temperature = -17°c, a) for ρ = 1.8 g/cm³, b) for ρ = 1.7 g/cm³, c) for ρ = 1.61 g/cm³, d) for ρ = 1.51 g/cm³ and e) for ρ = 1.42 g/cm³

Figures 3.3 compare the resistivity predicted by the NN model (red dashed line) with experimental data from Shan et al. (2015) (blue line) across varying water content levels at -17°C for different dry densities. The model captures the general trend of decreasing resistivity with increasing water content, reaching a minimum before slightly rising at higher levels. While the predicted values align well with experimental data at moderate and high water content, some deviations occur at lower water content values, particularly for higher dry densities. Overall, the model demonstrates a strong ability to approximate resistivity trends, with minor refinements needed for enhanced precision in specific regions.

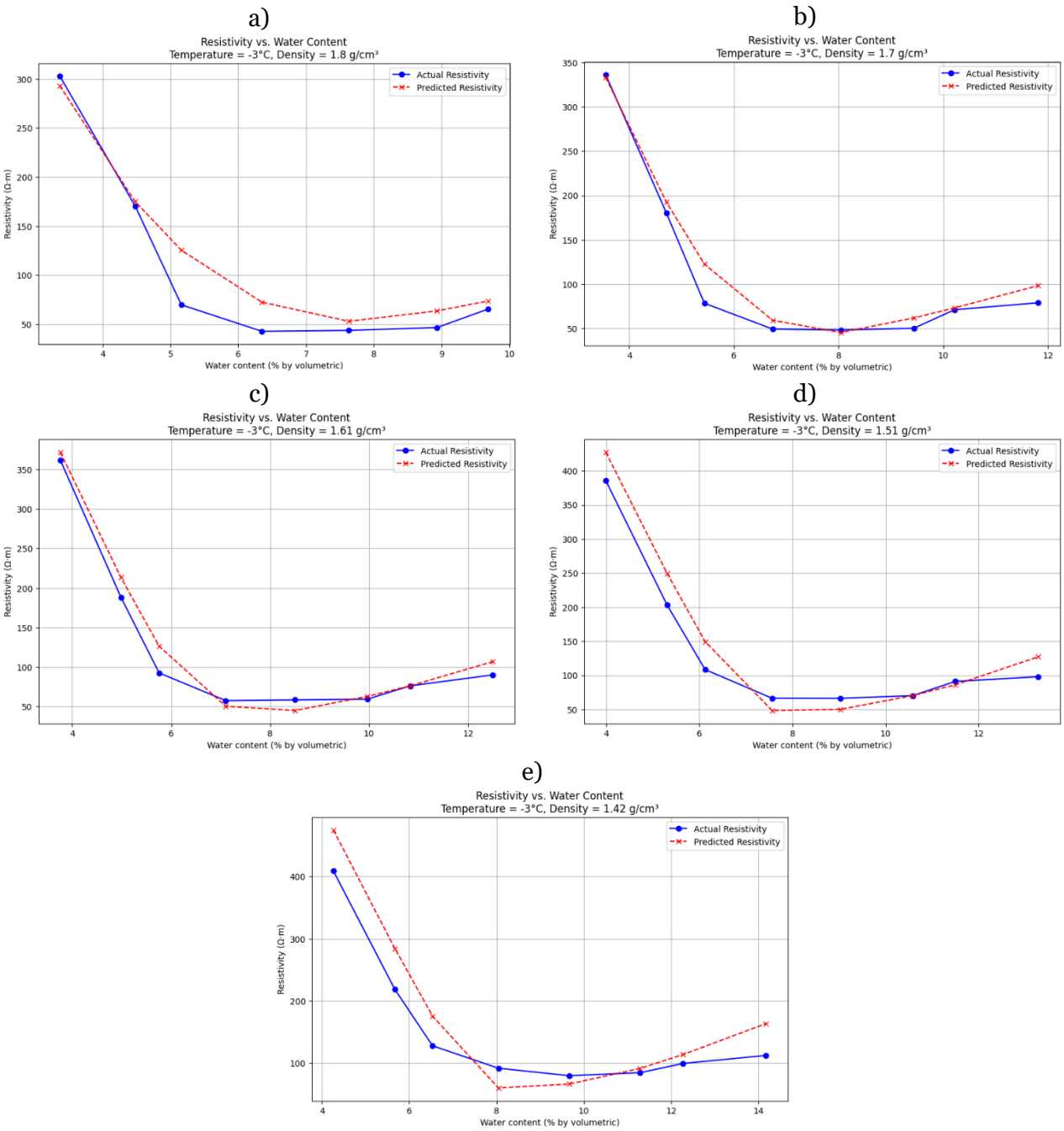

Figure 3.4 - Comparison between experimental data and the proposed model for different dry densities at a constant temperature = -3°c, a) for ρ = 1.8 g/cm³, b) for ρ = 1.7 g/cm³, c) for ρ = 1.61 g/cm³, d) for ρ = 1.51 g/cm³ and e) for ρ = 1.42 g/cm³

In comparison to the resistivity trends at -17°C, the figures for -3°C show lower overall resistivity values due to the higher temperatures, which reduce ice content and increase water mobility within the soil. While the predicted resistivity (red dashed lines) still aligns closely with the experimental data (blue solid lines), the deviation is more pronounced at lower water contents and lighter densities, such as 1.42 g/cm³. This highlights the challenge of accurately modeling resistivity at transitional temperatures where ice content diminishes. Unlike the -17°C case, the resistivity minima at -3°C occur at slightly higher water content levels, reflecting the temperature's impact on phase behavior and soil conductivity. These observations underscore the sensitivity of resistivity predictions to both temperature and soil density.

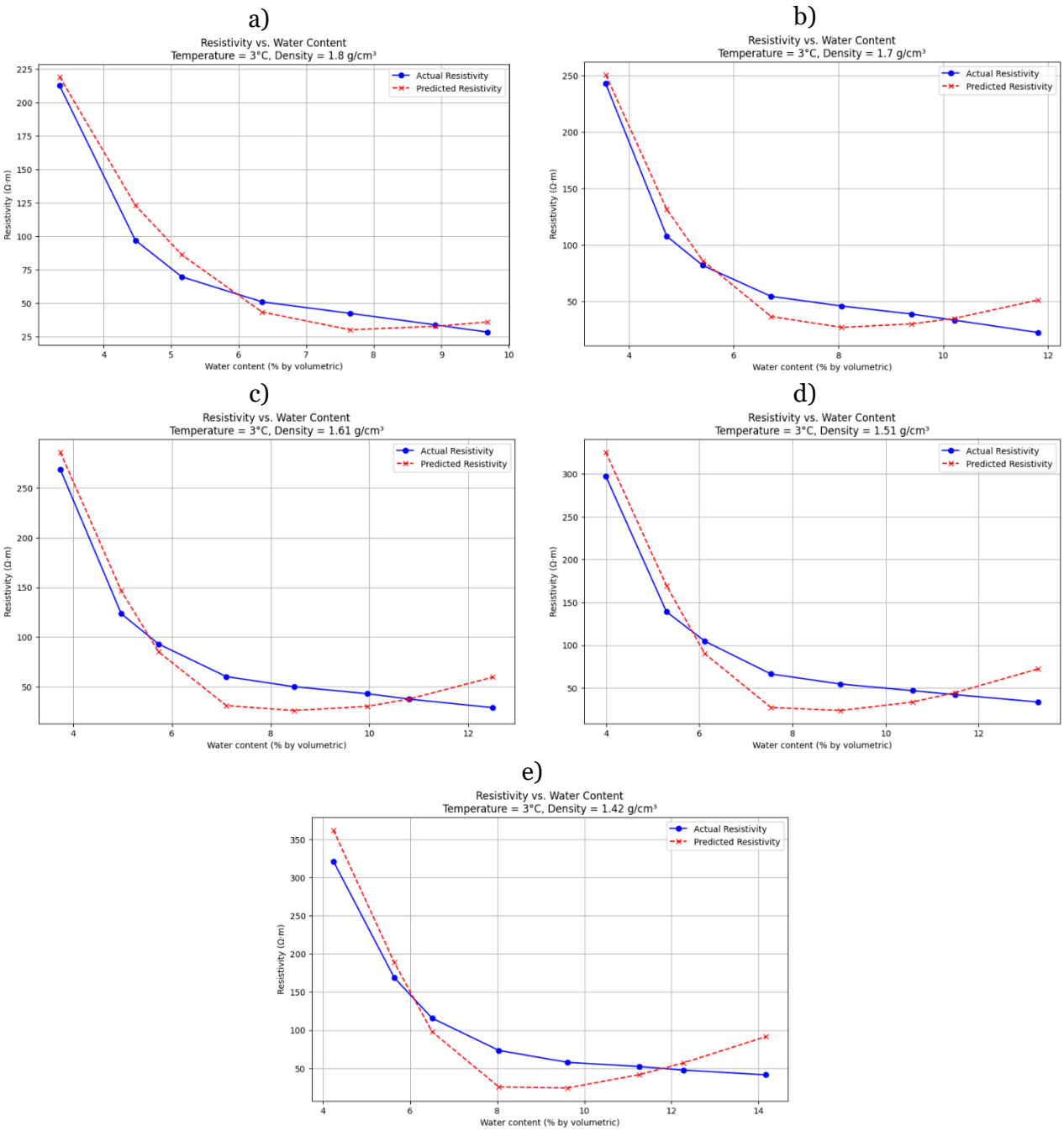

Figure 3.5 - Comparison between experimental data and the proposed model for different dry densities at a constant temperature = 3°c, a) for ρ = 1.8 g/cm³, b) for ρ = 1.7 g/cm³, c) for ρ = 1.61 g/cm³, d) for ρ = 1.51 g/cm³ and e) for ρ = 1.42 g/cm³

Figure 3.5 showcases the resistivity predictions at 3°C, a temperature above freezing, compared to the two previous figures at sub-zero temperatures (-17°C and -3°C). In this warmer phase, the resistivity exhibits a more pronounced decline with increasing water content, reflecting the dominant influence of liquid water on resistivity. Unlike the previous figures where phase change (ice to liquid) played a key role, here the resistivity variations are primarily dictated by the liquid water's conductivity. The predicted values align closely with experimental data at lower water content levels, but as water content increases, the model slightly overestimates resistivity in certain cases, especially at lower densities. This behavior suggests that at temperatures above freezing, the model's ability to capture resistivity influenced by purely liquid-phase water could still be refined.

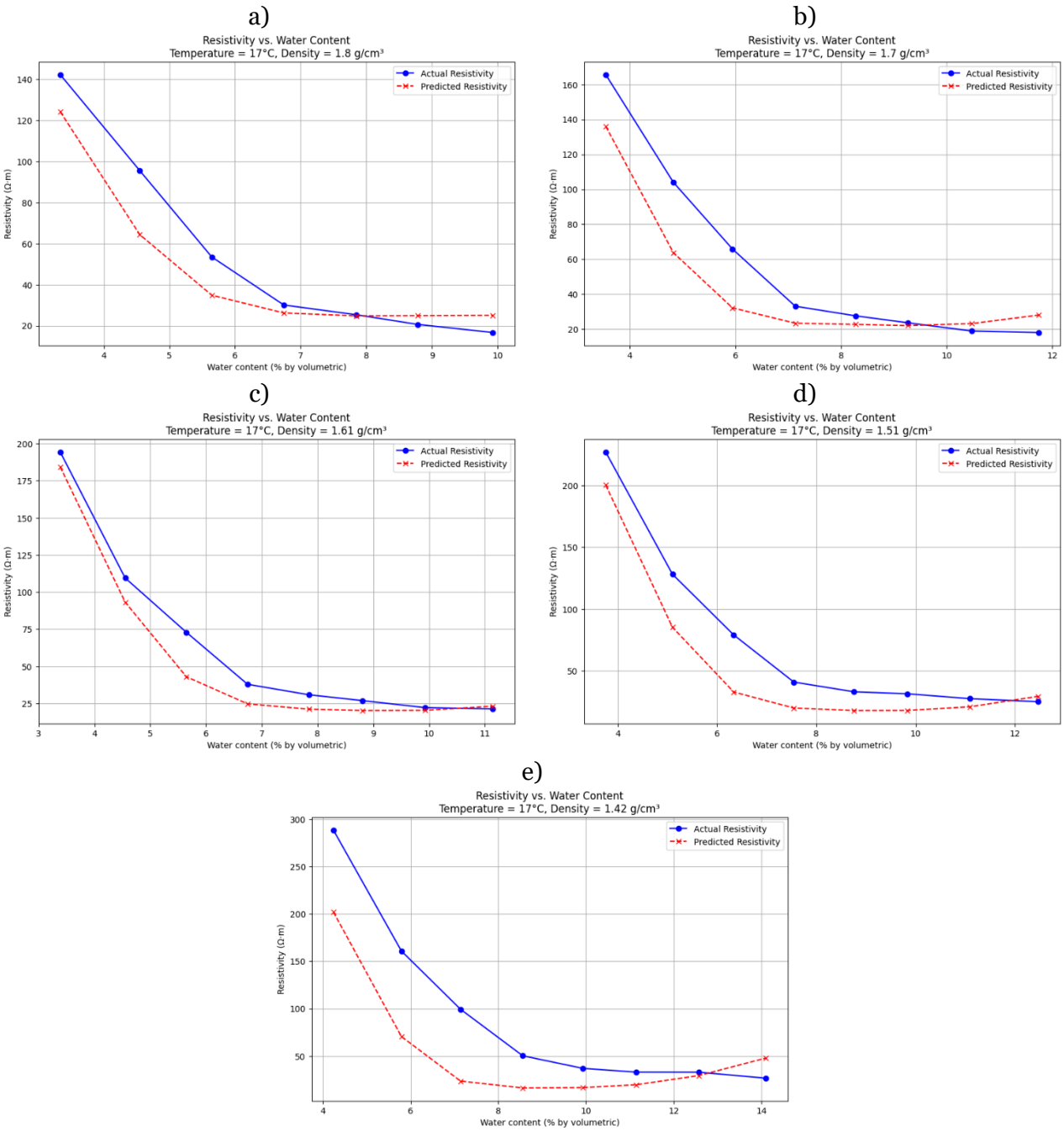

Figure 3.6 - Comparison between experimental data and the proposed model for different dry densities at a constant temperature = 17°c, a) for ρ = 1.8 g/cm³, b) for ρ = 1.7 g/cm³, c) for ρ = 1.61 g/cm³, d) for ρ = 1.51 g/cm³ and e) for ρ = 1.42 g/cm³

Figure 3.6 illustrates the resistivity trends of permafrost at a temperature of 17°C across different dry densities (1.8, 1.7, 1.61, 1.51, and 1.42 g/cm³) as a function of water content. Compared to the colder temperatures in the previous figures, the resistivity values are significantly lower. The predicted resistivity (red dashed lines) follows the general decreasing trend with increasing water content seen in the actual data (blue lines), but with a noticeable deviation at lower densities. This comparison highlights how the model adapts to temperature changes, capturing the reduced resistivity characteristic of higher temperatures, albeit with some limitations in accurately representing low-density conditions.

3.3.4 Training and Validation Loss

Figure 3.7 shows the training and validation loss curves over the 160 training epochs for the NN model. The loss decreases steadily for both training and validation sets, indicating effective learning and convergence. By the end of training, the model achieves stable, low loss values for both sets, suggesting minimal overfitting and good generalization capability.

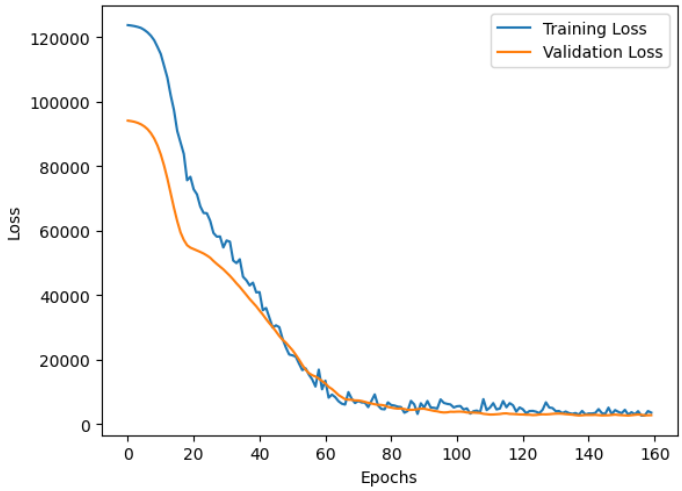

Figure 3.7 - Training and validation loss curves over the 160 training epochs

3.3.5 Evaluation of Model Predictions: Actual vs. Predicted Resistivity

This section presents a comparison between the actual and predicted resistivity values for each model, illustrating the accuracy and reliability of each approach in predicting permafrost resistivity. The figure 3.8 provide a visual assessment of how closely each model's predictions align with the actual values, with the red line representing the perfect prediction line (where predicted values would exactly match actual values).

1. Neural Network (NN): The neural network model shows a strong alignment with the perfect prediction line, with most points clustering closely along it. This indicates that the neural network accurately captured the resistivity values, achieving high predictive performance with a minimal average error. The high R^2 score (0.975) and low error metrics (MSE, MAE, MAPE) further confirm its effectiveness.

2. Random Forest: Similar to the neural network, the Random Forest model's predictions closely follow the perfect prediction line, especially at lower resistivity values. Although there is a slight deviation at higher values, the Random Forest model achieved a comparable R^2 score (0.973), making it a strong alternative for resistivity prediction.

3. SVR: The SVR model demonstrates significant deviation from the perfect prediction line, with scattered points indicating large prediction errors, especially for higher resistivity values. This is reflected in its low R^2 score (0.597) and high error metrics, suggesting that SVR is not well-suited for this prediction task.

4. Gradient Boosting: The Gradient Boosting model generally aligns with the perfect prediction line, although there is some deviation at higher resistivity values. This model achieved a reasonable R^2 score (0.967) and moderate error metrics, indicating it can effectively predict resistivity, though with slightly less precision compared to the neural network and Random Forest.

5. k-NN: The k-NN model's predictions align with the perfect prediction line at lower resistivity values, with some spread observed at higher values. Its R^2 score of 0.967 suggests that it performs reasonably well, though not as accurately as the neural network for this task.

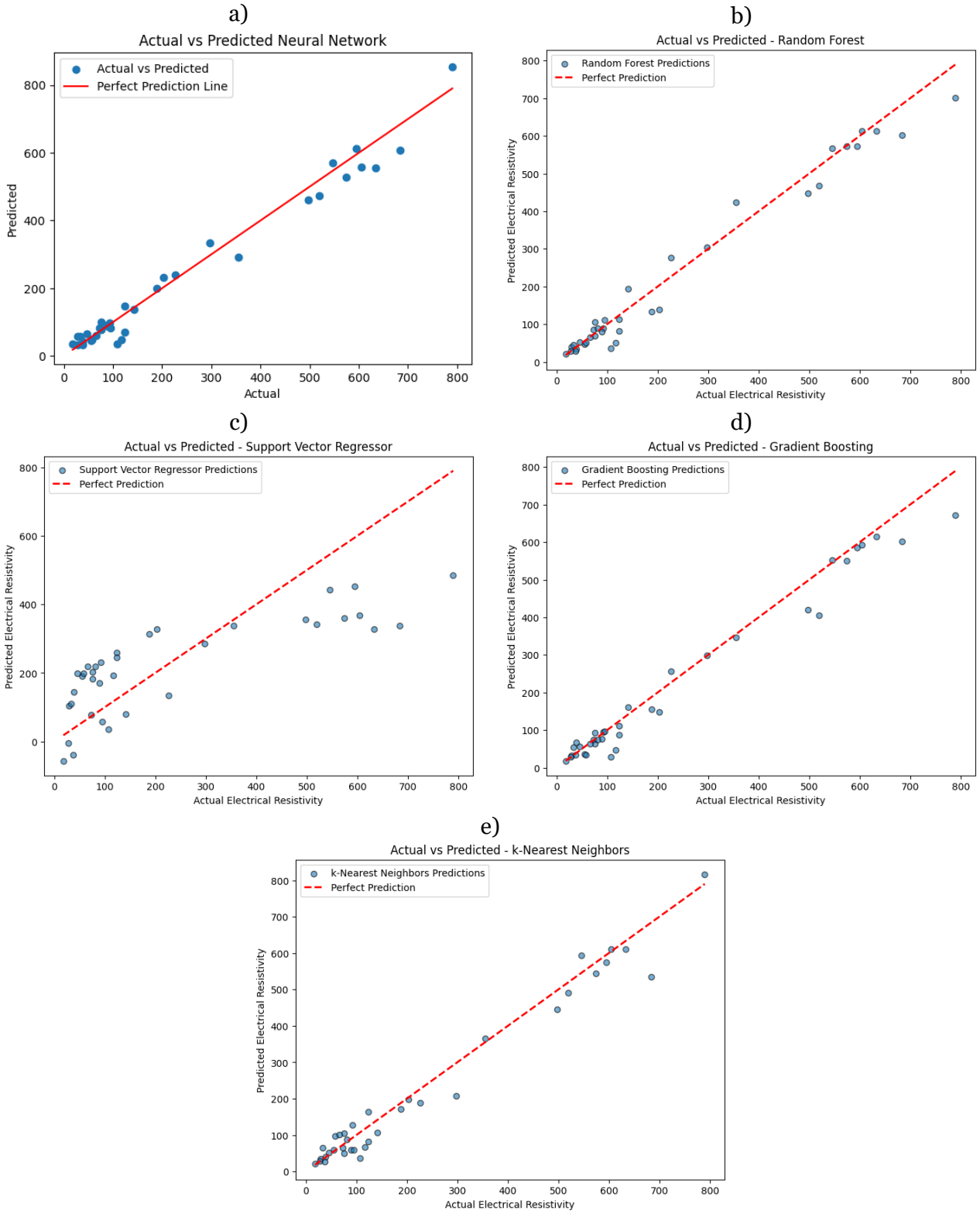

Figure 3.8 - Comparison between the actual and predicted resistivity values for each model, a) for NN, b) for Random Forest, c) for SVR, d) for gradient boosting and e) for k-NN.

3.4 Generating dataset of representative 2D models of permafrost regions

In a ML-based approach for monitoring permafrost regions, the first critical step is to establish a dataset that simulates a wide range of conditions and configurations of frozen and thawed soils. The primary objective is to represent sedimented permafrost regions and capture their discontinuities in a realistic manner. By assigning reliable and scientifically validated properties which is selected earlier to each region, numerous models were generated to emulate a variety of scenarios, allowing for robust training and evaluation of predictive algorithms.

Each model consisted of four primary layers, designed to reflect key characteristics of permafrost environments:

- Active Layer: This surface layer undergoes seasonal freeze-thaw cycles, significantly influencing the resistivity profile. The active layer was modeled with a thickness ranging from 1.5 to 2 meters, higher temperatures, and relatively lower resistivity compared to the underlying frozen layers. This layer was crucial in simulating dynamic changes in subsurface resistivity due to environmental factors such as temperature and moisture variations.
- Thaw Layer: Located below the active layer, the thaw layer represented regions where ice has melted. It was characterized by lower resistivity than the permafrost layer, temperatures ranging between -4°C and 1°C, and densities similar to the permafrost. This layer also featured higher water content, highlighting transitional zones that are vital for understanding permafrost degradation.
- Permafrost Layer: The permafrost layer simulated stable, frozen ground typical of permafrost regions. It was characterized by high resistivity, low temperatures (ranging from -15°C to -4°C), moderate density (1.2 to 1.8 g/cm^3), and variable water content (0.10 to 0.40). This layer played a central role in monitoring permafrost stability and detecting potential degradation.
- Base Layer: This foundational layer represented stable, fully thawed soil beneath the permafrost. It featured relatively lower resistivity varied from 200 to 400 ohm-m, providing a stable reference for deeper, unfrozen ground.

To enhance realism, discontinuities in permafrost and thaw regions were introduced through the random assignment of ellipsoidal shapes. By superimposing multiple ellipsoids, complex geometries resembling natural subsurface structures were generated. This approach allowed for the creation of realistic models that captured the spatial heterogeneity and intricate patterns typical of permafrost environments. These models serve as essential tools for training ML algorithms to identify and predict permafrost conditions and their discontinuities under diverse scenarios.

A total of 500 representative models were generated to simulate diverse conditions and configurations of permafrost regions with varying degrees of discontinuity. Figure 3.9 provides examples of these models, where distinct regions are color-coded for clarity:

- Orange Areas: Represent the active layer, simulating seasonal freeze-thaw cycles.
- Light Purple Areas: Correspond to the thaw layer, illustrating transitional zones with melted ice and higher water content.
- Light Gray Areas: Denote permafrost regions, characterized by high resistivity and stable frozen conditions.

The generated models clearly showcase exaggerated discontinuities within the permafrost regions, highlighting their potential to simulate complex and realistic subsurface structures. These models provide a valuable foundation for training ML algorithms to detect and predict permafrost characteristics and discontinuities under varied scenarios.

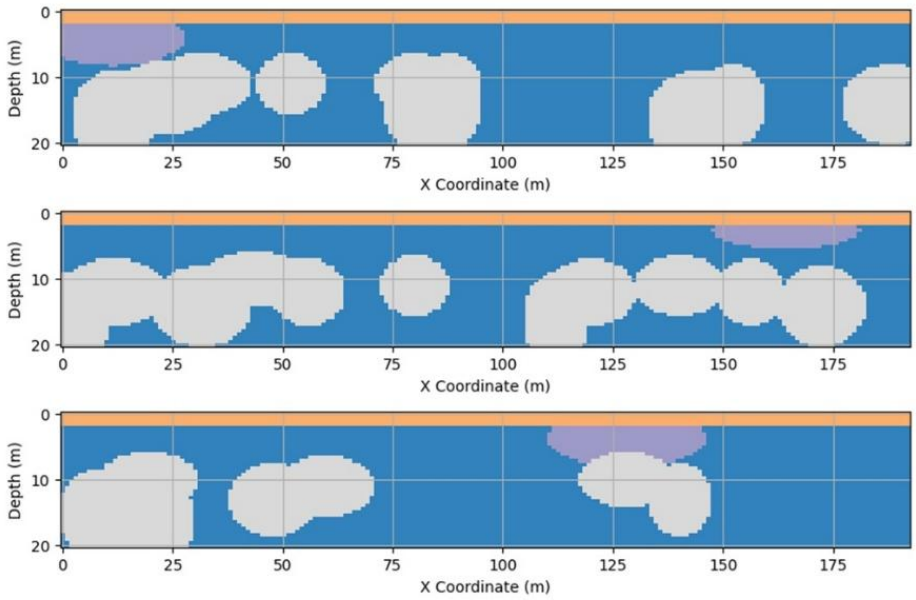

Figure 3.9 – Some examples of generated representative models

3.4.1 Assigning Resistivity of Each Region Using the Best Performing ML Model

Following a comprehensive evaluation of multiple ML models, the best-performing model was selected based on its accuracy and reliability in predicting resistivity. This model was then employed to assign resistivity values to each region in the generated synthetic models based on their assumed properties: Temperature (θ), Dry Density (ρd), and Water Content (W).

The process involved the following steps:

1. Input Feature Preparation: For each region (active layer, thaw layer, permafrost, and base layer), the input features were derived based on the assumed temperature, dry density, and water content ranges. These input features were pre-processed using the scaling techniques specified in the data preprocessing step to ensure compatibility with the trained ML model.
2. Model Prediction: The best-performing model, determined during the evaluation phase, was deployed to predict resistivity for each set of input features. This ensured that the resistivity assigned to each region reflected the realistic variations in permafrost and surrounding layers.
3. Integration into Synthetic Models: The predicted resistivity values were assigned to their respective regions within the synthetic models. This process resulted in realistic resistivity distributions across the models, accurately representing the physical and thermal properties of each layer.

The generated 2D models capture the complex spatial resistivity distributions found in permafrost regions. Each layer in these models is characterized by specific resistivity values, temperatures, densities, and water content levels that reflect natural permafrost environments.

Figure 3.10 illustrates examples of these generated 2D models, showing the distinct properties of each layer. The visualizations highlight how the synthetic models replicate the layered structure commonly found in permafrost regions, with discontinuities and transitions between layers clearly visible. These 2D models are valuable tools for simulating and analyzing permafrost characteristics and can be used for further inversion studies to improve our understanding of subsurface conditions in cold regions.

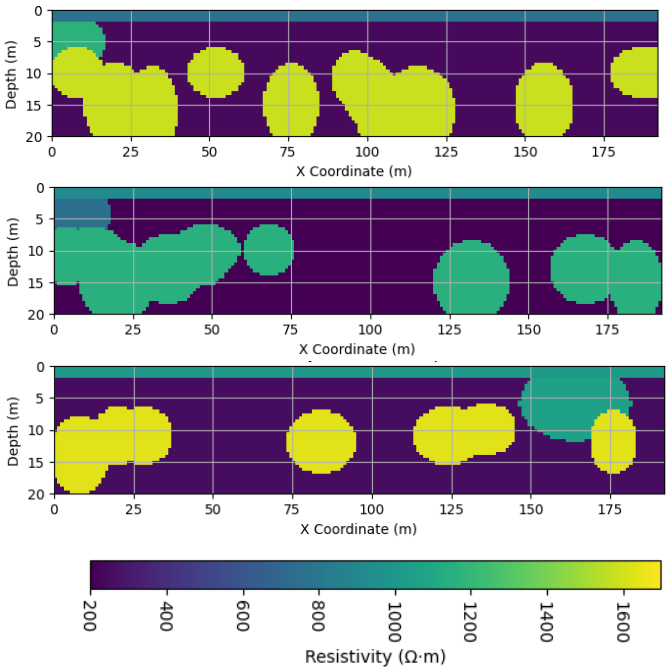

Region	T°c	density	Water content	Resistivity
Active	5	1.61	0.13	765
Thaw	-3	1.37	0.15	1163
Permafrost	-13	1.36	0.14	1580
Region	T°c	density	Water content	Resistivity
Active	2	1.49	0.25	919
Thaw	-3	1.78	0.12	752
Permafrost	-9	1.58	0.25	1154
Region	T°c	density	Water content	Resistivity
Active	5	1.37	0.14	1003
Thaw	-4	1.5	0.34	1058
Permafrost	-13	1.29	0.27	1631

Figure 3.10 – Some generated 2D models samples with properties for each region

3.4.2 Forward Modeling

Forward modeling was conducted using ResiPy (Blanchy et al., 2020) to simulate apparent resistivity values for each of the 500 runs. This process involved setting up an electrode array and defining a measurement sequence to create synthetic data for modeling permafrost and other soil layers.

- Electrode Configuration: The model utilized a 48-electrode linear array configuration, with electrodes spaced 4 meters apart along a predefined path. The generate_electrode_coordinates() function was employed to calculate precise positions for each electrode, ensuring a consistent and accurate setup for all simulations.
- Sequence: The measurement sequence was defined using Wenner-Schlumberger array configuration, with a fixed spacing between potential electrodes of 4 meters and a maximum expansion n=16 (as shown in Figure 3.11). The apparent Resistivity of each point could be calculated as follows:

$$k = \pi n(n+1)a \qquad \textit{(Equation 3.2)}$$

$$\rho = \frac{\Delta V}{I} k \qquad \textit{(Equation 3.3)}$$

- Forward Modeling: Once the electrode configuration and measurement sequence were established, ResiPy was used to generate synthetic apparent resistivity data for each simulated run. This step involved creating a forward model that simulated electrical current flow through the subsurface, producing resistivity measurements that represented realistic field data. The resulting synthetic data served as input for subsequent inversion processes and predictive modeling.

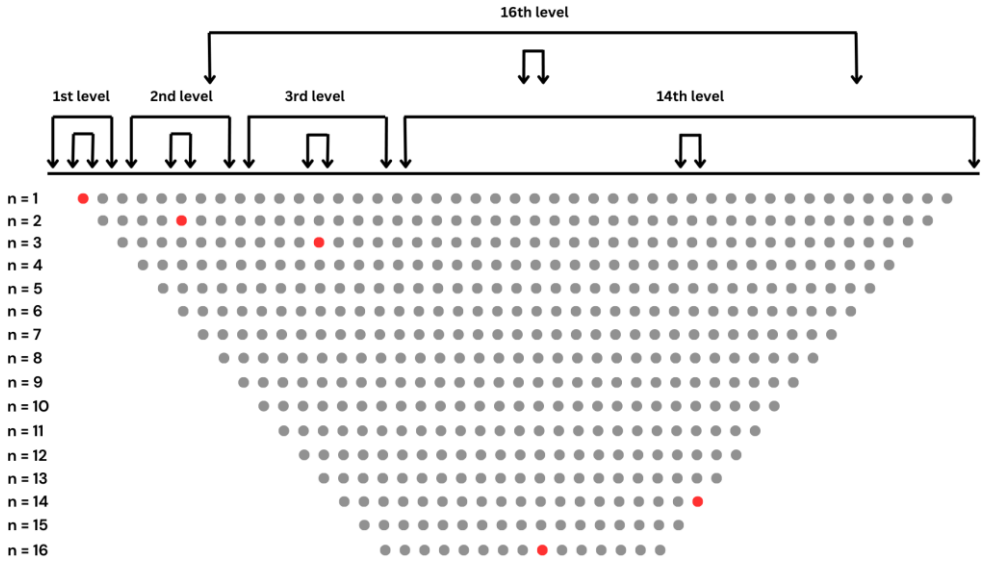

Figure 3.11 - Schematic representation of the Wenner–Schlumberger array with electrode locations and datum points.

Using these configurations, 480 apparent resistivity data points were generated for each representative model, capturing detailed spatial variations in subsurface resistivity. To enhance realism, the forward modeling process incorporated 5% noise, simulating the measurement inaccuracies typically encountered in field surveys.

The Wenner-Schlumberger array, with its consistent spacing and systematic measurement approach, enables detailed imaging of resistivity distributions across permafrost regions. By varying the n value, the array configuration enhances the model's ability to detect resistivity variations within different soil layers, such as the active, thaw and permafrost layers.

Figure 3.12 showcases examples of the generated 2D resistivity models alongside their corresponding pseudo-sections. These visualizations underline the detailed resistivity distributions within each representative model and the capability of the ResiPy-generated pseudo-sections to mimic realistic subsurface structures. By accurately reflecting the resistivity characteristics of layered permafrost regions, the pseudo-sections provide essential insights for further analysis.

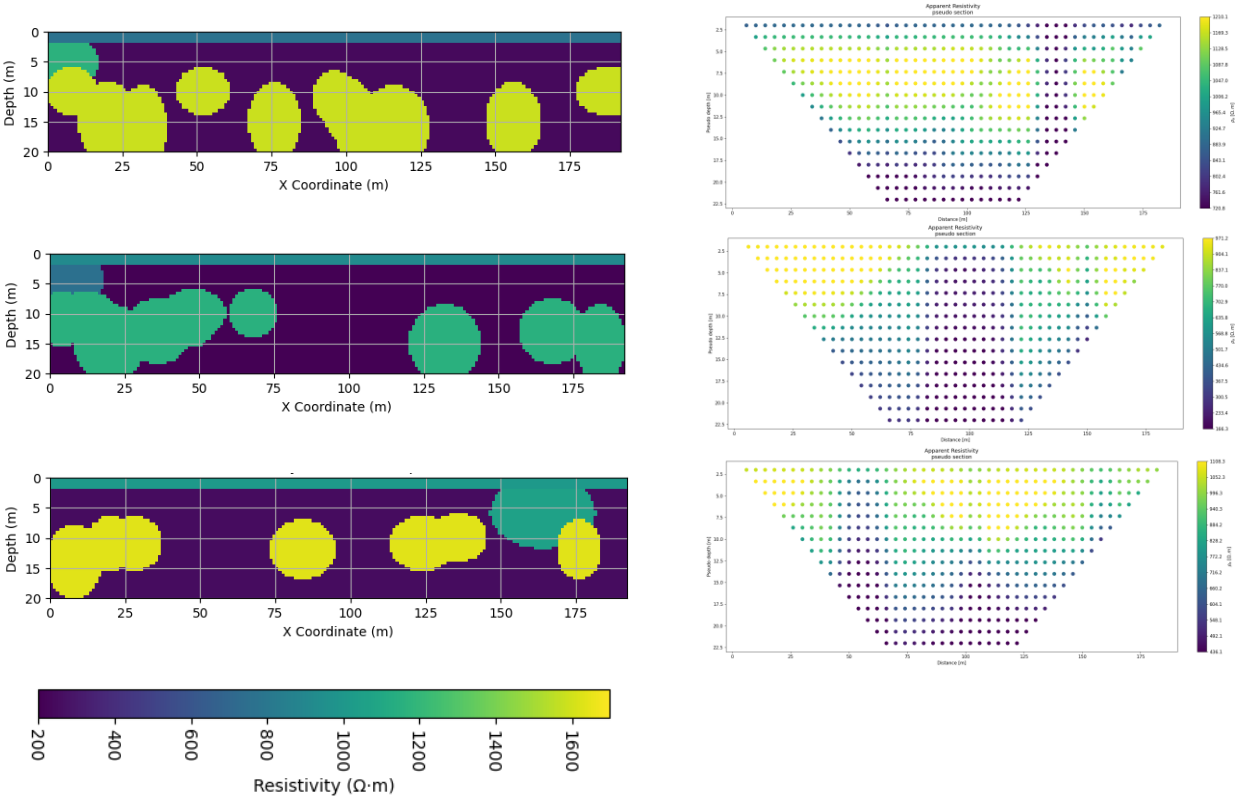

Figure 3.12 - Examples of generated 2D models alongside their corresponding pseudo-sections

3.4.3 Data management and storage

The data generated from each iteration, including detailed specifications of the modeled regions, was systematically stored for further analysis. This process involved storing the data in structured formats to ensure accessibility and compatibility with subsequent modeling and evaluation steps. Key information saved included:

- Region Specifications: Properties such as temperature, dry density, water content, and assigned resistivity values for each layer.
- Model Geometry: The spatial configuration of each synthetic model, including the dimensions and relationships between layers.
- Generated Resistivity Data: Apparent resistivity values derived from forward modeling, organized for use in inversion and ML tasks.

The stored dataset serve as the foundation for validating the models, comparing ML predictions, and conducting inversion analysis in later stages of the study.

3.5 Permafrost Resistivity Prediction

This section details the methodology for predicting permafrost resistivity using ML models, emphasizing the models utilized, their configurations, and the evaluation metrics applied to measure performance. In this context, the resistivity of permafrost in each simulated model was designated as the ground truth, while apparent resistivity data and electrode distances for each measurement sequence were employed as input features for training the models.

The ground truth resistivity values were derived from the predefined properties of each synthetic model, representing the true resistivity characteristics of the permafrost. Apparent resistivity, on the other hand, reflects the observed electrical resistivity influenced by subsurface heterogeneities and was computed for each pseudo-section. Additionally, spatial distances between electrodes within each measurement sequence were included as input features to capture critical spatial relationships affecting resistivity patterns.

By leveraging apparent resistivity and electrode distance data, the ML models were trained to understand the intricate relationships between these features and the actual resistivity values. This training enabled the models to predict permafrost resistivity with a high degree of accuracy. Given that resistivity is a crucial parameter for monitoring permafrost conditions, the ability of ML models to reliably predict it based on pseudo-section data demonstrates their potential as effective tools for permafrost assessment and monitoring.

3.5.1 Data Preparation

To ensure accurate and reliable training of ML models, the data underwent a systematic preprocessing procedure encompassing the following steps:

1. Loading Apparent Resistivity and Electrode Data: Apparent resistivity values and their corresponding electrode configurations were extracted from the ".dat" files produced during the pseudo-section modeling process. These files provided the foundational data required for feature generation and model training.
2. Feature Engineering: Spatial relationships within each electrode configuration were incorporated by calculating distances between electrode pairs. These distances, when combined with apparent resistivity values, formed a comprehensive feature set that encapsulated the spatial and electrical characteristics of the pseudo-sections.
3. Target Variable: Permafrost resistivity, calculated based on the predefined properties of each region in the simulated runs, was established as the target variable. This ground truth value served as the basis for training and evaluating the performance of the ML models.

Through this rigorous data preparation process, the input features and target variable were standardized, ensuring consistency and reliability for model training and evaluation.

3.5.2 Models and Comparison Indicators

To evaluate the ability of ML models to predict permafrost resistivity, five algorithms were tested: Linear Regression, Random Forest, Gradient Boosting, SVR, and Neural Networks. Each model was meticulously configured and trained on an 80-20 split of the dataset. The configurations for each model are detailed below:

- Gradient Boosting was configured with a learning rate of 0.1, which balanced the contribution of each decision tree to the final model. The number of estimators was set to 100, ensuring sufficient

complexity to learn patterns without overfitting, while the depth of each tree was limited to avoid overly complex models that might struggle to generalize.

- Random Forest, another ensemble method, was set up with a maximum tree depth of 10 to prevent overfitting while retaining its ability to capture essential patterns. The trees split when at least two samples were available, ensuring flexibility during the growth phase. A total of 200 trees were used to provide a robust ensemble capable of achieving high predictive accuracy without excessive computational cost.
- SVR was included to explore its potential for capturing linear relationships within the data. A regularization parameter of 10 was chosen to balance training accuracy and model simplicity. The kernel type was linear, which effectively modeled the relationships in this dataset, and the gamma parameter was automatically scaled based on the feature space, ensuring optimal kernel operation.
- The Neural Network model incorporated a deep learning approach with four dense layers. The first layer consisted of 250 neurons, followed by 150 neurons in the second, 40 neurons in the third, and a single output neuron. Each hidden layer utilized the ReLU activation function to capture nonlinear relationships, while the output layer had a linear activation for continuous predictions. Dropout layers were included after each hidden layer, applying a 20% dropout rate to mitigate overfitting by reducing dependencies among neurons. The network was trained with the Adam optimizer, known for its adaptive learning rate capabilities, and MSE was used as the loss function to minimize prediction errors.
- Lastly, k-NN relied on local patterns within the data to make predictions. The model considered the three nearest neighbors for each data point, with weights inversely proportional to their distances. This configuration allowed the model to prioritize closer points in the feature space, ensuring predictions were influenced more by the most relevant data points.

Each model was trained and tested on an 80-20 split of the dataset, ensuring that enough data was available for robust learning while reserving a portion for evaluating generalization.

3.5.3 Model Evaluation and Comparison

The table 3.2 presents a comparison of all models evaluated for permafrost resistivity prediction:

Table 3. 2 – comparison between ML models' performance for predicting resistivity (ρ) of Permafrost body

Model	MSE	MAE	MAPE	R^2 score
Gradient Boosting	23697.09	123.81	153.93	0.5501
Linear Regression	1291499.88	882.32	1136.44	-23.52
Random Forest	21687.18	117.59	147.26	0.5882
Support Vector Regressor	48964.5	183.31	221.27	0.0703
Neural Network	50165.12	178.83	223.97	0.0475

- Random Forest and Gradient Boosting achieved the lowest MSE, MAE, and RMSE values among the tested models, with R^2 scores of 0.5882 and 0.5501, respectively. This suggests that these two models provided the most accurate predictions among the options tested, although their R^2 values indicate only moderate predictive power.
- Linear Regression performed very poorly, with a highly negative R^2 score (-23.52), indicating that it was unable to capture the relationship between features and the target variable effectively. The high error values further emphasize its unsuitability for this task.
- Support Vector Regressor and Neural Network models also underperformed, with low R^2 scores (0.0703 and 0.0475, respectively) and relatively high error values, indicating limited predictive capability for this application.

Overall, the results suggest that tree-based models, particularly Random Forest and Gradient Boosting, were the most effective ML approaches for predicting permafrost resistivity in this dataset. These models showed better accuracy and predictive reliability compared to the other tested methods.

3.5.4 Evaluation of Model Predictions: Actual vs. Predicted Resistivity

This section provides a visual evaluation of the resistivity prediction accuracy for each ML model, comparing predicted resistivity values against actual values. The following scatter plots illustrate how closely each model's predictions align with the actual resistivity measurements, with the red dashed line representing a perfect prediction where predicted values would equal actual values (figure 4.12).

- Neural Network: The scatter plot for the neural network model shows a moderate alignment with the perfect prediction line, with predictions somewhat dispersed around it. While the neural network captures general trends, the spread indicates variability in predictive accuracy, contributing to its relatively low R^2 score.
- SVR: The SVR model exhibits a significant deviation from the perfect prediction line. The predicted values are mostly clustered around a narrow range, failing to capture the full variability of actual resistivity values. This reflects the SVR model's limited predictive performance, as indicated by its low R^2 score and high error metrics.
- Gradient Boosting: The Gradient Boosting model shows better alignment with the perfect prediction line compared to SVR, with predictions scattered closely around it. This indicates a reasonable predictive capability, capturing the general resistivity patterns, though some variance remains. The model's R^2 score and error metrics reflect this balanced performance.
- Random Forest: The Random Forest model also displays a close alignment with the perfect prediction line, with points clustered around it. This indicates that Random Forest performs well in capturing resistivity variations, and its relatively high R^2 score confirms its effectiveness in this prediction task.
- Linear Regression: The Linear Regression model shows a poor alignment with the perfect prediction line, with significant scattering of points. The predicted values diverge considerably from the actual values, resulting in a highly negative R^2 score and high error metrics. This plot clearly illustrates the unsuitability of Linear Regression for this dataset.

3.5.5 Summary of Findings

The findings indicate that Random Forest and Gradient Boosting are the preferred models for predicting permafrost resistivity, offering a balance between accuracy and interpretability. The limitations observed in SVR and Linear Regression underscore the need for models that can handle non-linear, complex relationships within environmental datasets. These results provide a foundation for further refinement and application of ML approaches in predicting soil resistivity, particularly in cold regions where permafrost characteristics are critical to geotechnical and environmental assessments.

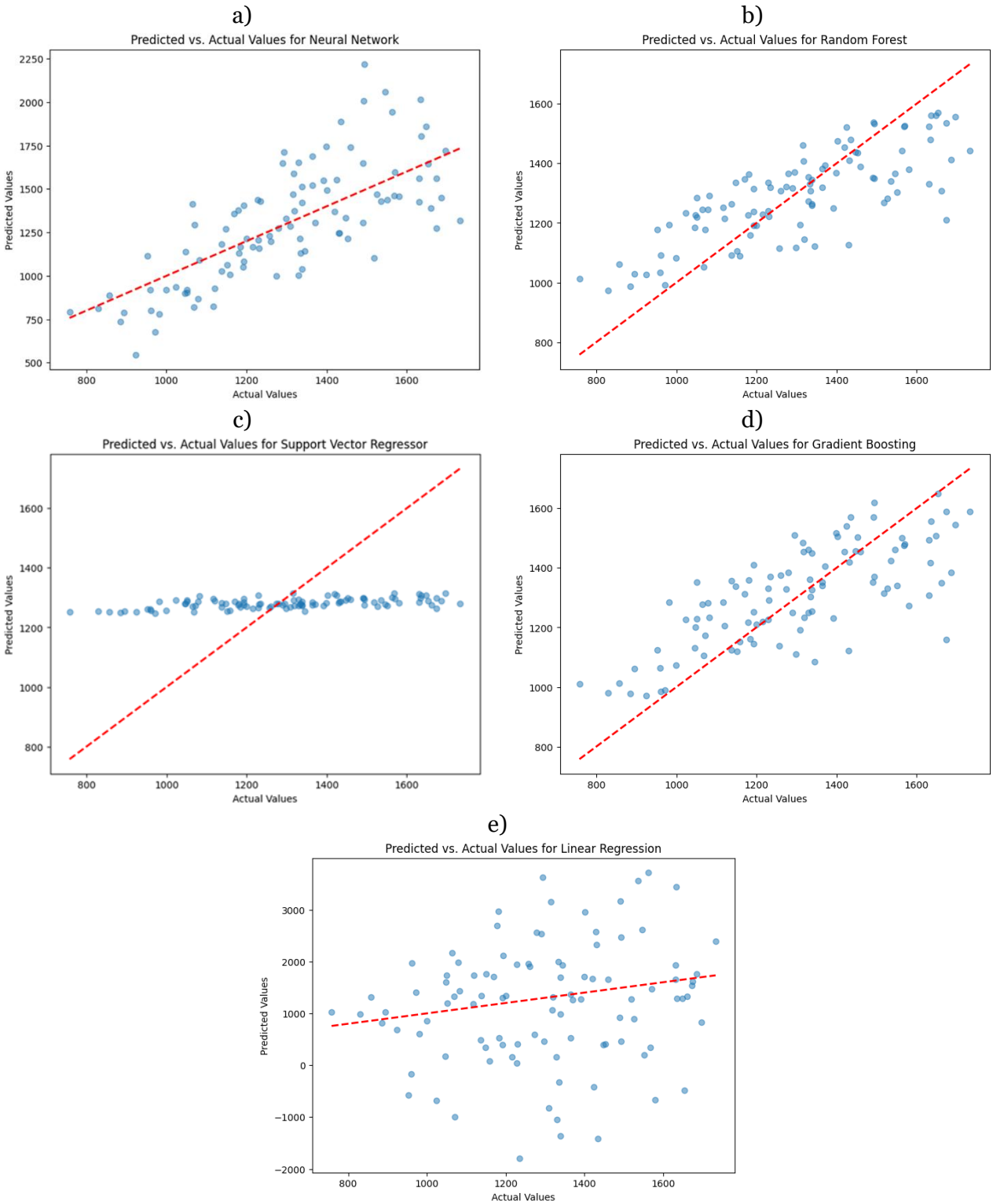

Figure 3.13 - Comparison between the actual and predicted resistivity values of permafrost for each model , a) for NN, b) for Random Forest, c) for SVR, d) for gradient boosting and e) for Linear Regression.

3.6 Water Content and Temperature Prediction Models

The subsequent stage of the methodology involved developing ML models to predict water content and temperature in permafrost regions. These predictions leveraged resistivity values obtained from earlier models, combined with additional features such as dry density, to estimate these critical environmental variables. By doing so, this step sought to extend the utility of the models beyond resistivity, offering insights into the physical and thermal characteristics of permafrost.

ML algorithms were employed for both prediction tasks, including Random Forest, Gradient Boosting, Support Vector Regressor, Neural Networks, and Linear Regression. The aim was to evaluate each model's performance across a variety of scaling techniques, including StandardScaler, MinMaxScaler, and MaxAbsScaler, to determine the most suitable model and preprocessing approach for each prediction target.

Water content prediction focused on understanding the distribution and dynamics of moisture within the permafrost layers, a crucial factor influencing permafrost stability and thermal conductivity. Similarly, temperature prediction was critical for assessing the thermal state and potential thawing of permafrost.

3.6.1 Data Preparation and Feature Engineering

For predicting water content and temperature in permafrost regions, data preparation involved utilizing key variables extracted from the generated pseudo-sections, including predicted resistivity, temperature, and dry density. These variables served as input features to develop robust ML models tailored to these specific prediction tasks.

Key features—predicted resistivity, temperature, dry density, and water content—were identified as the most relevant input variables. These features were scaled using various preprocessing techniques to evaluate the impact of normalization on model performance. The scaling methods applied included StandardScaler, MinMaxScaler, and MaxAbsScaler, along with a baseline scenario where no scaling was applied. This approach ensured that models were assessed under consistent conditions and allowed for identifying the most effective scaling method for each prediction task.

For water content prediction, the target variable was directly extracted from the dataset, representing the moisture content within permafrost layers. Similarly, for temperature prediction, temperature values were structured as the target variable, ensuring alignment with the prepared feature sets to maintain data integrity across tasks.

3.6.2 Temperature prediction model evaluation and comparison

The following table summarizes the performance of different ML models for temperature prediction in permafrost regions, evaluated under various scaling methods. The performance metrics include MAE, RMSE, and R^2 score.

Table 3.3 – comparison between ML models' performance for predicting temperature (θ) of Permafrost body with various scaling methods

Scaler	Model	MAE	RMSE	R^2
No Scaling	Linear Regression	1.6504	2.2727	0.4767
	Random Forest	1.6525	2.2926	0.4675
	Gradient Boosting	1.7014	2.3179	0.4557
	Support Vector Regressor	2.113	2.5172	0.358
	Neural Network	2.2207	2.683	0.2707
StandardScaler	Linear Regression	1.651	2.2727	0.4767
	Random Forest	1.645	2.2912	0.4681
	Gradient Boosting	1.7014	2.3179	0.4557
	Support Vector Regressor	1.6287	2.256	0.4843
	Neural Network	1.6981	2.2982	0.4649
MinMaxScaler	Linear Regression	1.651	2.2727	0.4767
	Random Forest	1.6463	2.2938	0.4669
	Gradient Boosting	1.7014	2.3179	0.4557
	Support Vector Regressor	1.6447	2.2607	0.4822
	Neural Network	1.7568	2.3362	0.447
MaxAbsScaler	Linear Regression	1.6526	2.2742	0.476
	Random Forest	1.6519	2.2969	0.4655
	Gradient Boosting	1.7014	2.3179	0.4557
	Support Vector Regressor	1.6412	2.2056	0.5071
	Neural Network	1.6365	2.266	0.4797

- SVR with MaxAbsScaler achieved the highest R^2 score (0.5071) with relatively low MAE and RMSE values, making it the most effective model-scaling combination for temperature prediction.
- Gradient Boosting showed consistent performance across all scaling methods, with a stable R^2 score around 0.4767, indicating robustness to different scaling techniques.
- Random Forest performed reasonably well, especially with StandardScaler and MinMaxScaler, with R^2 scores close to Gradient Boosting, but slightly lower.
- Neural Network performance varied with scaling methods, with MaxAbsScaler yielding the highest R^2 score of 0.4797, which was close to other models but still slightly below SVR.
- Linear Regression showed the lowest performance across all scaling methods, with R^2 scores consistently around 0.4557, indicating limited suitability for temperature prediction in permafrost regions.

3.6.3 Water Content prediction model evaluation and comparison

The table below presents the performance metrics (MAE, MSE, R^2) for different models under various scaling methods for predicting water content.

Table 3.4 – comparison between ML models' performance for predicting Water Content (W) of Permafrost body with various scaling methods

Scaler	Model	MAE	MSE	R^2
No Scaling	Linear Regression	0.0691	0.0068	-0.0658
	Random Forest	0.0735	0.0078	-0.2189
	Gradient Boosting	0.0748	0.0083	-0.2881
	Support Vector Regressor	0.0684	0.0065	-0.0101
	Neural Network	0.0799	0.0094	-0.4605
StandardScaler	Linear Regression	0.0691	0.0068	-0.0658
	Random Forest	0.0731	0.0078	-0.2114
	Gradient Boosting	0.0748	0.0083	-0.2881
	Support Vector Regressor	0.0749	0.0082	-0.281
	Neural Network	0.0815	0.0096	-0.4936
MinMaxScaler	Linear Regression	0.0691	0.0068	-0.0658
	Random Forest	0.0729	0.0077	-0.2022
	Gradient Boosting	0.0748	0.0083	-0.2881
	Support Vector Regressor	0.0743	0.008	-0.2489
	Neural Network	0.0706	0.0069	-0.0787
MaxAbsScaler	Linear Regression	0.0691	0.0068	-0.0658
	Random Forest	0.0732	0.0078	-0.2133
	Gradient Boosting	0.0748	0.0083	-0.2881
	Support Vector Regressor	0.0705	0.0069	-0.0687
	Neural Network	0.0684	0.0065	-0.0182

The Support Vector Regressor with MaxAbsScaler achieved relatively better performance, though overall R^2 values indicate that none of the models fully captured the relationships needed for reliable water content prediction. The reliance on previously predicted resistivity values as an input feature likely introduced biases, inflating performance metrics on seen data but reducing real-world applicability.

3.6.4 Summary of Findings

The results from temperature and water content prediction models indicate moderate performance across various ML approaches, highlighting several limitations. The moderate R^2 scores suggest that these models only partially capture the underlying relationships in the data, and their ability to generalize to unseen, real-world scenarios is limited.

A key factor influencing these results is the dependency on previously predicted resistivity values as input features, which introduces potential biases. This reliance, especially given that much of the dataset contains "seen" data, likely inflates model performance metrics, reducing their applicability in more variable, real-world settings.

Figures 3.14 and 3.15 illustrate the alignment between each model's predictions using MaxAbsScaler and the actual measurements for temperature. These visualizations provide a comparative insight into each model's effectiveness, underscoring the need for further refinement, unseen test data, and advanced feature engineering to improve the generalization capabilities of these models.

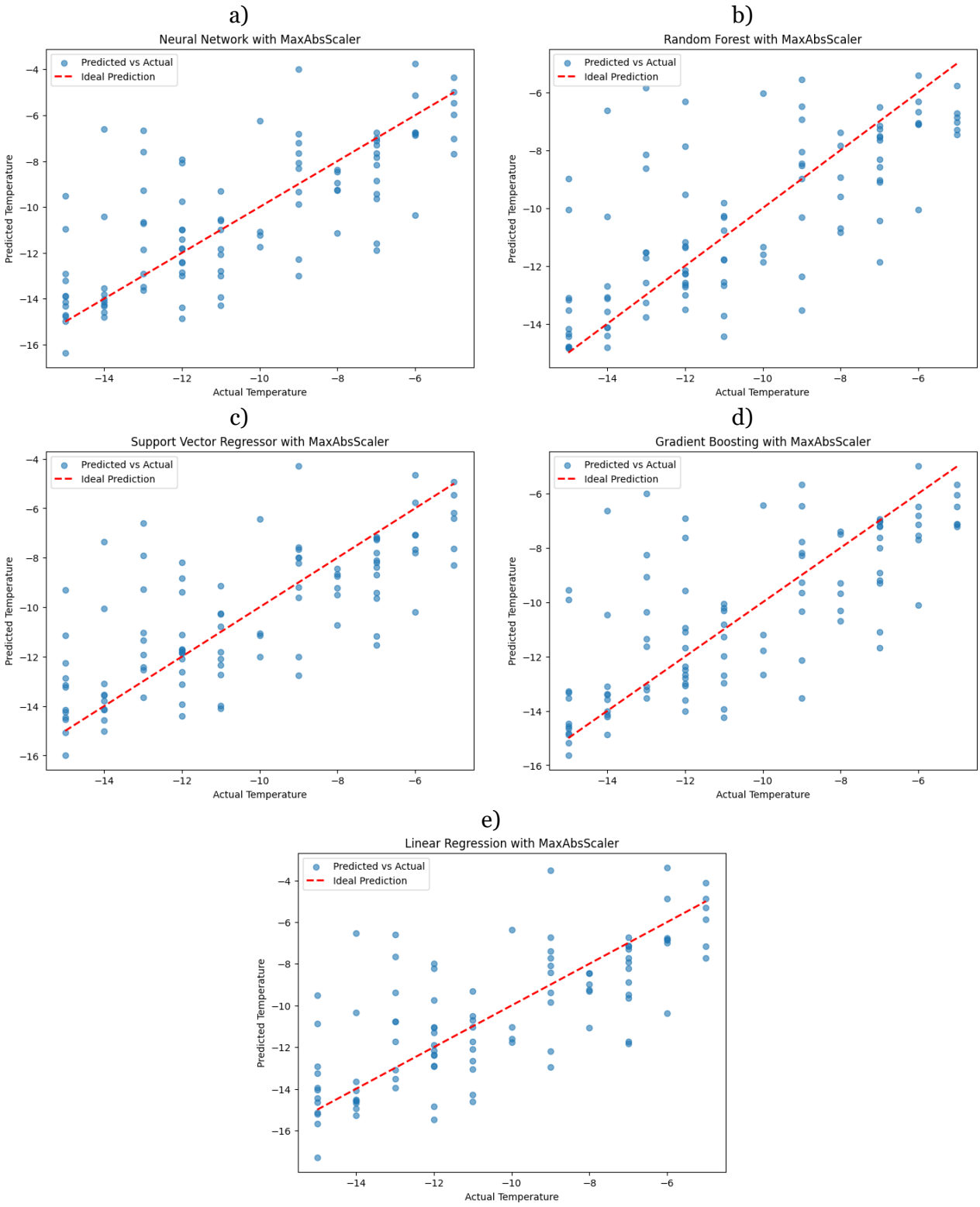

Figure 3.14 - Comparison between the actual and predicted temperature values of permafrost for each model using maximum absolute scaler method, a) for NN, b) for Random Forest, c) for SVR, d) for gradient boosting and e) for Linear Regression.

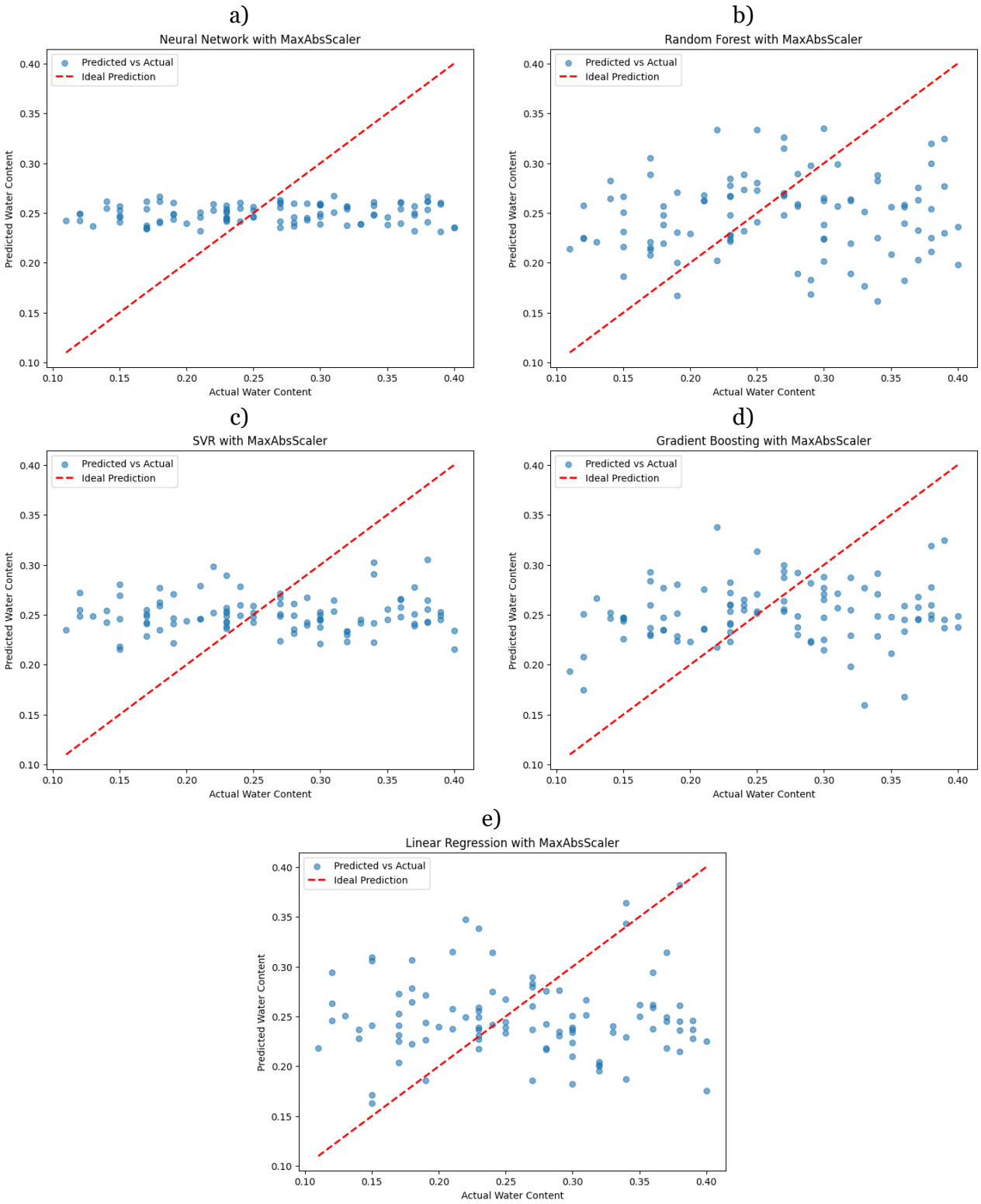

Figure 3.15 - Comparison between the actual and predicted water content values of permafrost for each model using maximum absolute scaler method, a) for NN, b) for Random Forest, c) for SVR, d) for gradient boosting and e) for Linear Regression.

Chapter 4: ERT and CNN Inversion

Summary: Chapter 4 explores the use of ERT and CNN for imaging permafrost regions. ERT is presented as a method that measures subsurface resistivity to distinguish between frozen (high resistivity) and thawed (low resistivity) ground. The chapter highlights the limitations of conventional inversion techniques in capturing sharp resistivity contrasts and introduces a CNN-based inversion model. This CNN model demonstrates improved accuracy in reconstructing detailed subsurface resistivity distributions, effectively identifying complex discontinuities within permafrost regions. Figure 4.1 represents the overall workflow of this chapter.

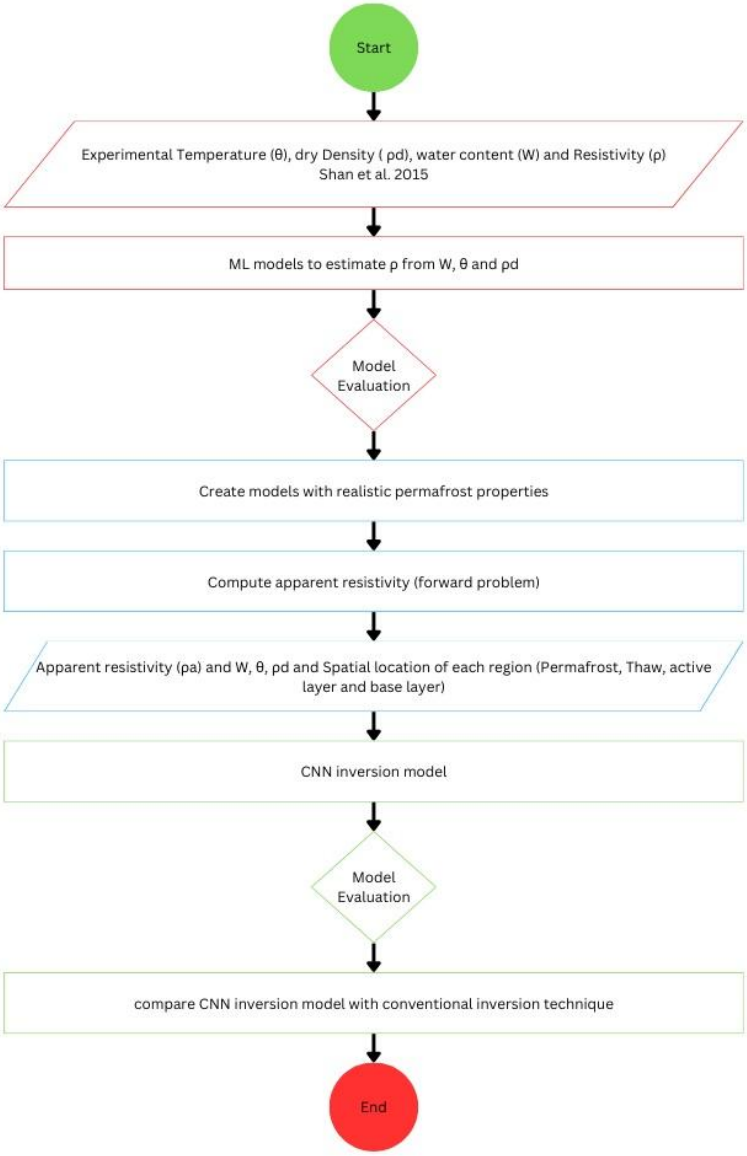

Figure 4.1 – The workflow of CNN inversion

4.1 ERT definition and application

ERT is a is a powerful geophysical method for monitoring permafrost conditions, providing insights into the physical properties of the subsurface by measuring the resistance of soil or rock to the flow of electrical current. This technique is particularly useful for characterizing permafrost because frozen ground, which contains ice, has significantly higher resistivity compared to thawed ground, where water serves as a conductor (Hilbich et al., 2008).

It involves injecting electrical current into the ground through a pair of electrodes and measuring the resulting potential differences at other electrode pairs. By systematically varying the positions of the current and potential electrodes, a dataset of apparent resistivity measurements is obtained, which can be inverted to produce a two-dimensional (2D) or three-dimensional (3D) model of the subsurface resistivity (Loke et al., 2013).

ERT involves three main stages:

1. Data Acquisition: Involves collecting resistivity data in the field using specific electrode arrays.
2. Data Preprocessing and Inversion: Converts raw measurements into resistivity models through computational algorithms.
3. Interpretation: Identifies geological or hydrological features from the resistivity models.

In permafrost regions:

- Frozen ground: Exhibits high resistivity due to the low conductivity of ice.
- Thawed ground: Shows lower resistivity because liquid water increases the conductivity.
- Mixed phases: Areas with partially frozen ground have intermediate resistivity values.

This contrast enables the delineation of permafrost boundaries, the active layer, and transitions between frozen and unfrozen zones.

4.1.1 Data Acquisition for ERT

Collecting electrical resistivity (ER) data involves a systematic approach to ensure accurate measurements and reliable subsurface interpretations. The process begins with equipment setup, which includes deploying a resistivity meter, power supply, and electrodes in the field. Proper electrode spacing and alignment are essential to achieve the desired depth of investigation and resolution (Loke et al., 2021).

Survey design is critical and involves selecting an appropriate electrode configuration, such as Wenner or Schlumberger arrays, based on the specific objectives and geological conditions of the study area. Data acquisition is performed by injecting electrical current into the ground through current electrodes and measuring the resulting potential difference at receiving electrodes, which is then used to calculate apparent resistivity (Dahlin, 2001).

4.1.2 Different inversion techniques

ERT involves transforming apparent resistivity data collected in the field into meaningful subsurface models. This transformation is achieved through inversion techniques, which convert raw resistivity measurements into a distribution of resistivity values that represent the electrical properties of the subsurface. These models help identify variations in lithology, moisture content, or ice presence, making them particularly valuable for permafrost studies (Loke et al., 2013).

Conventional inversion methods, such as deterministic inversion employs a systematic approach to find the best-fitting resistivity distribution by solving the inverse problem with predefined

mathematical constraints. It typically relies on optimization techniques, such as least-squares or Occam's inversion, which iteratively minimize the objective function representing the misfit between observed and calculated resistivity values. However, they often struggle to capture sharp boundaries or lateral heterogeneities, such as those found in discontinuous permafrost zones (Dahlin & Zhou, 2004; Zhong et al., 2021).

Also, robust inversion focuses on minimizing the influence of outliers and emphasizes capturing sharp resistivity contrasts, making it better suited for complex geological settings like discontinuous permafrost zones. Unlike deterministic inversion, which assumes smoothness, robust inversion uses L1-norm or hybrid L1-L2-norm regularization techniques to achieve more distinct boundaries in resistivity models.

Advanced inversion techniques, including 2D and 3D resistivity inversion, have improved subsurface imaging by accounting for spatial complexities. Additionally, time-lapse inversion methods enable monitoring temporal changes in resistivity, which is critical for studying seasonal freeze-thaw cycles in permafrost (Kneisel et al., 2008). Hybrid approaches, such as joint inversion, combine resistivity data with other geophysical datasets, such as seismic, to improve model accuracy and resolution (Buckel et al., 2021).

ML-based inversion techniques are emerging as a promising alternative to traditional methods. These approaches leverage the power of neural networks and ensemble algorithms to predict resistivity distributions more accurately, particularly in areas with complex geological structures. Such methods have demonstrated the ability to detect anomalies and discontinuities in permafrost regions, offering enhanced sensitivity and precision compared to conventional techniques (Thaler et al., 2023; Liu et al., 2024).

4.2 Conventional deterministic inversion using ResiPy

Following the generation of apparent resistivity through forward modeling for the dataset generated in section 3.4, ResiPy was used for the inversion process. This step converted the synthetic apparent resistivity data into detailed ERTs. These visualized maps of the resistivity distribution within the soil, capturing the distinct characteristics of each layer and facilitating further analysis of the soil's properties.

4.2.1 Mesh Configuration

ResiPy employs triangular meshes for resistivity inversion, with a default configuration of three elements between each electrode and a growth factor of 20% to 50% for deeper regions. However, for direct comparison with the CNN inversion results, a fine mesh configuration with 1x1 meter elements and growth factor equal to 20% was used. This ensured consistency in resolution across both methods, allowing for meaningful evaluations of their respective performances.

4.2.2 Regularization and inversion configuration

ResiPy utilizes a smoothness-constrained least-squares inversion technique, commonly referred to as Tikhonov regularization. This method aims to stabilize the inversion process by balancing the trade-off between fitting the observed data and maintaining a smooth resistivity model. The following features characterize ResiPy's inversion methodology:

- Misfit Threshold: The inversion process iteratively minimizes the difference between observed and modeled data, halting when the misfit falls below a predefined threshold. This ensures that the final model adequately represents the input data without excessive computation.
- Iteration Limits: To prevent overfitting and manage computational demands, the inversion typically runs for 10–20 iterations by default.
- Sensitivity Matrix Normalization: ResiPy normalizes the sensitivity matrices to account for variations in electrode spacing and subsurface coverage, ensuring consistent results across different configurations.
- Smoothing Factor: A regularization parameter (lambda) is applied to balance data misfit and model smoothness, optimizing the trade-off between capturing fine details and avoiding noise amplification.

Figures 4.2 to 4.4 illustrate examples of generated 2D models alongside their corresponding ERT results obtained through the conventional inversion technique. These figures highlight the strengths and limitations of traditional inversion methods:

- While the conventional inversion technique is generally effective at mapping large-scale resistivity patterns, it struggles to accurately capture discontinuities within the permafrost regions.
- This limitation may be partly due to the Wenner-Schlumberger array configuration, which, while useful for producing general resistivity profiles, has some weaknesses in detecting sharp transitions and discontinuities within the subsurface.

These observations underscore the potential need for enhanced modeling and inversion techniques to better resolve fine-scale features within permafrost regions, especially where discontinuities play a critical role in understanding subsurface dynamics.

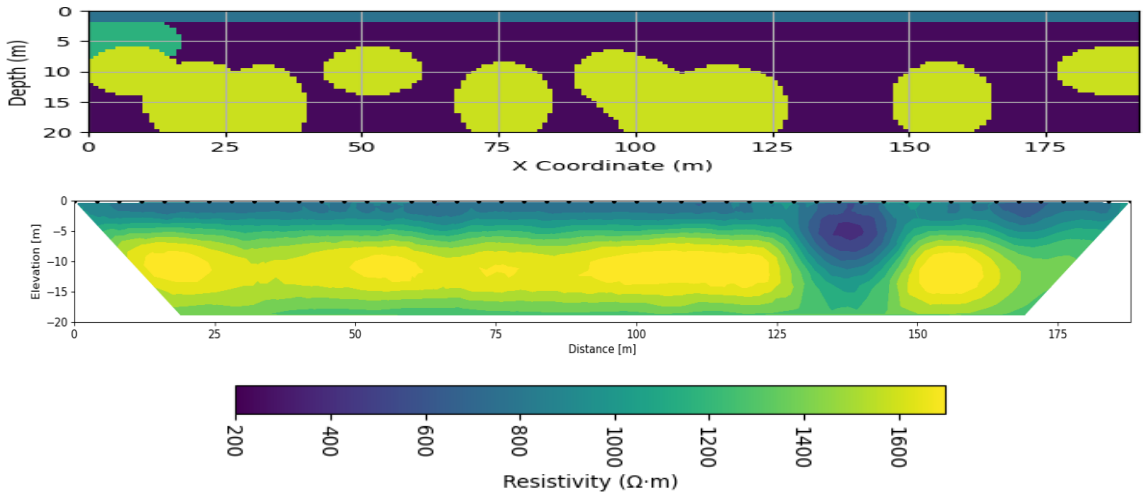

Figure 4.2 – First example of generated 2D models alongside their corresponding ERT

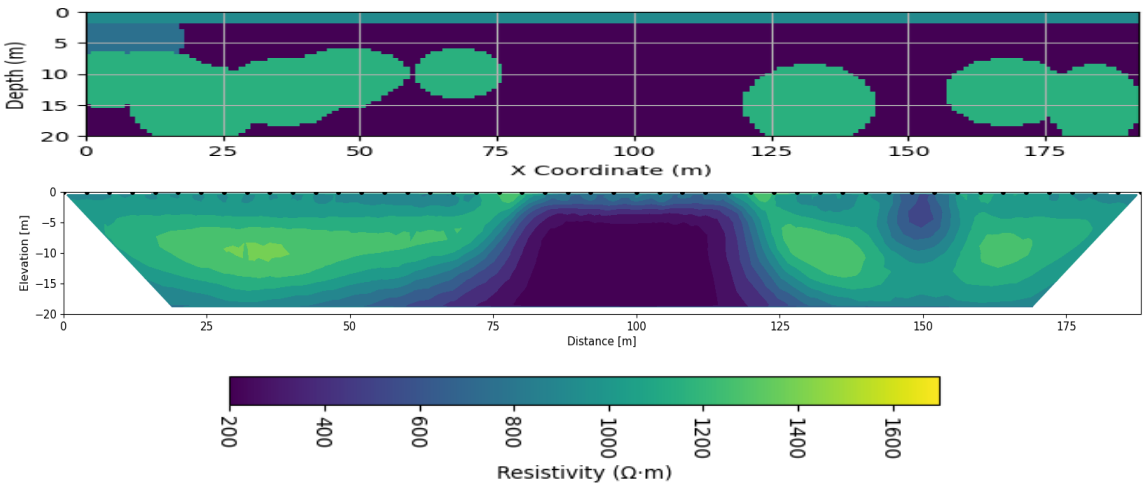

Figure 4.3 – Second example of generated 2D models alongside their corresponding ERT

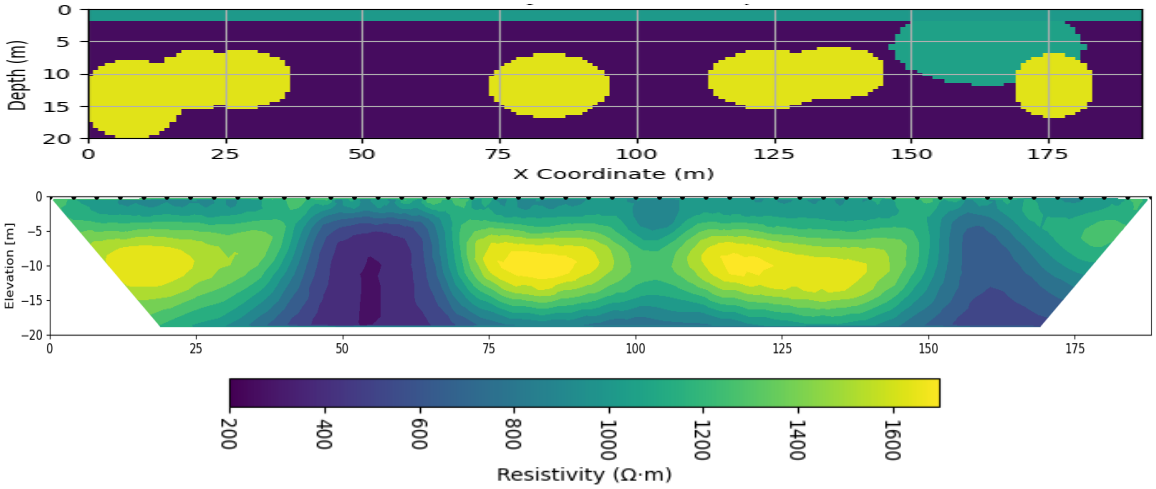

Figure 4.4 – Third example of generated 2D models alongside their corresponding ERT

4.3 CNN Model for Resistivity Inversion

The concluding stage of this study focused on leveraging a CNN model for resistivity inversion, targeting the transformation of synthetic apparent resistivity data into true resistivity distributions. Using the generated 2D apparent resistivity dataset, which represented permafrost regions with discontinuities as outlined in Section 3.4, the CNN model was designed to address the challenges posed by conventional inversion methods.

The CNN-based inversion methodology aimed to provide a more automated and precise approach to inversion in permafrost environments. By capturing complex spatial resistivity variations, the model sought to overcome limitations such as the inability of traditional methods to resolve sharp lateral heterogeneities or intricate subsurface features. This approach was particularly valuable for imaging the resistivity distributions of frozen and thawed soil configurations, providing insights into the permafrost's structural characteristics.

The use of a CNN for resistivity inversion represents a pioneering step towards improving inversion accuracy in geophysical studies. The model's ability to learn from diverse synthetic datasets and predict detailed resistivity maps underscores its potential for real-time imaging applications in permafrost research and monitoring. This innovative approach demonstrates the applicability of deep

learning techniques in geophysical inversions, paving the way for future advancements in this domain.

4.3.1 Mesh Creation and Data Preparation

To prepare for training the CNN model, a fine spatial mesh was created to represent the resistivity distribution across each permafrost model. The preparation process involved the following steps:

- Mesh Creation: The Gmsh library was employed to generate a fine, rectangular mesh with a resolution of 1 x 1 meter. This high-resolution mesh was designed to accurately capture the spatial variations in resistivity across the permafrost models, ensuring a realistic representation of subsurface configurations.
- Resistivity Assignment: Resistivity values, previously saved for each model, were assigned to individual mesh elements based on the region type (e.g., permafrost, thaw, base, or active layers). The properties of these regions, such as temperature, water content, and density, were used to determine the corresponding resistivity values, ensuring consistency with the predefined characteristics of each generated model.

This structured approach to mesh creation and resistivity assignment facilitated the preparation of high-quality datasets for CNN training, enabling the model to learn the spatial and resistivity patterns critical for accurate inversion.

4.3.2 CNN Model Architecture

The CNN model was designed to interpret apparent resistivity data and predict a detailed resistivity distribution across the mesh, accurately reflecting the complex spatial patterns present in permafrost regions. The architecture of the CNN model included the following components:

- Input Layer: Configured to accept input data as a flattened array of apparent resistivity values, shaped to (480, 1, 1). This format ensured compatibility with the model's convolutional layers and allowed it to process the data effectively.
- Convolutional Layers:
    - First Layer: Implemented with 32 filters, a kernel size of (5, 1), and ReLU activation. This layer was followed by Batch Normalization to stabilize learning and a 10% dropout rate to prevent overfitting.
    - Second Layer: Used 64 filters, a kernel size of (3, 1), and ReLU activation, again followed by Batch Normalization and a 10% dropout rate.
    - Third Layer: Incorporated 128 filters with a kernel size of (3, 1) and ReLU activation to capture finer spatial features in the resistivity data.
- Flattening Layer: Transformed the 3D feature maps generated by the convolutional layers into a 1D array, making the data suitable for processing by the fully connected layers.
- Fully Connected Layers:
    - Dense Layer: Consisted of 256 neurons with ReLU activation, enabling the model to learn complex, nonlinear relationships in the data.
    - Output Layer: A dense layer reshaped to output a 2D resistivity matrix that matched the dimensions of the input mesh, providing the final predicted resistivity distribution.

The CNN model was compiled using the Adam optimizer, chosen for its adaptive learning rate and efficiency in training deep networks. The loss function was set to MSE to minimize the squared differences between predicted and actual resistivity values. Additionally, MAE was included as a supplementary evaluation metric to provide further insights into model performance.

This architecture was designed to leverage the spatial dependencies in the apparent resistivity data and produce highly detailed resistivity maps, advancing the capability to monitor and analyze permafrost regions.

4.3.3 Training and Evaluation

The training process for the CNN model used to predict resistivity distributions from apparent resistivity data was conducted as follows:

- Data Split: The dataset was divided into training and testing subsets, with 80% of the data allocated for training and 20% for testing. This split ensured that the model was evaluated on data it had not encountered during training, providing a realistic measure of its generalization capability.
- Training Parameters:
    - Epochs: The model was trained over 100 epochs, allowing sufficient iterations to learn patterns in the data while monitoring for signs of overfitting.
    - Batch Size: A batch size of 16 was used, balancing computational efficiency and model performance.
- Monitoring and Regularization:
    - Loss Monitoring: Both training and validation losses were tracked during the training process. This step was crucial to ensuring that the model converged effectively and did not overfit the training data.
    - Validation: Periodic evaluation on the validation set during training provided insights into the model's performance on unseen data, guiding potential adjustments to hyperparameters or early stopping criteria.
- Evaluation Metrics:
    - Loss: The MSE was calculated on the test set to evaluate how well the model minimized prediction errors.
    - MAE: As an additional evaluation metric, MAE was used to measure the average magnitude of errors in the predictions, providing a complementary view of model accuracy.

The test set evaluation confirmed the model's ability to predict detailed resistivity distributions, leveraging the spatial dependencies in the apparent resistivity data. These metrics provided a quantitative assessment of the model's performance and highlighted areas for further optimization or refinement.

4.3.4 Model Training and Evaluation

The CNN model was trained for resistivity inversion over 100 epochs with a batch size of 16. The final training metrics indicated a training loss of 46,064.20 and a MAE of 156.71, while the validation metrics showed a significantly higher validation loss of 165,696.27 and validation MAE of 296.05.

These results suggest potential overfitting, as the model performed better on the training set than on the validation set.

An additional evaluation on a separate test dataset yielded a test loss of 164,884.58 and a test MAE of 295.24. These test results confirm that the CNN model has some capacity for resistivity inversion but struggles to accurately predict resistivity distributions, especially in regions with complex patterns or discontinuities.

To improve the model's performance, expanding the dataset to include a wider variety of resistivity scenarios could be beneficial. A larger, more diverse dataset might help the CNN model learn more robust patterns and enhance its ability to generalize, thereby improving inversion accuracy in complex permafrost regions.

The training and validation loss curves (figure 4.5) and MAE curves (figure 4.6) display a divergence between training and validation results, supporting the hypothesis of overfitting.

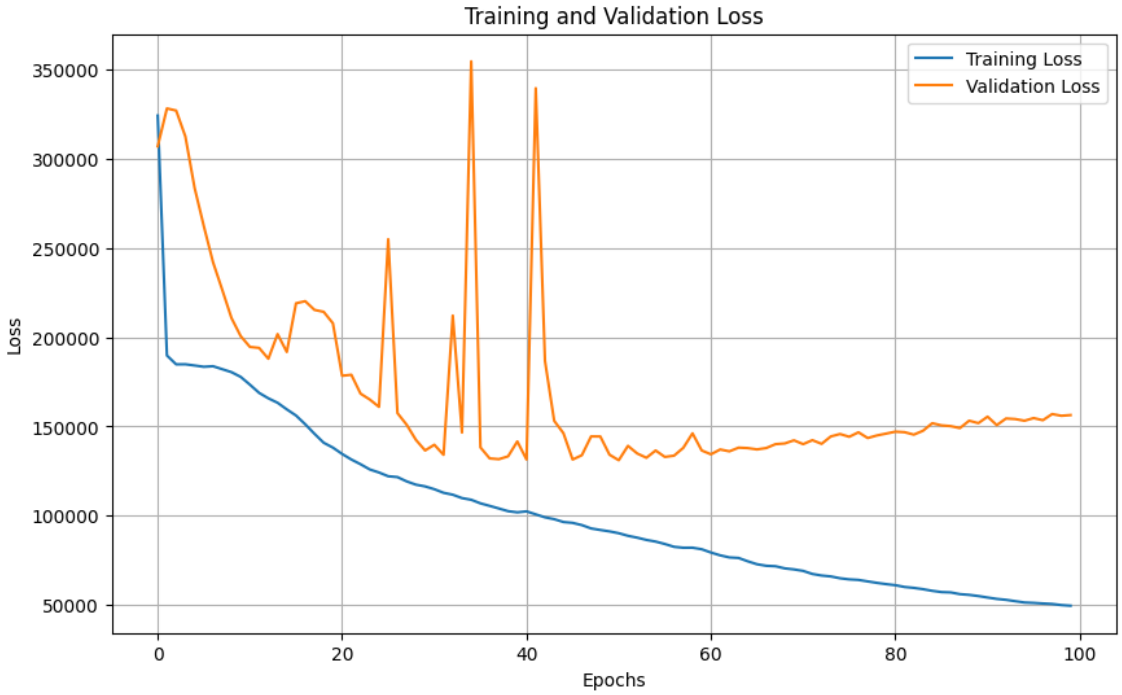

Figure 4.5 - Training and validation loss curves over the 100 training epochs

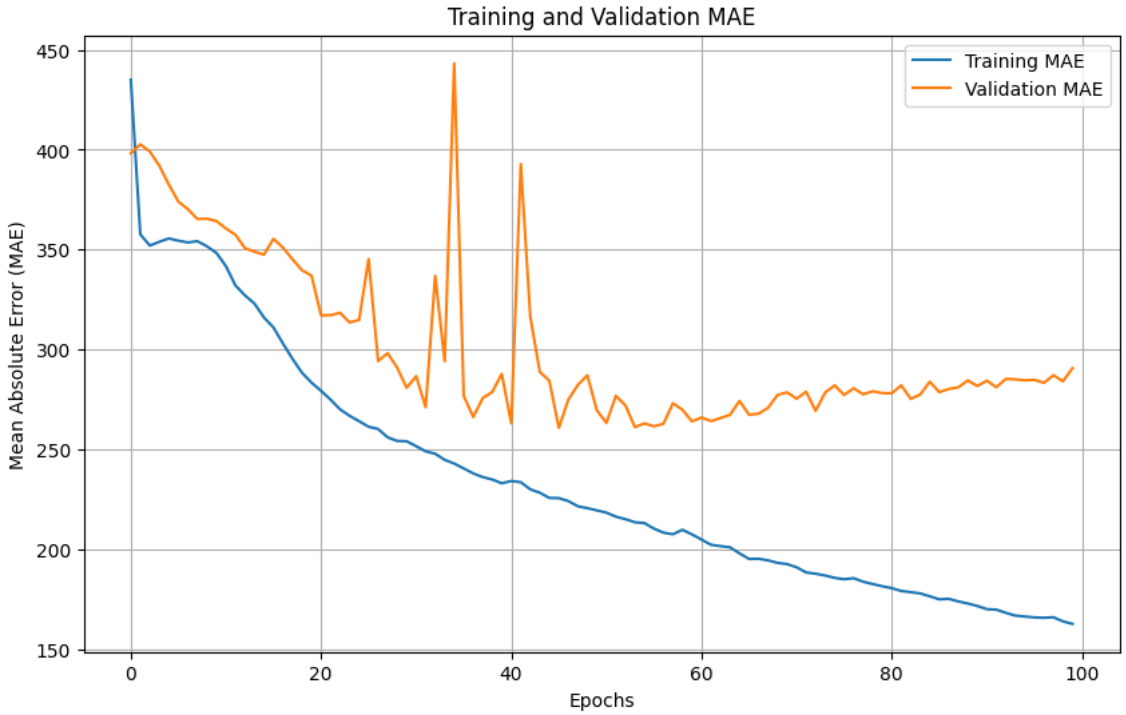

Figure 4.6 - Training and validation MAE curves over the 100 training epochs

4.3.5 Model Inversion Examples on Unseen Data

Despite some overfitting observed during training, the proposed CNN inversion model demonstrates promising performance on unseen data. Figures 4.7 to 4.16 present examples of actual resistivity models of permafrost, alongside results obtained from both the conventional inversion technique and the proposed CNN inversion model.

The comparison illustrates the CNN model's potential in capturing complex resistivity discontinuities, which are often challenging for traditional inversion methods to resolve accurately. The CNN model's ability to detect these discontinuities highlights its applicability in real-time imaging, offering a more detailed representation of subsurface structures in permafrost regions. This capability could be particularly valuable in applications where rapid, reliable imaging is essential for geotechnical and environmental assessments.

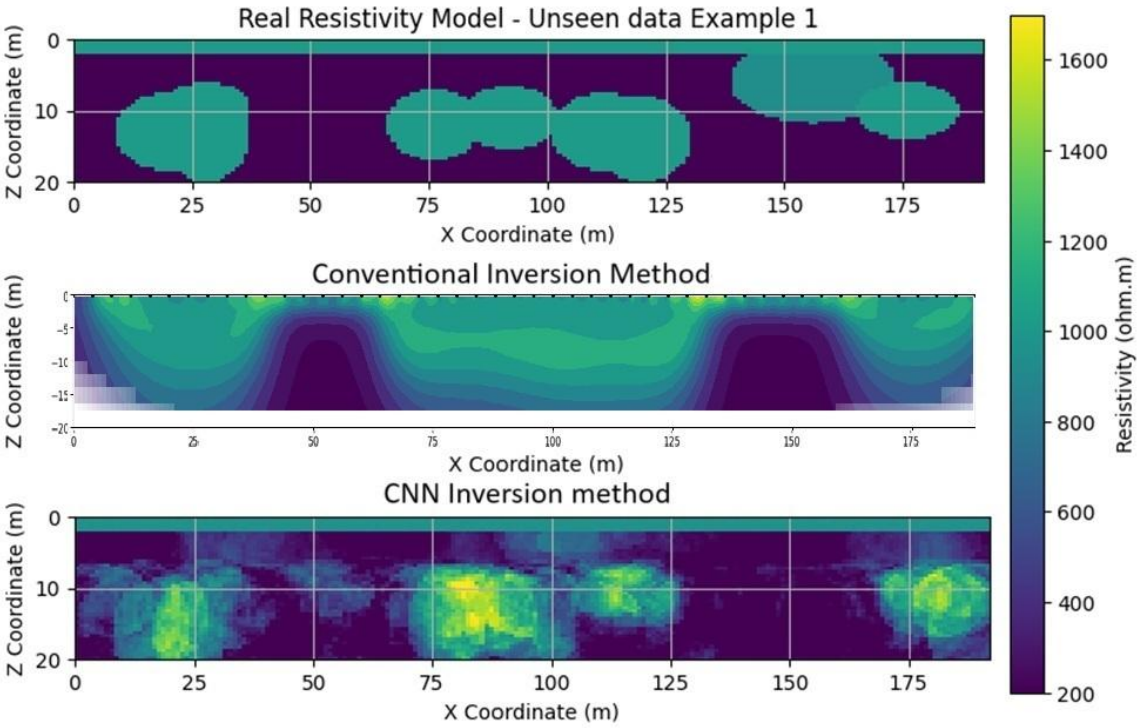

Figure 4.7 - Comparison between the CNN inversion and conventional inversion methods 1st example

In Figure 4.7, the comparison between the real resistivity model, conventional inversion method, and CNN inversion method highlights the performance of both approaches in reconstructing subsurface resistivity distributions. The conventional inversion method (middle) provides a smoother resistivity distribution but struggles to accurately capture sharp boundaries and smaller-scale resistivity variations. This results in a loss of detail and potential underrepresentation of localized resistivity anomalies.

On the other hand, the CNN inversion method (bottom) demonstrates a significant improvement in detecting fine details and capturing the true resistivity patterns, including sharp transitions and localized anomalies. Although some artifacts are present, the CNN inversion aligns more closely with the real resistivity model than the conventional method.

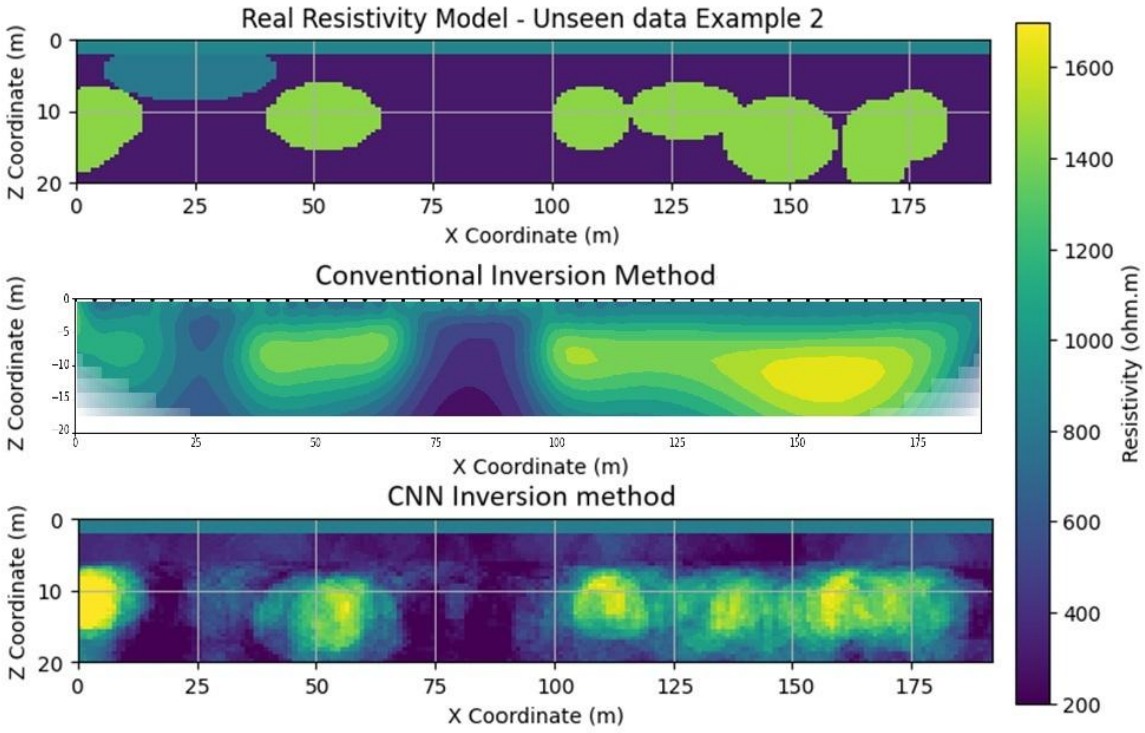

Figure 4.8 - Comparison between the CNN inversion and conventional inversion methods 2nd example

In Figure 4.8, the conventional inversion method (middle panel) provides a smoothed representation of these regions, where resistivity transitions are more gradual, and some high-resistivity zones are either underestimated or blended with surrounding areas. This smoothing effect is consistent with the conventional inversion's tendency to regularize the solution, sacrificing localized details for broader continuity.

Compared to the conventional method, the CNN inversion (bottom panel) offers a sharper depiction of resistivity variations, successfully reconstructing the spatial characteristics and preserving boundary transitions. While the CNN approach shows enhanced localization of resistivity zones compared to the traditional method, the results here exhibit slightly less precision in capturing some finer variations compared to Figure 4.7. This difference may indicate how the CNN adapts differently depending on the complexity or overlap of resistivity features in unseen datasets.

Relative to Figure 4.7, this example emphasizes how the CNN excels in identifying multiple overlapping or closely spaced resistive regions, demonstrating its adaptability across various conditions. However, it also reflects that its performance may vary slightly depending on the density and distribution of resistivity anomalies, offering a trade-off between preserving resolution and managing noise. The conventional approach, on the other hand, continues to struggle with resolving finer resistivity patterns, showing similar limitations as in the prior example. Together, these results highlight the CNN's superior potential for reconstructing complex resistivity distributions over traditional methods, though both approaches require careful interpretation depending on application context.

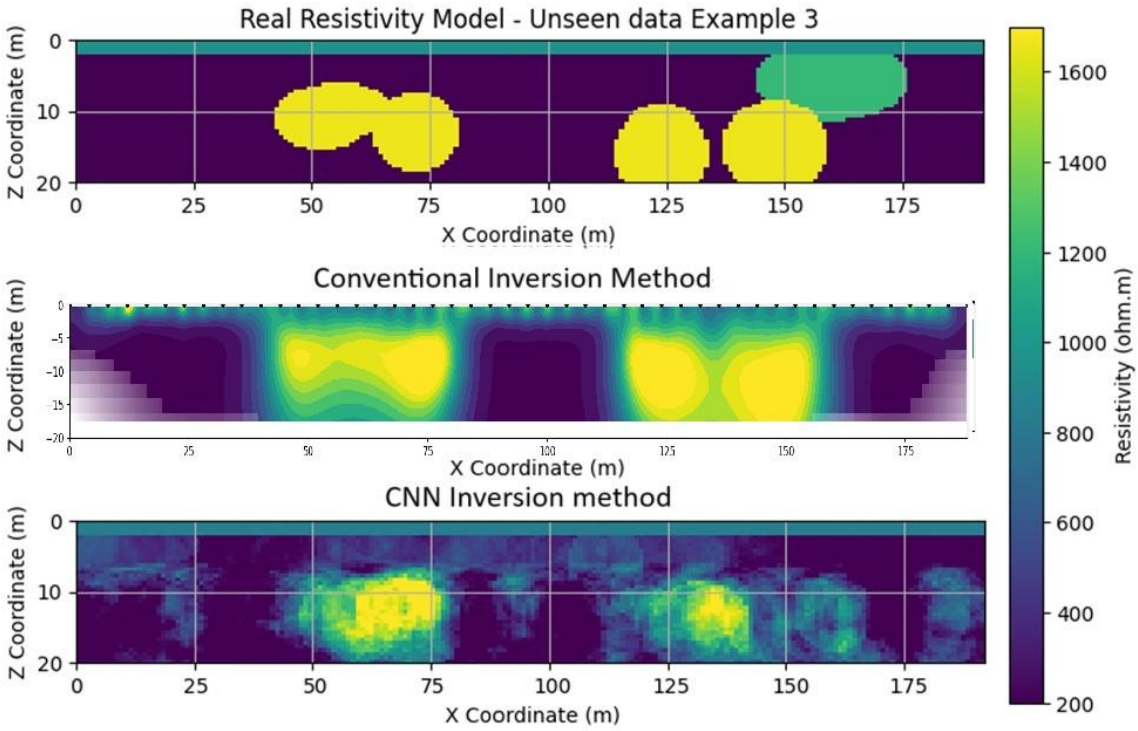

Figure 4.9 - Comparison between the CNN inversion and conventional inversion methods 3rd example

In Figure 4.9, the real resistivity model (top panel) represents a configuration with distinct high-resistivity regions characterized by sharper boundaries and varied spatial distribution. The conventional inversion method (middle panel) again exhibits its limitation in resolving abrupt transitions, as the sharp resistive boundaries appear blurred, and resistive zones are over-smoothed, blending with adjacent regions. This smoothing tendency persists across the examples, highlighting the limitations of conventional inversion in capturing localized features.

The CNN inversion (bottom panel) shows a notable improvement in reconstructing the resistivity profile, with sharper delineation of resistive regions and a better match to the real resistivity model. However, in this example, there are slight inaccuracies in reconstructing the geometry of smaller resistive zones compared to the earlier cases (Figures 4.7 and 4.8), suggesting that the CNN may face challenges when dealing with irregular or compact resistive features.

Compared to the previous examples, this figure illustrates how the CNN inversion remains consistent in capturing the primary resistive regions while showing some variability in resolving smaller or overlapping anomalies. Unlike the conventional method, which remains prone to over-smoothing, the CNN demonstrates adaptability across various scenarios. However, it also reveals the need for further refinement in handling cases with more intricate geometries or closely spaced anomalies.

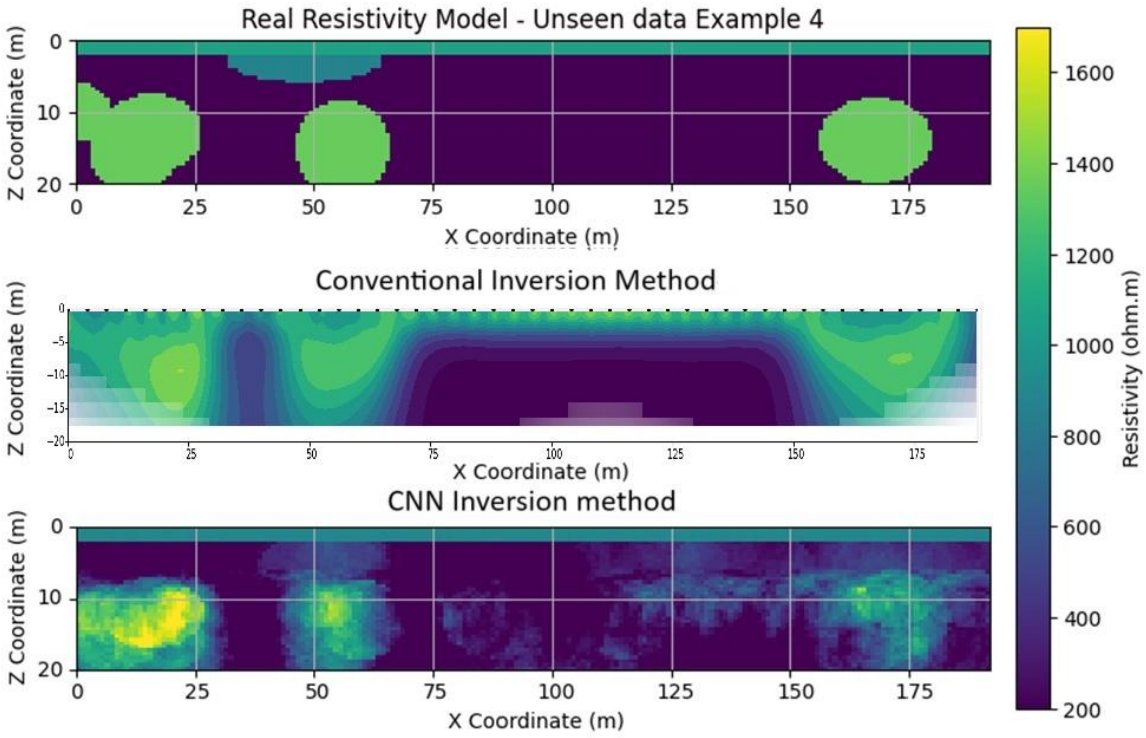

Figure 4.10 - Comparison between the CNN inversion and conventional inversion methods 4th example

In figure 4.10, the CNN inversion method (bottom panel) continues to show superior performance in identifying and reconstructing the resistive zones with greater precision and clarity. While minor discrepancies exist in capturing the exact shape and edges of some resistive regions, the CNN generally retains the spatial layout and intensity closer to the real model compared to the conventional approach. Notably, the CNN inversion captures smaller resistive features, which are almost entirely absent in the conventional inversion output.

Compared to the previous examples, Figure 4.10 demonstrates the CNN's consistent ability to adapt to different configurations, providing more accurate and detailed reconstructions. The conventional method's results remain largely unchanged in their smoothing tendency, further emphasizing the CNN's advantage in handling more intricate resistivity distributions.

The CNN's difficulty in detecting the uppermost features in these figures can be attributed to the size and composition of the dataset used for training. The dataset likely contains a higher density of data points from deeper regions of the models, as these are typically more abundant in synthetic datasets generated for geophysical studies. This imbalance in data representation causes the model to become more sensitive to patterns and features associated with deeper regions, while it struggles to adequately learn the characteristics of shallow, near-surface structures.

Furthermore, the lack of sufficient data for the uppermost regions may limit the model's ability to generalize to these features, especially when the training process prioritizes minimizing overall error. Since deeper regions contribute more significantly to the total resistivity profile in most cases, the model inherently focuses on learning these patterns at the expense of shallower details.

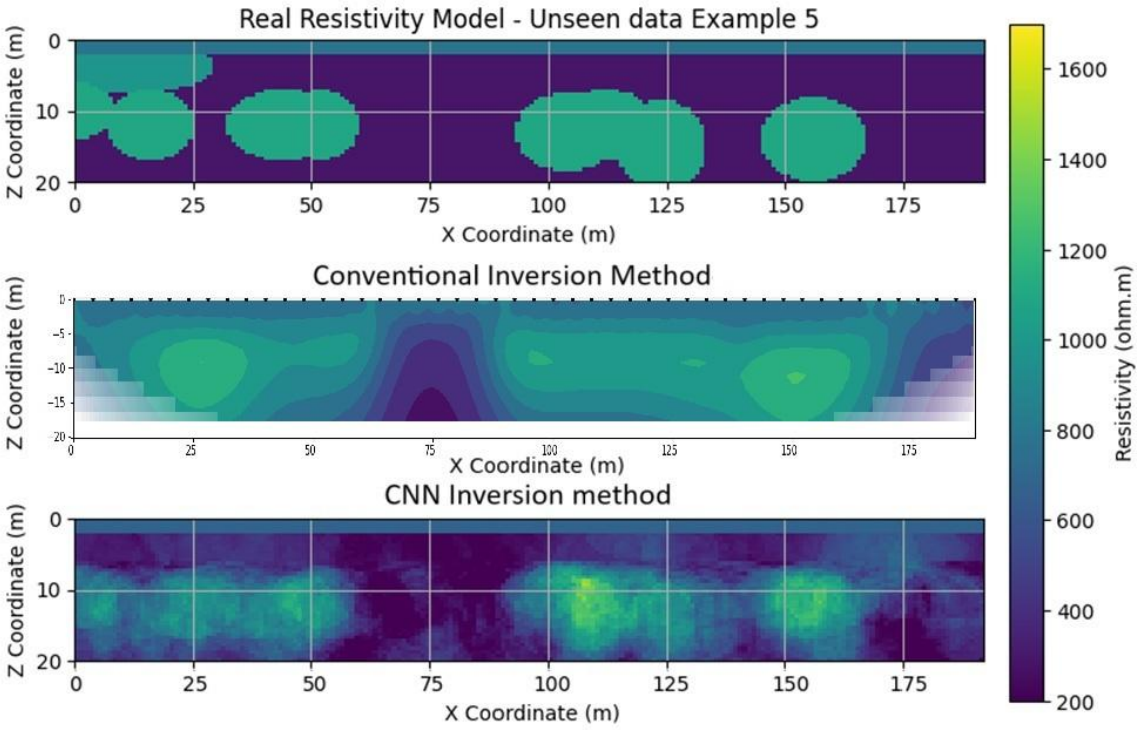

Figure 4.11 - Comparison between the CNN inversion and conventional inversion methods 5th example

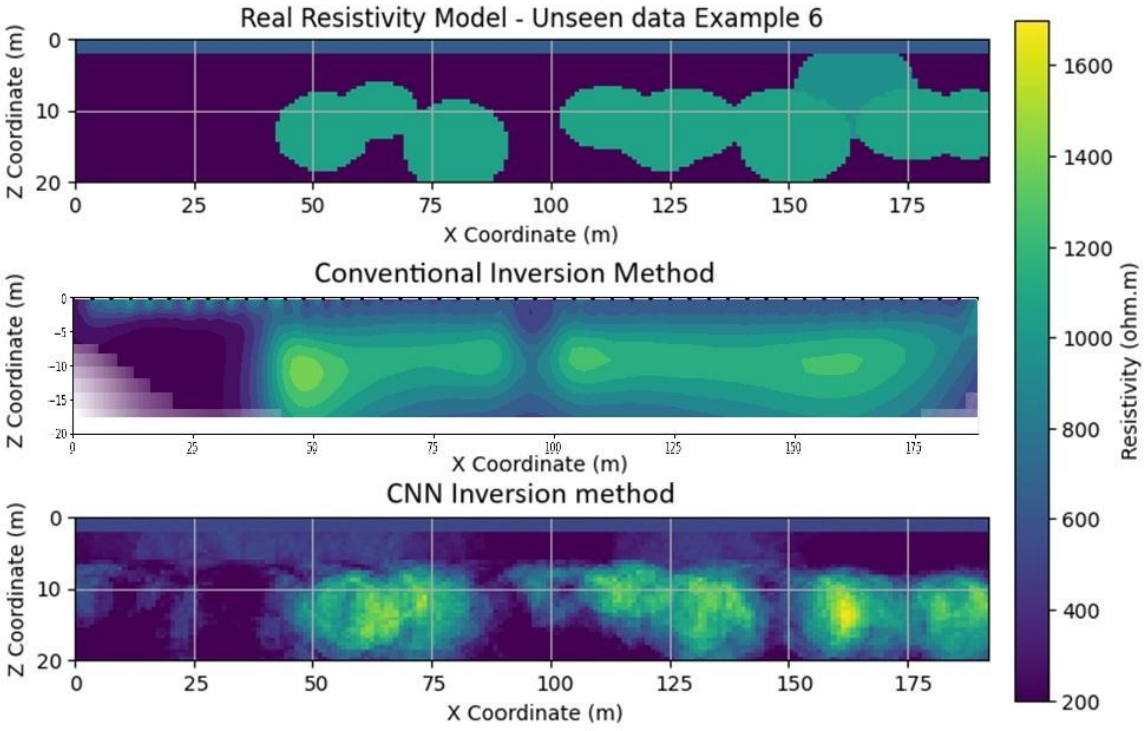

Figure 4.12 - Comparison between the CNN inversion and conventional inversion methods 6th example

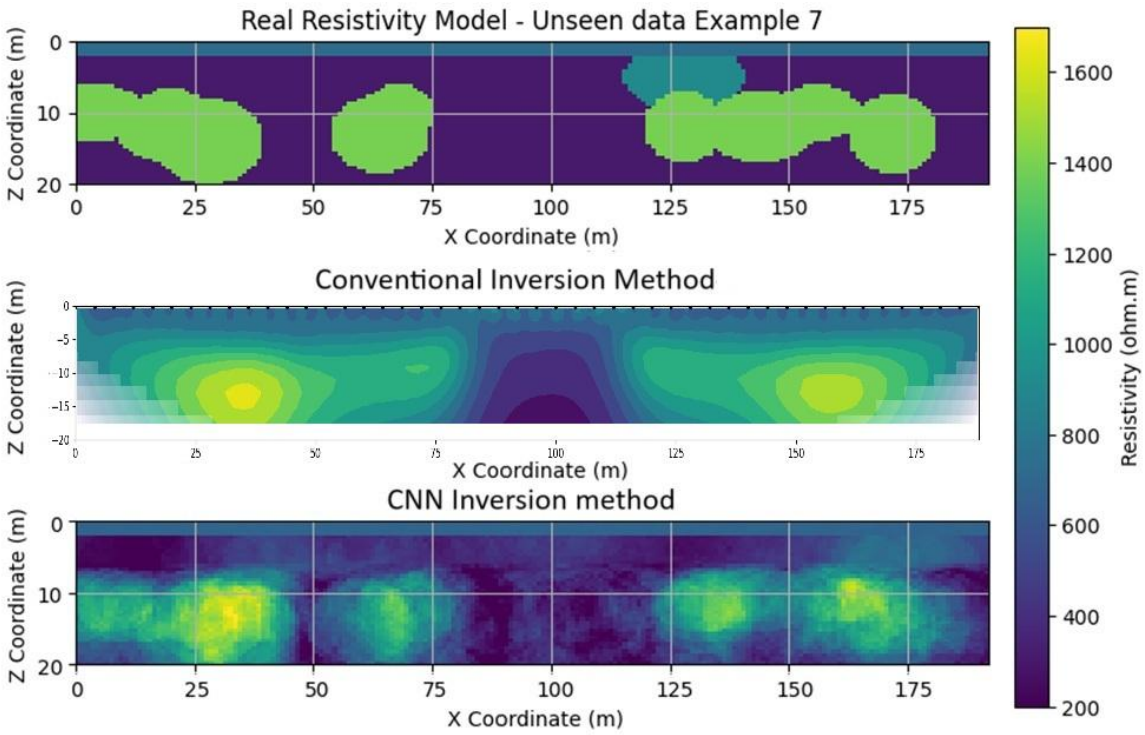

Figure 4.13 - Comparison between the CNN inversion and conventional inversion methods 7th example

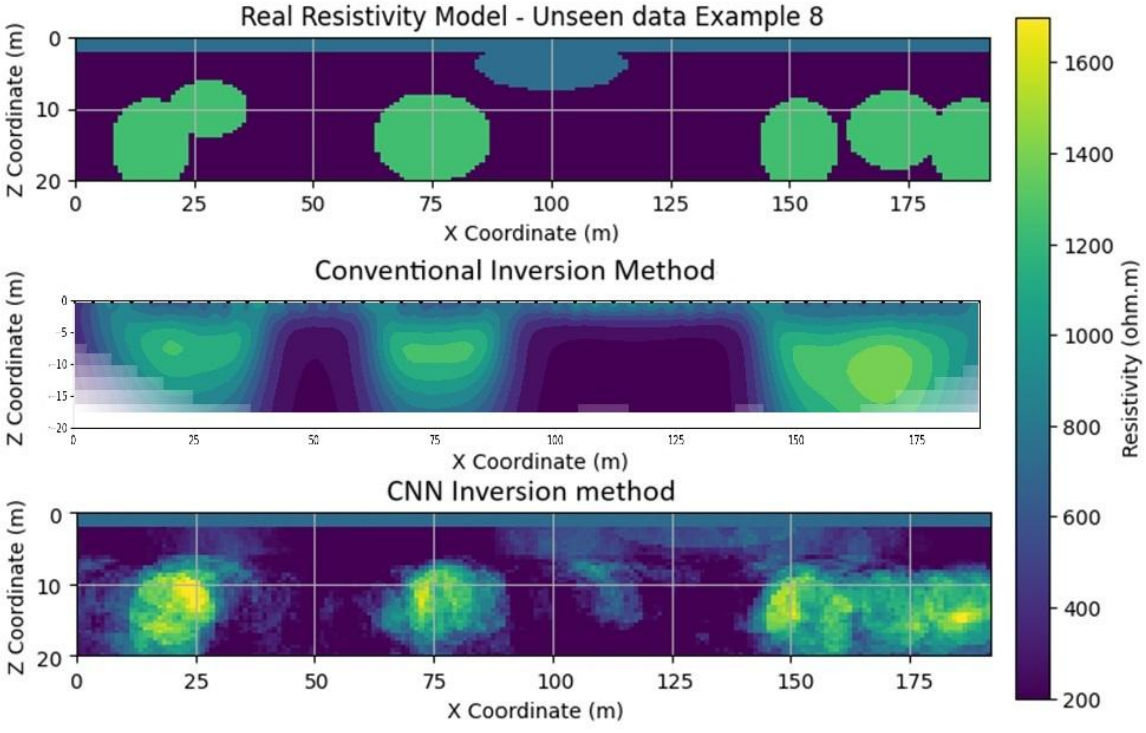

Figure 4.14 - Comparison between the CNN inversion and conventional inversion methods 8th example

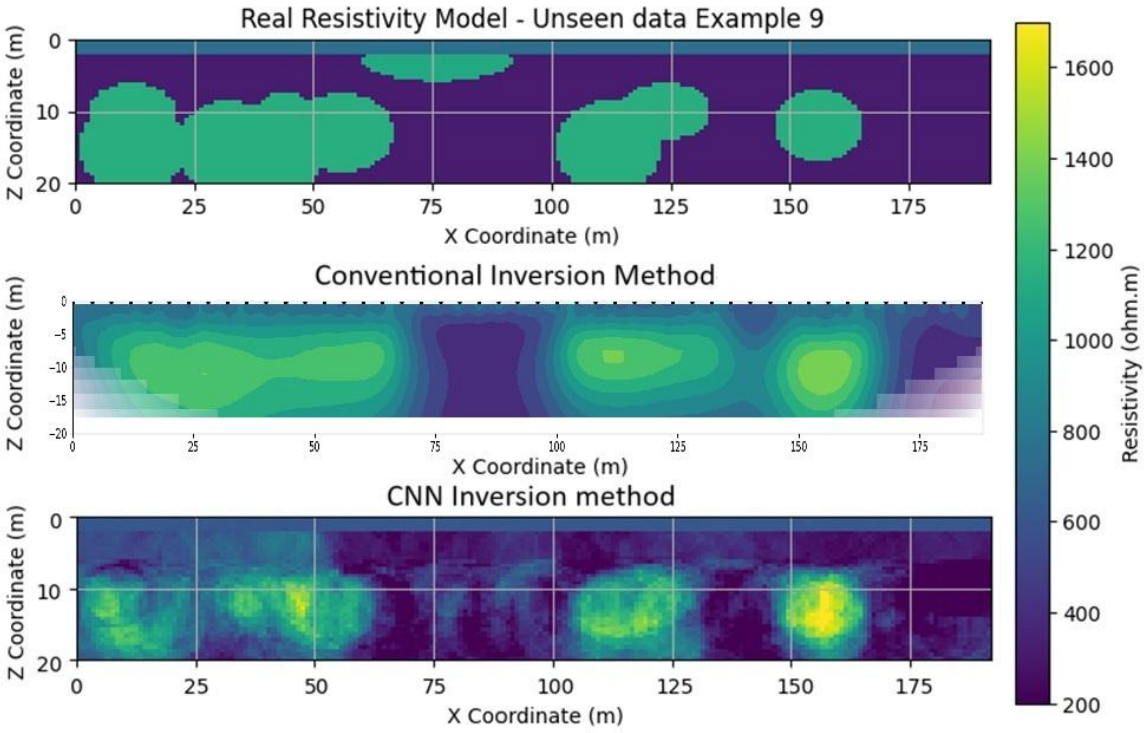

Figure 4.15 - Comparison between the CNN inversion and conventional inversion methods 9th example

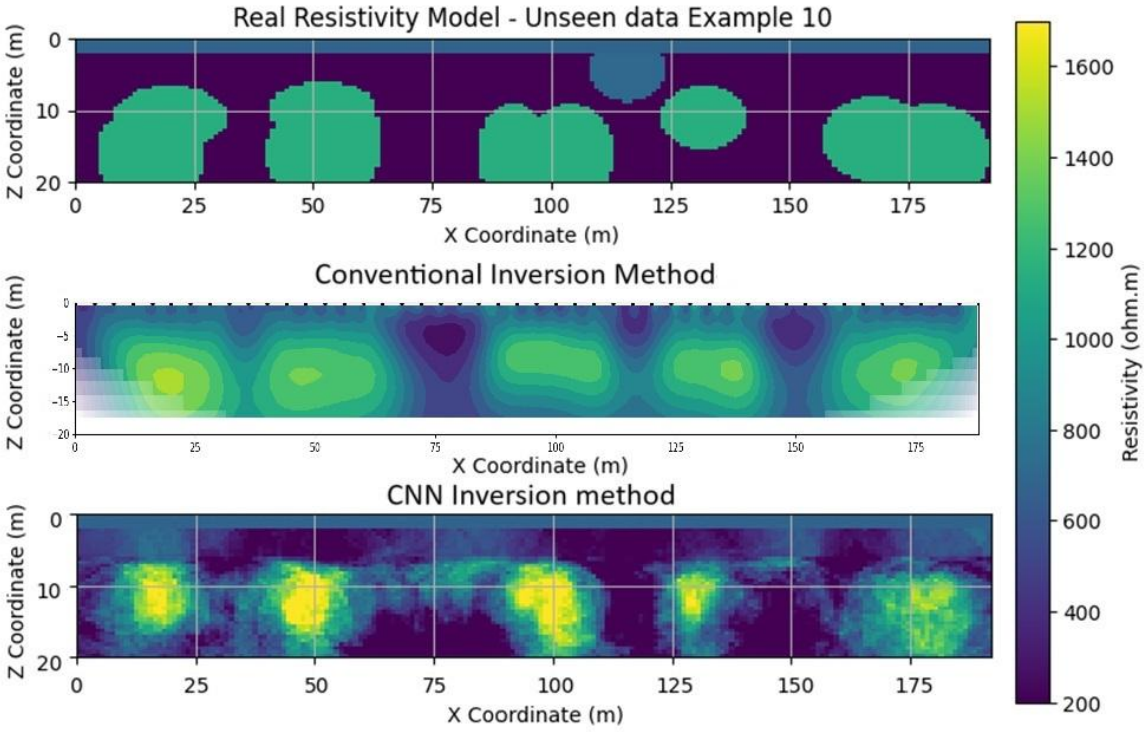

Figure 4.16 - Comparison between the CNN inversion and conventional inversion methods 10th example

The illustrations reveal that the conventional inversion method tends to produce a smoother resistivity map, capturing general resistivity zones but often failing to resolve finer discontinuities or intricate resistivity details. This results in a blurred or averaged interpretation, especially in areas where the permafrost layer is interspersed with thawed zones.

In contrast, the CNN model demonstrates a strong capability to capture more localized resistivity variations, providing a closer approximation to the actual resistivity model and highlighting discontinuities more effectively. The CNN method yields finer spatial details, showing potential for real-time imaging of resistivity structures. However, challenges remain, as the CNN output can sometimes include artifacts or show less precise boundaries compared to the ground truth.

The CNN-based inversion method thus shows considerable promise for identifying discontinuities and complex resistivity structures, which are crucial in permafrost mapping applications. While the CNN model's performance is promising, further improvements—such as additional data and optimized training—could enhance boundary precision and reduce artifacts. Meanwhile, the conventional method, although stable, lacks the spatial resolution required for high-detail mapping. This comparison underscores the CNN model's advantage in scenarios that demand rapid and detailed resistivity mapping, highlighting its value in capturing the intricate heterogeneity characteristic of permafrost regions.

Chapter 5: Discussion and conclusion

Summary: This chapter outlines the critical discussions and limitations observed throughout the study, focusing on the challenges in predicting the petrophysical properties of permafrost, limitations in the temperature and water content prediction models, and the constraints of the CNN-based inversion methodology. It also provides directions for future work to address these limitations.

5.1 Discussion

This study explored the application of ML and geophysical methods to monitor permafrost regions, focusing on predicting the resistivity of frozen soil, modeling permafrost characteristics, and improving resistivity inversion techniques. The key findings are as follows:

1. Resistivity Prediction Models: The Neural Network model demonstrated superior performance in predicting the resistivity of frozen soil, achieving the highest R^2 score (0.975) and the lowest error metrics among all tested models. The model effectively captured the complex relationships between soil properties (temperature, dry density, water content) and resistivity, closely aligning with experimental data from Shan et al. (2015). Random Forest and Gradient Boosting models also showed strong predictive capabilities but were slightly less accurate than the Neural Network.

2. Generation and Inversion of 2D Permafrost Models: Synthetic 2D models representing permafrost regions with discontinuities were successfully generated, incorporating layers like the active layer, thaw layer, permafrost, and base layer with realistic properties. Conventional inversion methods, using the Wenner-Schlumberger array configuration, were able to map large-scale resistivity patterns but struggled to resolve finer discontinuities within permafrost regions.

3. Permafrost Resistivity Prediction: Tree-based models, particularly Random Forest and Gradient Boosting, were most effective in predicting permafrost resistivity from synthetic data, achieving moderate R^2 scores (0.5882 and 0.5501, respectively). Linear Regression and SVR models underperformed, indicating their limitations in handling the non-linear relationships present in the data.

4. Temperature and Water Content Prediction: ML models showed moderate performance in predicting temperature within permafrost regions, with the Support Vector Regressor using MaxAbsScaler achieving the highest R^2 score (0.5071). Models struggled to accurately predict water content, with negative R^2 scores suggesting poor model fit and reliability. The dependency on previously predicted resistivity values introduced biases, highlighting a methodological limitation.

5. CNN Model for Resistivity Inversion: A CNN model was developed for resistivity inversion, transforming apparent resistivity data into true resistivity distributions with enhanced accuracy. The CNN outperformed conventional inversion methods, effectively capturing complex resistivity discontinuities and providing detailed subsurface imaging. While overfitting was observed, the model showed promise in resolving sharp boundaries and localized anomalies within permafrost regions.

5.2 Limitation

- Predicting resistivity of frozen soil and feature selection:

A significant limitation in predicting the resistivity of frozen soil lies in the difficulty of determining appropriate petrophysical properties. The current methodology relies on a limited dataset, primarily digitized from published experimental results. While this provides a foundational framework, predicting resistivity based on such constrained properties may not capture the full complexity of frozen soil behavior.

Key factors, such as porosity, grain size distribution, and mineral composition, were excluded from the model due to the unavailability of data. Including these properties could lead to a more robust and comprehensive model. However, achieving this would require extensive experimental efforts across diverse permafrost regions to quantify these additional parameters under varying environmental conditions. Such efforts are critical to developing a universally applicable and precise model for predicting frozen soil resistivity.

- Temperature and Water Content Prediction Models

The methodology for predicting temperature and water content using ML models demonstrated moderate accuracy but revealed inherent limitations. A critical issue is the reliance on predicted resistivity values as input features for these models. These resistivity values were derived using the best-performing model trained on 80% of the dataset, resulting in a significant proportion of "seen" data being used for subsequent predictions. This introduces potential biases, inflating the model's performance metrics and reducing its generalizability to real-world scenarios.

Moreover, the absence of additional critical features such as porosity, grain size distribution, and thermal conductivity further limits the accuracy of temperature and water content predictions. Future efforts should focus on incorporating such features, supported by field data, to develop more reliable and generalizable models.

- CNN Inversion Models

The CNN-based inversion model exhibited promising results in reconstructing resistivity distributions with fine spatial details and capturing complex discontinuities within permafrost regions. However, several limitations must be addressed:

1. Overfitting: The training process indicated signs of overfitting, as the model performed better on the training data than on the validation or test sets. This suggests the need for a richer and more diverse dataset to improve the model's generalization capabilities.
2. Dependency on Fixed Configurations: The CNN inversion model was trained on data generated with fixed configurations, such as specific electrode sequences, spacing, and mesh sizes. Any changes to these configurations significantly influenced the model's performance, highlighting its limited adaptability compared to conventional inversion techniques, which can be adjusted dynamically.
3. Lack of Real Data Validation: While the CNN model was tested on synthetic data, the absence of real electrical resistivity data corresponding to the assumed configurations represents a critical limitation. The inability to validate the model with real-world data restricts its applicability and reliability in practical scenarios. Future studies should prioritize applying CNN inversion techniques to real datasets to assess their robustness and performance under real-world conditions.

5.3 Implications and Future Directions

The initial goal of this thesis was to predict the petrophysical properties of permafrost using electrical resistivity models and ML techniques. While the study achieved significant progress, the following areas require further exploration:

- Expanded Experimental Datasets: Developing a robust predictive model for frozen soil resistivity necessitates broader experimental data, including additional properties such as porosity, grain size distribution, and mineral composition.
- Generalization of CNN Models: Addressing overfitting in CNN inversion models through the development of richer, more varied datasets is essential. Incorporating multiple configurations for electrode spacing, sequences, and mesh sizes could enhance the adaptability and generalizability of these models.
- Integration of Real Data: Future studies should focus on acquiring real electrical resistivity datasets corresponding to the assumed configurations. This would enable a direct evaluation of the CNN inversion model's performance in real-world scenarios, bridging the gap between synthetic and field data.
- Refinement of Temperature and Water Content Models: Incorporating additional features, such as porosity and thermal conductivity, into the temperature and water content prediction models could improve their accuracy. A move towards more advanced feature engineering and validation on unseen datasets is necessary.

5.4 Conclusion

This study highlights the potential of ML and CNN-based inversion techniques for modeling the complex properties of permafrost. However, the limitations identified underscore the need for extensive data collection, methodological refinement, and validation on real-world datasets. Addressing these challenges is crucial for advancing the application of ML in permafrost research, enabling more accurate predictions and effective monitoring of these critical environments.

References (Bibliography)

- Afan, H., Ibrahem Ahmed Osman, A., Essam, Y., Ali Najah Ahmed, A.-M., Huang, Y., Kisi, O., Sherif, M., Sefelnasr, A., Chau, K., & El-Shafie, A. (2021). Modeling the fluctuations of groundwater level by employing ensemble deep learning techniques. *Engineering Applications of Computational Fluid Mechanics*, *15*, 1420–1439. https://doi.org/10.1080/19942060.2021.1974093
- Auken, E., Christiansen, A. V., Kirkegaard, C., Fiandaca, G., Schamper, C., Behroozmand, A. A., Binley, A., Nielsen, E., Effersø, F., Christensen, N. B., Sørensen, K., Foged, N., & Vignoli, G. (2015). An overview of a highly versatile forward and stable inverse algorithm for airborne, ground-based and borehole electromagnetic and electric data. Exploration Geophysics, 46(3), 223–235. https://doi.org/10.1071/EG13097
- Baral, P., & Haq, M. A. (2020). Spatial prediction of permafrost occurrence in Sikkim Himalayas using logistic regression, random forests, support vector machines and neural networks. Geomorphology, 371, 107331. https://doi.org/https://doi.org/10.1016/j.geomorph.2020.107331
- Biskaborn, B. K., Smith, S. L., Noetzli, J., Matthes, H., Vieira, G., Streletskiy, D. A., Schoeneich, P., Romanovsky, V. E., Lewkowicz, A. G., Abramov, A., Allard, M., Boike, J., Cable, W. L., Christiansen, H. H., Delaloye, R., Diekmann, B., Drozdov, D., Etzelmüller, B., Grosse, G., … Lantuit, H. (2019). Permafrost is warming at a global scale. Nature Communications, 10(1), 264. https://doi.org/10.1038/s41467-018-08240-4
- Blanchy, G., Saneiyan, S., Boyd, J., McLachlan, P., & Binley, A. (2020). ResIPy, an intuitive open source software for complex geoelectrical inversion/modeling. Computers & Geosciences, 137, 104423.
- Buckel, J., Mudler, J., Gardeweg, R., Hauck, C., Hilbich, C., Frauenfelder, R., Kneisel, C., Buchelt, S., Blöthe, J. H., Hördt, A., & Bücker, M. (2023). Identifying mountain permafrost degradation by repeating historical electrical resistivity tomography (ERT) measurements. The Cryosphere, 17(7), 2919–2940. https://doi.org/10.5194/tc-17-2919-2023
- Buckel, J., Reinosch, E., Hördt, A., Zhang, F., Riedel, B., Gerke, M., Schwalb, A., & Mäusbacher, R. (2021). Insights into a remote cryosphere: a multi-method approach to assess permafrost occurrence at the Qugaqie basin, western Nyainqêntanglha Range, Tibetan Plateau. The Cryosphere, 15(1), 149–168.
- Christensen, L. (2019). *Robot Navigation in Distorted Magnetic Fields*.
- Dahlin, T. (2001). The development of DC resistivity imaging techniques. Computers & Geosciences, 27(9), 1019–1029. https://doi.org/https://doi.org/10.1016/S0098-3004(00)00160-6
- Dahlin, T., & Zhou, B. (2004). A numerical comparison of 2D resistivity imaging with 10 electrode arrays. Geophysical Prospecting, 52(5), 379–398.
- Delaloye, R., & Lambiel, C. (2005). Evidence of winter ascending air circulation throughout talus slopes and rock glaciers situated in the lower belt of alpine discontinuous permafrost (Swiss Alps). Norsk Geografisk Tidsskrift-Norwegian Journal of Geography, 59(2), 194–203.
- Dobinski, W. (2006). Ice and environment: A terminological discussion. Earth-Science Reviews, 79(3), 229–240. https://doi.org/https://doi.org/10.1016/j.earscirev.2006.07.003
- Dobinski, W. (2011). Permafrost. Earth-Science Reviews, 108(3), 158–169. https://doi.org/https://doi.org/10.1016/j.earscirev.2011.06.007
- Everdigen, R. O. van. (1998). Definitions. Multi-language Glossary of Permafrost and Related Ground-ice Terms. International Permafrost Association, University of Calgary, 1–78.
- French, H. M. (2017). The periglacial environment. John Wiley & Sons.
- Hauck, C. (2013). New Concepts in Geophysical Surveying and Data Interpretation for Permafrost Terrain. Permafrost and Periglacial Processes, 24(2), 131–137. https://doi.org/https://doi.org/10.1002/ppp.1774

- Hauck, C., & Hilbich, C. (2024). Preconditioning of mountain permafrost towards degradation detected by electrical resistivity. Environmental Research Letters, 19(6), 64010. https://doi.org/10.1088/1748-9326/ad3c55
- Herring, T., & Lewkowicz, A. G. (2022). A systematic evaluation of electrical resistivity tomography for permafrost interface detection using forward modeling. Permafrost and Periglacial Processes, 33(2), 134–146. https://doi.org/https://doi.org/10.1002/ppp.2141
- Herring, T., Lewkowicz, A. G., Hauck, C., Hilbich, C., Mollaret, C., Oldenborger, G. A., Uhlemann, S., Farzamian, M., Calmels, F., & Scandroglio, R. (2023). Best practices for using electrical resistivity tomography to investigate permafrost. Permafrost and Periglacial Processes, 34(4), 494–512. https://doi.org/https://doi.org/10.1002/ppp.2207
- Hilbich, C., Hauck, C., Hoelzle, M., Scherler, M., Schudel, L., Völksch, I., Vonder Mühll, D., & Mäusbacher, R. (2008). Monitoring mountain permafrost evolution using electrical resistivity tomography: A 7-year study of seasonal, annual, and long-term variations at Schilthorn, Swiss Alps. Journal of Geophysical Research: Earth Surface, 113(F1). https://doi.org/https://doi.org/10.1029/2007JF000799
- Hilbich, C., Marescot, L., Hauck, C., Loke, M. H., & Mäusbacher, R. (2009). Applicability of electrical resistivity tomography monitoring to coarse blocky and ice-rich permafrost landforms. Permafrost and Periglacial Processes, 20(3), 269–284.
- Hjort, J., Streletskiy, D., Doré, G., Wu, Q., Bjella, K., & Luoto, M. (2022). Impacts of permafrost degradation on infrastructure. Nature Reviews Earth & Environment, 3(1), 24–38. https://doi.org/10.1038/s43017-021-00247-8
- Jin, X.-Y., Jin, H.-J., Iwahana, G., Marchenko, S. S., Luo, D.-L., Li, X.-Y., & Liang, S.-H. (2021). Impacts of climate-induced permafrost degradation on vegetation: A review. Advances in Climate Change Research, 12(1), 29–47. https://doi.org/https://doi.org/10.1016/j.accre.2020.07.002
- Jorgenson, M. T., Douglas, T. A., Liljedahl, A. K., Roth, J. E., Cater, T. C., Davis, W. A., Frost, G. v, Miller, P. F., & Racine, C. H. (2020). The Roles of Climate Extremes, Ecological Succession, and Hydrology in Repeated Permafrost Aggradation and Degradation in Fens on the Tanana Flats, Alaska. Journal of Geophysical Research: Biogeosciences, 125(12), e2020JG005824. https://doi.org/https://doi.org/10.1029/2020JG005824
- Jorgenson, M. T., Romanovsky, V., Harden, J., Shur, Y., O'Donnell, J., Schuur, E. A. G., Kanevskiy, M., & Marchenko, S. (2010). Resilience and vulnerability of permafrost to climate change. Canadian Journal of Forest Research, 40(7), 1219–1236. https://doi.org/10.1139/X10-060
- Kneisel, C., Emmert, A., & Kästl, J. (2014). Application of 3D electrical resistivity imaging for mapping frozen ground conditions exemplified by three case studies. Geomorphology, 210, 71–82. https://doi.org/https://doi.org/10.1016/j.geomorph.2013.12.022
- Kneisel, C., Emmert, A., Polich, P., Zollinger, B., & Egli, M. (2015). Soil geomorphology and frozen ground conditions at a subalpine talus slope having permafrost in the eastern Swiss Alps. CATENA, 133, 107–118. https://doi.org/https://doi.org/10.1016/j.catena.2015.05.005
- Kneisel, C., Hauck, C., Fortier, R., & Moorman, B. (2008). Advances in geophysical methods for permafrost investigations. Permafrost and Periglacial Processes, 19(2), 157–178. https://doi.org/https://doi.org/10.1002/ppp.616
- Krautblatter, M., Verleysdonk, S., Flores-Orozco, A., & Kemna, A. (2010). Temperature-calibrated imaging of seasonal changes in permafrost rock walls by quantitative electrical resistivity tomography (Zugspitze, German/Austrian Alps). Journal of Geophysical Research: Earth Surface, 115(F2). https://doi.org/https://doi.org/10.1029/2008JF001209
- Liu, B., Guo, Q., Li, S., Liu, B., Ren, Y., Pang, Y., Guo, X., Liu, L., & Jiang, P. (2020). Deep learning inversion of electrical resistivity data. IEEE Transactions on Geoscience and Remote Sensing, 58(8), 5715–5728.

- Liu, Q., Niu, J., Lu, P., Dong, F., Zhou, F., Meng, X., Xu, W., Li, S., & Hu, B. X. (2022). Interannual and seasonal variations of permafrost thaw depth on the Qinghai-Tibetan Plateau: A comparative study using long short-term memory, CNN, and random forest. Science of The Total Environment, 838, 155886. https://doi.org/https://doi.org/10.1016/j.scitotenv.2022.155886
- Liu, T., Zhang, F., Lin, C., Liang, Z., Wang, G., & Feng, D. (2024). Discontinuous permafrost detection from neural network-ensemble learning based electrical resistivity tomography. Cold Regions Science and Technology, 225, 104266. https://doi.org/https://doi.org/10.1016/j.coldregions.2024.104266
- Loke, M. H., Chambers, J. E., Rucker, D. F., Kuras, O., & Wilkinson, P. B. (2013). Recent developments in the direct-current geoelectrical imaging method. Journal of Applied Geophysics, 95, 135–156.
- Loke, M. H., Rucker, D. F., Chambers, J. E., Wilkinson, P. B., & Kuras, O. (2021). Electrical resistivity surveys and data interpretation. In Encyclopedia of solid earth geophysics (pp. 344–350). Springer.
- Loranty, M. M., Abbott, B. W., Blok, D., Douglas, T. A., Epstein, H. E., Forbes, B. C., Jones, B. M., Kholodov, A. L., Kropp, H., Malhotra, A., Mamet, S. D., Myers-Smith, I. H., Natali, S. M., O'Donnell, J. A., Phoenix, G. K., Rocha, A. v, Sonnentag, O., Tape, K. D., & Walker, D. A. (2018). Reviews and syntheses: Changing ecosystem influences on soil thermal regimes in northern high-latitude permafrost regions. Biogeosciences, 15(17), 5287–5313. https://doi.org/10.5194/bg-15-5287-2018
- McKenzie, J. M., Kurylyk, B. L., Walvoord, M. A., Bense, V. F., Fortier, D., Spence, C., & Grenier, C. (2021). Invited perspective: What lies beneath a changing Arctic? The Cryosphere, 15(1), 479–484. https://doi.org/10.5194/tc-15-479-2021
- Melo, A., & Li, Y. (2021). Geology differentiation by applying unsupervised machine learning to multiple independent geophysical inversions. Geophysical Journal International, 227(3), 2058–2078. https://doi.org/10.1093/gji/ggab316
- Natali, S. M., Bronen, R., Cochran, P., Holdren, J. P., Rogers, B. M., & Treharne, R. (2022). Incorporating permafrost into climate mitigation and adaptation policy. Environmental Research Letters, 17(9), 91001. https://doi.org/10.1088/1748-9326/ac8c5a
- Oldenborger, G. A., & LeBlanc, A.-M. (2018). Monitoring changes in unfrozen water content with electrical resistivity surveys in cold continuous permafrost. Geophysical Journal International, 215(2), 965–977. https://doi.org/10.1093/gji/ggy321
- Ran, Y., Li, X., Cheng, G., Che, J., Aalto, J., Karjalainen, O., Hjort, J., Luoto, M., Jin, H., Obu, J., Hori, M., Yu, Q., & Chang, X. (2022). New high-resolution estimates of the permafrost thermal state and hydrothermal conditions over the Northern Hemisphere. Earth System Science Data, 14(2), 865–884. https://doi.org/10.5194/essd-14-865-2022
- Romanovsky, V. E., Smith, S. L., & Christiansen, H. H. (2010). Permafrost thermal state in the polar Northern Hemisphere during the international polar year 2007–2009: a synthesis. Permafrost and Periglacial Processes, 21(2), 106–116. https://doi.org/https://doi.org/10.1002/ppp.689
- Sathiparan, N., Jeyananthan, P., & Subramaniam, D. (2024). Influence of metakaolin on pervious concrete strength: a machine learning approach with shapley additive explanations. *Multiscale and Multidisciplinary Modeling, Experiments and Design*, *7*. https://doi.org/10.1007/s41939-024-00455-x
- Schmidt, A., Dabas, M., & Sarris, A. (2020). Dreaming of perfect data: Characterizing noise in archaeo-geophysical measurements. Geosciences, 10(10), 382.
- Schuur, E. A. G., Abbott, B. W., Commane, R., Ernakovich, J., Euskirchen, E., Hugelius, G., Grosse, G., Jones, M., Koven, C., Leshyk, V., Lawrence, D., Loranty, M. M., Mauritz, M., Olefeldt, D., Natali, S., Rodenhizer, H., Salmon, V., Schädel, C., Strauss, J., … Turetsky, M.

(2022). Permafrost and Climate Change: Carbon Cycle Feedbacks From the Warming Arctic. Annual Review of Environment and Resources, 47(Volume 47, 2022), 343–371. https://doi.org/https://doi.org/10.1146/annurev-environ-012220-011847

- Schuur, E. A. G., McGuire, A. D., Schädel, C., Grosse, G., Harden, J. W., Hayes, D. J., Hugelius, G., Koven, C. D., Kuhry, P., Lawrence, D. M., Natali, S. M., Olefeldt, D., Romanovsky, V. E., Schaefer, K., Turetsky, M. R., Treat, C. C., & Vonk, J. E. (2015). Climate change and the permafrost carbon feedback. Nature, 520(7546), 171–179. https://doi.org/10.1038/nature14338
- Shan, W., Liu, Y., Hu, Z., & Xiao, J. (2015). A Model for the Electrical Resistivity of Frozen Soils and an Experimental Verification of the Model. Cold Regions Science and Technology, 119, 75–83. https://doi.org/https://doi.org/10.1016/j.coldregions.2015.07.010
- Shiklomanov, N. I., Streletskiy, D. A., Little, J. D., & Nelson, F. E. (2013). Isotropic thaw subsidence in undisturbed permafrost landscapes. Geophysical Research Letters, 40(24), 6356–6361. https://doi.org/https://doi.org/10.1002/2013GL058295
- Shur, Y., Hinkel, K. M., & Nelson, F. E. (2005). The transient layer: implications for geocryology and climate-change science. Permafrost and Periglacial Processes, 16(1), 5–17. https://doi.org/https://doi.org/10.1002/ppp.518
- Thaler, E. A., Uhleman, S., Rowland, J. C., Schwenk, J., Wang, C., Dafflon, B., & Bennett, K. E. (2023). High-Resolution Maps of Near-Surface Permafrost for Three Watersheds on the Seward Peninsula, Alaska Derived From Machine Learning. Earth and Space Science, 10(12), e2023EA003015. https://doi.org/https://doi.org/10.1029/2023EA003015
- Walvoord, M. A., & Kurylyk, B. L. (2016). Hydrologic Impacts of Thawing Permafrost—A Review. Vadose Zone Journal, 15(6), vzj2016.01.0010. https://doi.org/10.2136/vzj2016.01.0010
- Washburn, A. L. (1973). Periglacial processes and environments. Edward Arnold. https://cir.nii.ac.jp/crid/1130000794105701376
- Williams, P. J., & Smith, M. W. (1989). The Frozen Earth: Fundamentals of Geocryology. In *Studies in Polar Research*. Cambridge University Press. https://doi.org/DOI:10.1017/CBO9780511564437
- Xixi, L., Zou, C., Peng, C., & Wu, C. (2023). Uncertainty Quantification in Intelligent-Based Electrical Resistivity Tomography Image Reconstruction With Monte Carlo Dropout Strategy. IEEE Transactions on Geoscience and Remote Sensing, 61, 1–16. https://doi.org/10.1109/TGRS.2023.3262835
- Zhang, M., Li, R., Pei, W., Zhou, Y., Li, G., & Yang, S. (2024). Permafrost Degradation Risk Evaluation in the Qinghai-Tibet Plateau Under Climate Change Based on Machine Learning Models. Journal of Geophysical Research: Atmospheres, 129(2), e2023JD039611. https://doi.org/https://doi.org/10.1029/2023JD039611
- Zhong, S., Wang, Y., Zheng, Y., Wu, S., Chang, X., & Zhu, W. (2021). Electrical resistivity tomography with smooth sparse regularization. Geophysical Prospecting, 69(8–9), 1773–1789.
- Zhuo, J., Hou, X., Xiao, L.-Y., Zhuang, M., Shen, C., & Liu, Q. H. (2023). Machine-Learning Inversion of Resistivity Profiles From Multifrequency Electromagnetic Measurements on Undulating Terrain Surfaces. IEEE Transactions on Geoscience and Remote Sensing, 61, 1–9. https://doi.org/10.1109/TGRS.2023.3333917

Annex 1: Experimental Data Extracted from Shan et al. (2015)

This annex presents the experimental data extracted from Shan et al. (2015), which served as the basis for generating synthetic datasets and training ML models in this study. Tables A1.1 to A1.4 summarize the key data points, including resistivity values, water content, dry density, and temperature ranges.

Table A1.1 - Resistivity Values at -17°C

Temperature (°C)	Dry Density (g/cm³)	Water Content %	Resistivity (ohm-m)
-17	1.8	3.4	960.7
		4.5	647.9
		5.2	471.1
		6.3	412.2
		7.6	422.3
		8.9	497.5
		9.7	519.9
	1.7	3.5	1007.5
		4.7	670.2
		5.4	513.8
		6.7	458.9
		8.0	458.9
		9.4	523.9
		10.2	544.2
		11.8	615.4
	1.61	3.8	1072.5
		5.0	719.0
		5.7	560.5
		7.1	519.9
		8.5	513.8
		9.9	554.4
		10.8	574.7
		12.5	633.6
	1.51	4.0	1125.3
		5.3	790.1
		6.1	615.4
		7.6	546.3
		9.0	517.8
		10.6	586.9
		11.5	605.2
		13.3	662.1
	1.42	4.2	1186.2
		5.7	867.3
		6.5	680.4
		8.0	595.0
		9.6	552.4
		11.3	611.3
		12.2	637.7
		14.2	684.4

Table A1.2 - Resistivity Values at -3°C

Temperature (°C)	Dry Density (g/cm³)	Water Content %	Resistivity (ohm-m)
-3	1.8	3.4	303.2

		4.5	170.4
		5.2	69.6
		6.3	42.6
		7.6	43.5
		8.9	46.4
		9.7	65.3
	1.7	3.5	336.1
		4.7	180.4
		5.4	78.6
		6.7	49.6
		8.0	48.5
		9.4	50.4
		10.2	71.3
		11.8	79.1
	1.61	3.8	362.1
		5.0	188.4
		5.8	92.5
		7.1	57.5
		8.5	58.4
		10.0	59.3
		10.8	76.2
		12.5	90.0
	1.51	4.0	386.0
		5.3	203.3
		6.1	108.5
		7.6	66.5
		9.0	66.4
		10.6	70.2
		11.5	91.1
		13.3	98.0
	1.42	4.3	408.9
		5.7	218.3
		6.5	127.4
		8.0	91.4
		9.7	79.3
		11.3	84.1
		12.3	99.0
		14.2	111.9

Table A1.3 - Resistivity Values at 3°C

Temperature (°C)	Dry Density (g/cm³)	Water Content %	Resistivity (ohm-m)
3	1.8	3.3	212.5
		4.5	96.9
		5.2	69.5
		6.3	50.8
		7.7	42.2
		8.9	33.6
		9.7	28.1
	1.7	3.6	243.0
		4.7	107.8
		5.4	82.0
		6.7	54.7
		8.1	46.1
		9.4	39.1
		10.2	33.6
		11.8	22.7
	1.61	3.7	268.8
		5.0	123.4
		5.7	93.0
		7.1	60.2
		8.5	50.0
		10.0	43.0
		10.8	37.5
		12.5	28.9
	1.51	4.0	297.7
		5.3	139.1
		6.1	104.7
		7.5	66.4
		9.0	54.7
		10.6	46.9
		11.5	42.2
		13.3	33.6
	1.42	4.2	321.1
		5.6	168.8
		6.5	115.6
		8.0	73.4
		9.6	57.8
		11.3	52.3
		12.3	47.7
		14.2	41.4

Table A1.4 - Resistivity Values at 17°C

Temperature (°C)	Dry Density (g/cm³)	Water Content %	Resistivity (ohm-m)
17	1.8	3.3	142.3
		4.5	95.5
		5.6	53.5
		6.7	30.1
		7.8	25.3
		8.8	20.6
		9.9	16.7
	1.7	3.5	165.6
		4.8	104.1
		5.9	65.9
		7.1	33.2
		8.3	27.7
		9.3	23.7
		10.5	19.0
		11.7	18.1
	1.61	3.4	194.4
		4.6	109.5
		5.6	72.9
		6.7	37.8
		7.8	30.8
		8.8	26.8
		9.9	22.1
		11.1	21.3
	1.51	3.8	227.0
		5.1	128.2
		6.3	79.1
		7.5	40.9
		8.8	33.1
		9.8	31.5
		11.1	27.5
		12.5	25.1
	1.42	4.2	288.4
		5.8	160.8
		7.1	99.3
		8.6	50.2
		9.9	36.9
		11.1	32.9
		12.6	32.9
		14.1	26.6

Annex 2: ML Models and Data Normalization Methods

This annex provides detailed explanations of the ML models and data normalization techniques used in this study. It outlines the strengths, limitations, and justifications for each approach, alongside the equations and metrics that guided model evaluation.

A2.1 ML Regression Models

- **Random Forest**

Figure A2.1 illustrates the architecture of the Random Forest algorithm. The dataset is used to create multiple decision trees, each trained on a different subset of the data. For regression tasks, the individual results (Result-1, Result-2, …, Result-N) from each decision tree are averaged to produce the final output. This ensemble approach helps reduce overfitting and increases the model's ability to generalize, resulting in a more accurate and stable prediction. The process of averaging the results from each tree improves the model's robustness, especially in handling complex, non-linear relationships within the data.

- Justification: Random Forest was chosen for its robustness in handling complex, non-linear relationships and its ability to reduce overfitting through ensemble learning. Given the variability in permafrost data, Random Forest's capability to generalize by averaging predictions from multiple decision trees made it an ideal choice.
- Strengths: Random Forest is highly interpretable, relatively resistant to overfitting, and can handle large datasets with high dimensionality.
- Limitations: Random Forest can be computationally intensive with large datasets, and it may struggle with datasets where relationships are highly linear, as it inherently Favors non-linear patterns.

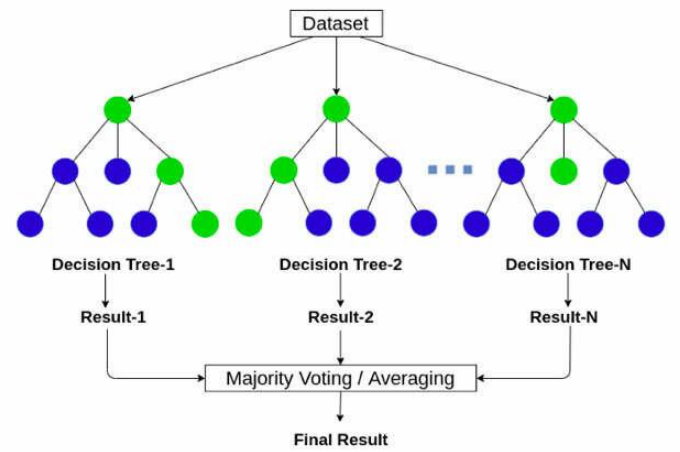

Figure A2.1- Structure of random forest regressor algorithm (Sathiparan et al. 2024)

- **Support Vector Regressor (SVR)**

The SVR model attempts to fit a hyperplane (solid line) through the data points in such a way that most data points are within a margin of tolerance (ε). Figure A2.2 illustrates the concept of Support Vector Regression (SVR). The dashed lines represent the boundary of this margin, where points outside the margin contribute to the error. The left graph shows a non-linear relationship, with SVR using kernel functions to transform the input into a higher-dimensional space, while the right graph

depicts a linear relationship. This tolerance zone enables SVR to generalize well, even with complex or noisy data.

- Justification: SVR was selected due to its ability to handle both linear and non-linear relationships by applying kernel functions, making it suitable for complex geophysical data that may contain mixed relationships.
- Strengths: SVR provides flexibility in model complexity through kernel functions and is effective with high-dimensional data.
- Limitations: SVR can be sensitive to outliers, and it may not perform as well as other models with very large datasets due to its computational demands. Additionally, tuning kernel parameters can be complex.

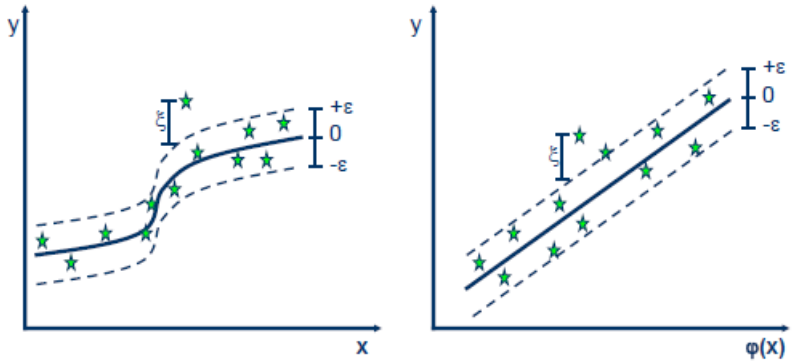

Figure A2.2 - Support Vector Regressor (SVR) Approach (Christensen, 2019)

➢ Gradient Boosting

Gradient Boosting is an ensemble learning method that builds a series of weak learners, typically decision trees, in a sequential manner. The key idea is that each new model attempts to correct the errors made by the previous models, ultimately improving the overall predictive accuracy. This process is known as "boosting," where each subsequent model is "boosted" to perform better on the mistakes of the previous ones.

This iterative approach allows Gradient Boosting to build a powerful predictive model by sequentially focusing on the hardest-to-predict cases. However, it is essential to tune the number of iterations, learning rate, and tree depth, as an overly complex model can lead to overfitting, while an insufficient number of iterations can result in underfitting.

- Justification: Gradient Boosting was chosen for its iterative learning process, where each model in the ensemble corrects the errors of the previous models. This approach is valuable in capturing intricate patterns and reducing error sequentially, which aligns well with the layered nature of permafrost data.
- Strengths: Gradient Boosting is powerful for non-linear data and can achieve high predictive accuracy by refining model predictions iteratively.
- Limitations: Gradient Boosting is prone to overfitting, particularly with noisy data. It is also computationally intensive, and its performance is highly sensitive to parameter tuning, which requires careful validation.

➢ k-Nearest Neighbors (k-NN)

k-NN is a simple, non-parametric ML algorithm used for both classification and regression tasks. It operates based on the principle that data points with similar features are likely to have similar outcomes. In regression tasks, k-NN predicts the output for a data point by taking the average (or sometimes a weighted average) of the outputs of its closest neighbors.

- Justification: The k-NN algorithm was included as a simple yet effective non-parametric model that can capture localized relationships in the data, which is important for detecting variations within permafrost regions.
- Strengths: k-NN is straightforward, interpretable, and does not make assumptions about data distribution, making it flexible for diverse data types.
- Limitations: k-NN can become computationally expensive with large datasets and may struggle with high-dimensional data. Its performance is sensitive to the choice of k, and it may perform poorly with imbalanced datasets.

➢ Neural Network

In a regression task, Neural Networks (NNs) work by mapping input features to a continuous output value through a series of interconnected layers and transformations. Here's a step-by-step outline of how NN models work for regression:

1. Input Layer: The input layer takes in the feature data, with each neuron representing one feature of the input dataset. This layer simply forwards the data to the next layer without any transformations.
2. Hidden Layers: The input data is then passed through one or more hidden layers. Each hidden layer consists of neurons, which apply weights to the incoming data and apply an activation function to introduce non-linearity. Common activation functions include ReLU (Rectified Linear Unit), sigmoid, or tanh, which help the network capture complex patterns in the data by transforming the inputs in non-linear ways. During the training process, the weights of the connections between neurons are adjusted to minimize the error in the model's predictions.
3. Forward Propagation: In forward propagation, data flows from the input layer, through each hidden layer, to the output layer. The inputs are multiplied by weights, and biases are added before applying the activation function. This process is repeated layer by layer, with each layer transforming the data according to its learned weights and biases.
4. Output Layer: In a regression NN, the output layer typically has a single neuron that outputs a continuous value, representing the predicted target variable. Unlike classification tasks where an activation function like softmax is used in the output layer, regression tasks may use a linear activation function or no activation function at all, as the goal is to produce a continuous output.
5. Loss Calculation: After the model generates its predictions, it calculates the loss (error) by comparing the predicted values to the actual target values from the training data. A common loss function for regression tasks is the MSE, which computes the average squared difference between the predicted and actual values.
6. Backpropagation and Optimization: To minimize the loss, the NN adjusts its weights and biases through a process called backpropagation. In backpropagation, the model calculates the gradient of the loss function with respect to each weight and bias. Using an optimization algorithm such as Gradient Descent or Adam, the network updates the weights in the direction that reduces the loss, thereby improving its predictions in future iterations.
7. Training Iterations: The NN repeats forward propagation, loss calculation, and backpropagation over many iterations (epochs), gradually minimizing the loss and improving its predictive accuracy on the training data.

8. Generalization: After training, the model's performance is evaluated on unseen test data to assess its generalization ability. The goal is for the NN to learn patterns in the training data that allow it to make accurate predictions on new data without overfitting (memorizing) specific data points.

Neural networks are particularly effective for complex regression tasks because they can model non-linear relationships between input features and the target variable, capturing intricate patterns that simpler models like linear regression may miss. However, they require a large amount of data and computational resources to train effectively, and careful tuning is often needed to avoid overfitting or underfitting.

- Justification: Neural Networks were selected for their capability to model highly complex, non-linear relationships, which are often present in environmental and geophysical data. The flexibility of neural networks makes them well-suited for capturing subtle patterns and dependencies in permafrost data.
- Strengths: Neural Networks can learn complex representations and relationships, especially with enough data, and are highly adaptable for various tasks.
- Limitations: Neural Networks require large datasets and significant computational resources. They can overfit easily if not managed with techniques such as regularization. Additionally, they are often viewed as "black boxes," lacking interpretability.

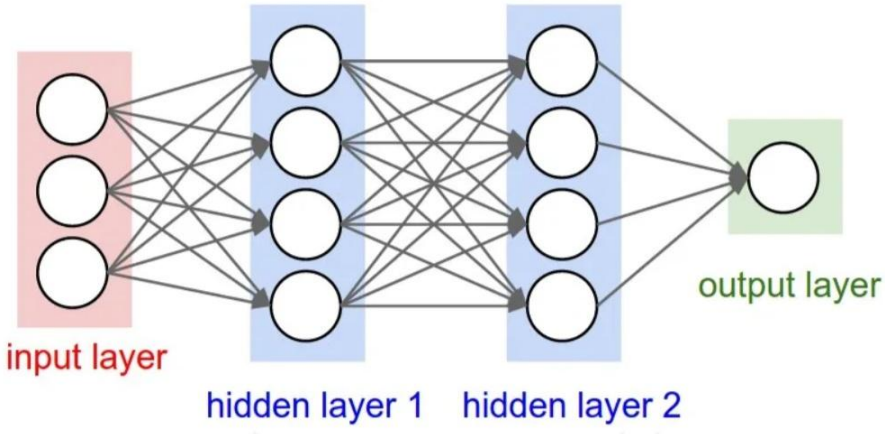

Figure A2.3 – A simple 2 hidden layer neural network structure (Afan et al. 2021)

➢ Linear Regression

Linear regression is one of the simplest and most widely used methods for predicting a continuous target variable based on one or more predictor (independent) variables. The core idea of linear regression is to find the best-fit line that represents the relationship between the predictors and the target variable.

In simple linear regression, we assume a linear relationship between a single predictor x and the target y, represented by the equation:

$$y = mx + b \qquad \text{(Equation A2.1)}$$

Where m is the slope of the line (indicating how much y changes for a unit change in x), b is the y-intercept (the value of y when x is zero).

In multiple linear regression, which involves multiple predictors x_1, x_2, ..., x_n, the relationship is extended to:

$$y = w_1x_1 + w_2x_2 + \cdots + w_nx_n + b \quad \text{(Equation A2.2)}$$

where w_1, w_2, ..., w_n, are the weights or coefficients associated with each predictor, and b is the intercept.

How It Works:

1. Model Fitting: Linear regression finds the values of w and b (for simple regression, m and b) that minimize the error between the predicted and actual values of y. This error is often measured using the MSE, which calculates the average of squared differences between actual and predicted values.
2. Optimization: The process of minimizing the MSE to find the best-fitting line is usually done using a method called Ordinary Least Squares (OLS). OLS adjusts w and b iteratively to minimize the total squared errors, finding the optimal line that fits the data.
3. Interpretation: The coefficients w provide insight into the relationship between each predictor and the target variable. A positive coefficient indicates a positive correlation (as the predictor increases, so does the target), while a negative coefficient suggests an inverse relationship.

- Justification: Linear Regression was included as a baseline model to assess how well the relationships in the data could be captured through linear patterns. It is also straightforward to interpret, offering insights into the influence of each predictor.
- Strengths: Linear Regression is simple, easy to interpret, and computationally efficient, making it ideal for benchmarking and exploratory analysis.
- Limitations: Linear Regression assumes a linear relationship, which may not hold for complex permafrost data. It is also sensitive to outliers and can perform poorly if relationships between features and the target variable are non-linear.

A2.2 CNN Model

A CNN is a deep learning model widely used for tasks involving spatial data, such as image processing, but it can also be adapted for structured data in regression tasks. CNN are particularly effective when the input data has spatial relationships, making them suitable for resistivity inversion tasks where capturing spatial patterns and local variations is essential.

A CNN is a deep learning model widely used for tasks involving spatial data, such as image processing, but it can also be adapted for structured data in regression tasks. CNN are particularly effective when the input data has spatial relationships, making them suitable for resistivity inversion tasks where capturing spatial patterns and local variations is essential.

The CNN architecture typically consists of three main types of layers: convolutional layers, pooling layers, and fully connected layers. For regression tasks, CNN can be modified to output continuous values in the final layer, allowing them to predict target variables like resistivity.

1. Convolutional Layers:
    - The convolutional layer is the core building block of a CNN. In this layer, small filters (or kernels) slide over the input data, performing an element-wise multiplication and summing the

results. This process, called convolution, extracts features from the input data, such as edges, textures, or spatial patterns.

- For resistivity data, the convolutional layers can capture spatial variations and discontinuities within permafrost, identifying patterns that might correlate with underlying resistivity structures.

2. Pooling Layers:
   - Pooling layers are used to reduce the spatial dimensions of the data, which helps to decrease computation and control overfitting. Typically, max pooling or average pooling is applied. Max pooling, for example, takes the maximum value in each region of the feature map, preserving the most prominent features while discarding less important information.
   - Pooling layers help the model generalize by focusing on the most significant patterns, which can improve its robustness and prevent overfitting to specific details in the training data.
3. Fully Connected Layers:
   - After several convolutional and pooling layers, the extracted features are flattened and passed through fully connected layers. These layers combine the features detected by previous layers to learn higher-level patterns and relationships.
   - In regression tasks, the final fully connected layer typically has a single neuron with a linear activation function, producing a continuous output value that represents the model's prediction.
4. Output Layer:
   - In this study, the output layer has a single neuron with a linear activation function, as the goal is to produce a continuous output that represents the predicted resistivity. Unlike classification tasks, which use activation functions like softmax, regression tasks often use a linear output.

- Justification for Using CNN in Resistivity Inversion: CNN are well-suited to this study due to their ability to capture spatial relationships within data. Resistivity data from permafrost regions typically exhibit complex spatial patterns and discontinuities that are difficult to capture using traditional methods. CNN, with their layer-by-layer feature extraction approach, can identify subtle spatial variations that may correspond to different resistivity zones, making them ideal for inversion tasks that require a detailed and accurate spatial representation.
  - Handling Complex Spatial Patterns: Conventional resistivity inversion techniques often smooth out details and may miss finer discontinuities in resistivity distribution. CNN, however, can capture these intricate spatial patterns through convolutional filters, allowing the model to detect sharp boundaries and regions with abrupt resistivity changes, which are common in permafrost structures.
  - Feature Hierarchies: CNN create feature hierarchies, allowing the model to recognize both local and global patterns. This is particularly important in resistivity inversion, as it enables the model to detect both small-scale variations within a single layer and larger structural patterns across different layers.
  - Efficiency in Large Datasets: CNN are designed to handle large datasets efficiently, which is advantageous when working with spatial data across multiple pseudo-sections or resistivity models. This scalability is essential for real-time imaging, where rapid and detailed analysis is required for environmental and geotechnical assessments.

- Strengths: CNN are well-suited to tasks where spatial relationships are important, as they can capture both local and global patterns effectively. They can identify intricate structures in resistivity data, potentially providing more accurate and detailed inversion results compared to traditional methods.
- Limitations: CNN require large amounts of labelled data for training to generalize effectively. They are also computationally intensive and can be prone to overfitting if the dataset is not diverse enough. For resistivity inversion, increasing the dataset size or incorporating more varied patterns can help improve the model's robustness.

In summary, the CNN model offers a promising approach for resistivity inversion by capturing spatially complex structures within permafrost regions. Its ability to detect discontinuities and subtle resistivity variations provides a valuable tool for real-time imaging, though it requires sufficient data and careful tuning to achieve reliable results. The choice of CNN in this study is justified by its capacity to capture and process the spatial dependencies in resistivity data, making it more suitable than traditional inversion methods for accurate permafrost mapping.

A2.3 Model Evaluation Metrics

To assess the performance and accuracy of the ML regression models used in this study, various evaluation metrics were employed. These metrics provide insights into the predictive power of the models and their ability to generalize across unseen data. The following key metrics were used:

- **R^2 (Coefficient of Determination)**

R^2 is a statistical measure that indicates the proportion of the variance in the dependent variable that is predictable from the independent variables. It ranges from 0 to 1, where an R^2 value of 1 indicates that the model perfectly explains the variance in the data, while an R^2 value close to 0 implies that the model fails to capture the variability. Equation:

$$R^2 = 1 - \frac{\sum_{i=1}^{n}(y_i - \hat{y}_i)^2}{\sum_{i=1}^{n}(y_i - \bar{y})^2} \quad \text{(Equation A2.3)}$$

where y_i represents the actual value, $\hat{y}_i$ is the predicted value, and $\bar{y}$ is the mean of the actual values.

Justification: R^2 is a fundamental metric for understanding the model's overall fit. In the context of permafrost resistivity, temperature, and water content prediction, a high R^2 value would suggest that the model captures the essential relationships between input features and target variables, making it a good indicator of predictive strength. However, R^2 alone does not indicate the magnitude of errors, which is why other metrics are also necessary.

- **RMSE (Root Mean Squared Error)**

RMSE is a measure of the average magnitude of the error between the actual and predicted values. It provides an indication of how well the model performs by giving more weight to larger errors. Equation:

$$RMSE = \sqrt{\frac{1}{n}\sum_{i=1}^{n}(y_i - \hat{y}_i)^2} \quad \text{(Equation A2.4)}$$

Justification: RMSE is valuable in this study because it penalizes large errors more heavily, which is crucial in applications like resistivity and temperature prediction, where large deviations can significantly impact the interpretation of subsurface properties. A high RMSE might indicate that the model struggles with certain extreme values or specific regions in the data. However, because it amplifies larger errors, RMSE might be less desirable when outliers heavily influence the data.

- **MSE (Mean Squared Error)**

MSE is the mean of the squared differences between the actual and predicted values. It is a commonly used metric that penalizes larger errors more than smaller ones, making it suitable for identifying models that perform well across all data points.

$$MSE = \frac{1}{n}\sum_{i=1}^{n}(y_i - \hat{y}_i)^2 \qquad \text{(Equation A2.5)}$$

Justification: MSE is often preferred when evaluating overall performance because it provides a measure that reflects both the bias and variance of the model. In the context of this study, a low MSE would suggest that the model generally performs well across all data points, while a high MSE would indicate consistent prediction errors. However, MSE's sensitivity to outliers may sometimes exaggerate errors due to occasional large deviations.

- **MAE (Mean Absolute Error)**

MAE represents the average absolute difference between the actual and predicted values. Unlike RMSE and MSE, MAE does not square the errors, which means it provides a more direct measure of prediction error that is less sensitive to outliers. Equation:

$$MAE = \frac{1}{n}\sum_{i=1}^{n}|y_i - \hat{y}_i| \qquad \text{(Equation A2.6)}$$

Justification: MAE provides a straightforward and interpretable measure of average prediction error, which is beneficial for understanding the typical error magnitude in model predictions. In this study, MAE is especially useful for examining the consistency of predictions across permafrost properties without allowing a few large errors to disproportionately influence the overall assessment.

- **MAPE (Mean Absolute Percentage Error)**

MAPE expresses the prediction error as a percentage, allowing for easy interpretation of the model's performance in terms of relative accuracy. It is particularly useful when comparing models on datasets with varying scales. Equation:

$$MAPE = \frac{100\%}{n}\sum_{i=1}^{n}\left|\frac{y_i - \hat{y}_i}{y_i}\right| \qquad \textit{(Equation A2.7)}$$

Justification: MAPE allows for an intuitive understanding of model accuracy in percentage terms. For this study, MAPE is helpful for interpreting how closely the predicted values align with actual measurements relative to their magnitudes. However, MAPE can be misleading when actual values are near zero, as it may produce extremely high values that skew the interpretation of accuracy.

By combining these metrics, this study can gain a comprehensive understanding of each model's strengths and limitations. High RMSE or MSE values would indicate a need for further refinement to reduce large errors, while high MAE or MAPE values might suggest broader issues with model generalization. In essence, using a mix of these metrics allows for a balanced assessment, ensuring that the models perform well across various dimensions of prediction accuracy and reliability.

A2.4 Data Normalization Methods

Data normalization is an essential preprocessing step in ML, especially for algorithms sensitive to feature scaling. Normalization ensures that features contribute equally to the model's performance and can lead to faster convergence and improved accuracy. This section outlines the different normalization methods employed in this study:

➢ StandardScaler

The StandardScaler standardizes the features by removing the mean and scaling them to unit variance. This results in a distribution with a mean of 0 and a standard deviation of 1. Equation:

$$X' = \frac{X - \mu}{\sigma} \qquad \textit{(Equation A2.8)}$$

where X represents the original feature, μ is the mean of the feature, and σ is the standard deviation.

Characteristics:

- Ensures that each feature contributes equally, which can be beneficial for algorithms that rely on distance metrics, such as Support Vector Regressors and k-Nearest Neighbors.
- Works well when the data follows a Gaussian distribution.
- Can improve the numerical stability of the models and speed up training.

➢ MinMaxScaler

The MinMaxScaler scales and translates each feature individually so that it lies within a given range, typically [0, 1]. It is useful when the distribution of the data does not follow a normal distribution. Equation:

$$X' = \frac{X - X_{min}}{X_{max} - X_{min}} \qquad \textit{(Equation A2.9)}$$

where X_{min} and X_{max} are the minimum and maximum values of the feature, respectively.

Characteristics:

- Preserves the relationships among data points and does not change the shape of the distribution.

- Suitable for algorithms where small-scale differences need to be preserved.
- Works best when the minimum and maximum values are known and consistent across datasets.

➢ **MaxAbsScaler**

The MaxAbsScaler scales the data by dividing each feature by its maximum absolute value, ensuring that all features are in the range [-1, 1] for both positive and negative values. Equation:

$$X' = \frac{X}{|X_{max}|} \qquad \textit{(Equation A2.10)}$$

where $|X_{max}|$ is the maximum absolute value of the feature.

Characteristics:

- Maintains sparsity in the dataset, making it useful for models with sparse data representations, such as text data or one-hot encoded features.
- Does not shift or center the data, which can be beneficial when preserving the original feature distribution is essential.
- Effective when features have different scales but need to be normalized without altering their zero-centered properties.